This dissertation has been
microfilmed exactly as received

68-17,476

CALUSIO, Joseph Charles, 1939-

THE MAGNETO-OPTIC AND ELECTRICAL PROPERTIES OF HYDROUS FERRIC OXIDES.

The University of Oklahoma, Ph.D., 1968
Physics, molecular

University Microfilms, Inc., Ann Arbor, Michigan

Downloaded from SHAREOK. Persistent Handle URL: https://hdl.handle.net/11244/2406

THE UNIVERSITY OF OKLAHOMA

GRADUATE COLLEGE

THE MAGNETO-OPTIC AND ELECTRICAL PROPERTIES OF HYDROUS FERRIC OXIDES

A DISSERTATION

SUBMITTED TO THE GRADUATE FACULTY

in partial fulfillment of the requirements for the

degree of

DOCTOR OF PHILOSOPHY

BY

JOSEPH CHARLES CALUSIO

Norman, Oklahoma

1968

THE MAGNETO-OPTIC AND ELECTRICAL PROPERTIES

OF HYDROUS FERRIC OXIDES

APPROVED BY

Sylvard Moerome

Stanley E. Babb, Jr.

J M Canfield

C C Lin

W. N. Huff

DISSERTATION COMMITTEE

ACKNOWLEDGEMENTS

The author wishes to express his sincere appreciation to Professor Sybrand Broersma for directing this work and for his many suggestions and his advice given to solve the many problems as they arose in the course of these studies.

Also it is a pleasure to acknowledge the support of the National Science Foundation. Their support throughout the course of this work made possible the purchase of equipment needed for these studies. In addition, financial support was provided in the form of a research assistantship.

Finally he wishes to express his appreciation of the constant encouragement and patience of his wife, Carol.

TABLE OF CONTENTS

		Page
ACKNOWLEDGMENTS		iii
LIST OF TABLES		v
LIST OF ILLUSTRATIONS		vi
Chapter		
I.	INTRODUCTION	1
	References	8
II.	FARADAY EFFECT	9
	References	61
III.	ELECTRICAL PROPERTIES	62
	References	74
IV.	OPTICAL ABSORPTION	75
	References	97
V.	RELATED EXPERIMENTS	98
	Electron Microscope Results	98
	EPR Measurements	104
	Effect of Pressure on the Resistance	107
	Photoconductivity	113
	References	115
VI.	THIN FILMS	116
	References	134
VII.	SUMMARY	135

LIST OF TABLES

Table		Page
1.	Magnet Current "I" and Field	17
2.	Summary of Data for Interference Filters Used.	18
3.	Summary of the Signs of the A, B, and C Terms for SFO's.	54
4.	Summary of the α's for the SFO's	56
5.	Effect of the Contact Material on the Experimental Energy Levels E_i	69
6.	Summary of Results from Resistance-(1/T) Data.	71
7.	Molar Extinction Coefficients for SFO #5C-1.	77
8.	Weak Absorption Peaks Observed for the SFO's	83
9.	Maximum Values of ε in The Range 200-1700 Millimicrons .	88
10.	Oscillator Strengths	95
11.	Comparison of Particle Size Data	101
12.	g_{eff} Values Obtained by ESR Measurements	107
13.	Resistance Relaxation Data for SFO #5A-4	109
14.	Thickness of Films Used in the Study of Faraday Rotation	121
15.	Verdet Constants in the "Linear" Regions for Several Ferromagnetics	127
16.	Saturation Rotation for Nickel	128

LIST OF FIGURES

Figures		Page
1.	Cells used in measuring the Faraday rotation	17
2.	MORD for $CoSO_4 \cdot 7H_2O$.	25
3.	Magnetic field dependence of the FR for SFO #5C-1. . . .	29
4.	Wavenumber dependence of the FR for SFO #5C-1.	30
5.	Magnetic field dependence of the FR for SFO #5B-6. . . .	32
6.	Wavenumber dependence of the FR for SFO #5B-6.	33
7.	Magnetic field dependence of the FR for SFO #6A-1. . . .	36
8.	Wavenumber dependence of the FR for SFO #6A-1.	37
9.	Magnetic field dependence of the FR for SFO #6'-8. . . .	38
10.	Wavenumber dependence of the FR for SFO #6'-8.	39
11.	Magnetic field dependence of the FR for SFO #10B-2 . . .	41
12.	Wavenumber dependence of the FR for SFO #10B-2	42
13.	Magnetic field dependence of the FR for SFO #10'-(7+8+9)	43
14.	Wavenumber dependence of the FR for SFO #10'-(7+8+9) . .	44
15.	Magnetic field dependence of the FR For SFO #11A-3 . . .	46
16.	Wavenumber dependence of the FR for SFO #11A-3	47
17.	Magnetic field dependence of the FR for SFO #11-C. . . .	48
18.	Wavenumber dependence of the FR for SFO #11-C.	49
19.	Magnetic field dependence of the FR for SFO #14.	51

LIST OF FIGURES (Cont'd.)

Figures		Page
20.	Wavenumber dependence of the FR for SFO #14.	52
21.	Schematic of apparatus used in measuring resistance values	63
22.	Temperature dependence of the resistance of SFO #5C-2. .	66
23.	Temperature dependence of the resistance of SFO #14. . .	67
24.	Resistance voltage characteristic of a typical SFO . . .	68
25.	Method of separating small absorption from large broad absorption	81
26.	Extinction coefficients for some ferric salt solutions .	86
27.	Extinction coefficients of SFO's #5C-1, #5B-6 and #14. .	91
28.	Extinction coefficients of SFO's #6A-1 and #6'-8	92
29.	Extinction coefficients of SFO's #10B-2 and #10'-(7+8+9)	93
30.	Extinction coefficients of SFO's #11A-3 and #11-C. . . .	94
31.	Photomicrographs of some SFO's	100
32.	Relaxation effect in SFO #5A-4	110
33.	Temperature dependence of the resistance of SFO #5A-4 at several pressures.	112
34.	Schematic of the vacuum system used to produce metal films.	117

LIST OF FIGURES (Cont'd.)

Figures Page

35. Schematic of apparatus used to measure the thickness of the metal films. 119

36. Faraday rotation of thin iron film as a function of magnetic field 123

37. Faraday rotation of thin cobalt film as a function of magnetic field 124

38. Faraday rotation of thin nickel film as a function of magnetic field 125

39. Faraday rotation of thin iron film as a function of the wavenumber 129

40. Faraday rotation of thin cobalt film as a function of wavenumber 130

41. Faraday rotation of thin nickel film as a function of wavenumber 131

42. Faraday rotation of thin copper film as a function of wavenumber 132

43. Field dependence of the rotation θ_D at 18,500 cm^{-1} in thin nickel film 133

CHAPTER I

INTRODUCTION

This thesis concerns the magneto-optic, electrical and structural properties of a group of "stabilized ferric oxides". In the following description we shall refer to these compounds as SFO's. Ferric oxide-(or hydroxide) macromolecules have been stabilized with a glucose polymer. This polysaccharide makes the ferric oxides particles soluble in water and retards the coagulation and subsequent precipitation of the colloidal particles. The sizes of the ferric oxide macromolecules are 100 Angstroms and smaller. Hence some differences are observed in magneto-optic properties between the SFO's and ordinary ionic solutions. They are described later. The sizes of the macromolecules are not so large however, that complete optical absorption takes place within a macromolecule and hence meaningful Faraday rotation measurements on the SFO's can be taken. The stability and size of the stabilized ferric oxides makes them ideal for experimental studies.

The major part of this thesis concerns the Faraday rotation-(FR)-of the SFO's. At the onset several goals were set. First, it had become desirable to measure the dispersion of the magneto-optic rotation-(MORD)-in the visible since measurements made previously with white light were not sufficient for a theoretical analysis. But these

data revealed a pressure dependence FR for the SFO's. Secondly, since little specific theory concerning the MORD of the ferric oxides had been written at that time it was of interest to test some of the more general theories. This task was simplified when, before our measurements of the MORD's were completed, a new theoretical paper appeared, encompassing FR measurements in spectral regions of large optical absorption. This publication was important to us since previous published theories were not valid in regions of large optical absorption and especially since the SFO's all have very large absorption coefficients at the wavelengths which we used.

Except for SFO #14 all commercial samples have a rather broad distribution of particle sizes. Some of the early experiments showed that the magnetic properties were very dependent upon the particular specimen.[1] Therefore, we fractionated the SFO's with a gel column.[2] It is from this separation that the terminology for designating a particular SFO fraction has arisen. The meaning of the symbols may be illustrated for a particular case, for example, SFO #5'B-3. The "five" refers to the unfractionated commercial SFO. The prime implies that this SFO has been fractionated with the G-200 Sephadex column (up to molecular weight 200,000). No prime refers to a fractionation with the G-100 column. The "B" refers to a particular portion of the SFO which was fractionated. Most important the "3" refers to the particular fraction of SFO #5. The heaviest (largest size) fraction comes through the column first and is labeled "1". Normally 5 to 15 fractions are obtained from a particular fractionation. SFO #14 is the only one that did not fractionate in our Sephadex column.

Information on the chemical composition of the fractions was obtained with a commercial analysis. This furnished the iron, carbon, and hydrogen content for many of the SFO fractions. The high fractions are characterized by iron contents of the order of 50 per cent by weight whereas the low fractions have iron contents of the order of 5 per cent. This continuous range of concentrations also justifies this research on otherwise complex systems. X-ray studies[2] and electron microscope studies reported in Chapter V show that the ferric oxides themselves are small crystallites in general ranging from 45 Angstroms diameter to less than 20 Angstroms. The crystallites of #14 are approximately rectangular with a size of 150 by 50 Angstroms.

As is to be expected the MORD of a particular sample closely follows the optical absorption. The optical absorption is very large in the UV but falls off rather sharply in the visible. This behavior is exhibited by the FR. Measurements of the MORD were taken in the range of 800 millimicrons to 365 millimicrons. The FR increases by as much as 100 times approaching the smaller wavelength. The newer theories predict this very sharp frequency dependence of the MORD whereas the older work did not. From the MORD data, the sign of the matrix elements of the electric dipole moment can be ascertained.

Examination of the magnetic field-(H)-dependence of the FR yields very interesting results. The dependence is not linear as one finds for molecular solutions. In order to fit the H dependence of the FR it is necessary to use functions such as tanh αH, so that "saturation" occurs for 10 kilogauss and at room temperature.

Evidently, the FR is proportional to the magnetization of the entire crystallite. This is analogous to superparamagnetism and is supported by measurements on the susceptibility, χ.[2] This may be the first time that such "superparamagnetic" FR has been reported. This effect is, of course, dependent on particle size and our success in observing it is a consequence of the fact that we were able to use particles small enough for light to be transmitted.

The FR is analytically related to the optical absorption spectra, in that the frequency functions needed to describe the MORD are centered at the absorption band maxima. Therefore, the absorption spectra for all SFO's were measured. We used water solutions of the SFO's for these measurements. The experiments showed that the absorption is due to the iron (iron ions) in the SFO's. The extinction coefficients for the SFO's are the same order of magnitude as that observed for the Fe^{3+} ion. However, the shape of the extinction coefficient spectra differs from the Fe^{3+} spectra, but it resembles the spectra of colloidal ferric hydroxide.

The absorption in the visible and in the infrared (IR) is dominated by the "wings" of the strong UV absorption band. The electronic transitions in the visible and IR correspond to forbidden electric dipole transitions and thus are very weak whereas the UV transitions are allowed. The positions of several absorption band maxima $\bar{\nu}_o$ in the visible are estimated from inflections in the curves displaying the excitation coefficient spectra. They are located at 17,000±1,000 cm^{-1}, 22,500±1,000, 26,500±1,000 cm^{-1}, and 32,000±2,000 cm^{-1}. Using frequency functions centered at these wavelengths it is possible to fit the FR data satisfactorily.

Because the SFO showed some electrical conductivity we decided to study this phenomenon and its mechanism. It was found that the resistance varied roughly as exp(a/T). A typical sample resistivity was 10^{14} ohm cm at room temperature and 10^{9} ohm cm at 200 °C, a change by a factor of 10^{5}.

Initially, we hoped to use the resistance versus temperature data to verify the $\bar{\nu}_o$ values found from the absorption spectra. However, except for 5C-1, the interpretation is complicated by the resistance due to the organic polymer. SFO #5C-1 is an exception, it has a resistance and energy gap quite similar to Fe_3O_4. For this SFO the resistance is likely to be determined solely by the ferric oxide, which must resemble Fe_3O_4. In the other SFO's the organic polymer shields the crystallites from one another.

Several short investigations were conducted on the SFO's to further enhance our understanding of their structure. Electron microscope pictures were made of several of the fractions. Standard electron microscope grids were prepared by placing a drop of the SFO solution onto the grid and then evaporating the water. Photomicrographs were taken at a magnification of over 100,000. Only the ferric oxide crystallites are visible. The sizes of these crystallites were measured and the results compared with those of the X-ray diffraction data.[2] The results of the two measurements are quite close: if the interpretation is correct they agree within experimental error. This confirms that the ferric oxide exists in crystallites. The sizes range from the rectangular shaped crystallites of #14, 150 Angstroms by 50 Angstroms, to crystallites

less than 20 Angstroms. Particles less than 15 Angstroms diameter were below the limit of resolution of this technique. It confirmed the magnetic and chemical results which showed that the highest fraction had the largest iron oxide crystallites for a particular SFO.

A brief study of the EPR spectra of the SFO's was made as well. The measurements were taken at room temperature. A value of the "g-factor" was found by estimating the magnetic field at the center of the relatively broad microwave absorption band. All of these values were found to be very nearly equal to 2.0. This is the value that one would expect for ferric ions since the angular momentum "L" is zero. No significant bands corresponding to other values of "g" could be discerned. This measurement gave us confidence that the iron was present in the SFO's in the +3 oxidation state through the possibility of the existence of some Fe^{2+} could not be completely ruled out by these measurements.

Measurements of the pressure dependence of the electrical conductivity were made. Since the crystallites are kept separated by the organic molecules it was felt that application of a pressure of the order of a few kilobar would produce a considerable change in the distance between crystallites and a correspondingly large change in the sample resistance. The measurements indeed showed that the resistance decreased by as much as 50 per cent on application of only 1.35 kilobar pressure. Also observed in these experiments was a tendency for the resistance to "relax" after the initial application of the pressure (or after its release). This double process was also observed in the pressure dependence of the magnetic susceptibility χ.[2] We believe

that this relaxation is due to either a slow rearrangement of the surface atoms in the crystallites or perhaps a release of the pressure on the polymers by the penetration of the pressurized oil into the exterior of the SFO. The time constants for this relaxation were measured and found to be the order of several minutes at room temperature and somewhat less than this value at elevated temperatures. It was found, however, that the activation energy of the SFO changed very little from its value at one atmosphere on raising the pressure to 1.35 kilobar.

The last experiments described are those on the Faraday rotation of thin ferromagnetic films. The dispersion and the field dependence of iron, cobalt and nickel films were measured. These films were prepared by vacuum deposition. The metal films were deposited onto microscope cover slips at a pressure below 0.1 micron of mercury. Measurements of the FR were taken after removal from the vacuum system but care was taken to store the films in a dry, evacuated container until the actual data were taken.

The magnetic field dependence of the FR showed that the nickel film "saturated" below 10 kilogauss. For the other films the saturation could be attained below 100 kilogauss. The ferromagnetic films saturate at high fields because the films are not thick enough to form domains with a magnetization perpendicular to the film plane. Finally, the thickness of these films was measured and the Verdet constant evaluated. Measurements of film thicknesses of 1000 Angstroms can be accomplished by use of multiple beam interferometry. Because of the difficulty of these thickness measurements the Verdet constant of thin films are seldom given.

REFERENCES

1. Skaggs, F. L., M. S. Thesis, University of Oklahoma 1964; S. Broersma, Rev. Sci. Instr. 34, 277 (1963).
2. Wilson, D. M., M. S. Thesis, University of Oklahoma, 1968, (in preparation).

CHAPTER II

FARADAY EFFECT

General Information

The first and most extensive study of the SFO's discussed in this thesis is of their magneto-optic rotation. Only the so called longitudinal magneto-optic rotation - Faraday effect - will be considered. In the Faraday effect the magnetic field, H, and the light beam are parallel. The terms longitudinal magneto-optic rotation and Faraday effect will be used interchangeably.

Initially, the SFO's were studied because they showed a considerable pressure effect on the magneto-optic rotation - MOR for short. It was found that the effect of pressure on the magnetic susceptibility was about a five per cent decrease per kilobar. Hence it was expected that the MOR would have a comparable effect. This was indeed found to be true and the results have been published.[1]

Attempts to analyze the pressure dependence of the MOR were thwarted because of a lack of knowledge of the structure of the SFO's. Also, in order to obtain a better understanding the wavelength dependence was studied first. A few years ago very little theoretical work on the dispersion of the magneto-optic rotation - MORD - had been published. Since then several publications have appeared and use can be

made of these now. Hence, the purpose of the present study was to measure the MORD's of the SFO's, especially as it relates to the structure and components of the SFO's. We also hoped to provide an experimental test for the proposed theories. Quite possibly the magnetic properties - MORD's and magnetic susceptibilities, etc., can furnish a new understanding of the diverse, and sometimes contradictory, properties of the "ferric complexes".

Experiment

The Faraday effect is named for its discoverer, who observed it as early as 1846. The Faraday effect is similar to natural optical activity, which one observes in many sugars, in that a rotation of polarized light occurs. However, here the effect is induced by a magnetic field, H, so that the rotation is zero at zero magnetic field. A schematic diagram of the optics involved in a Faraday effect measurement is given below.

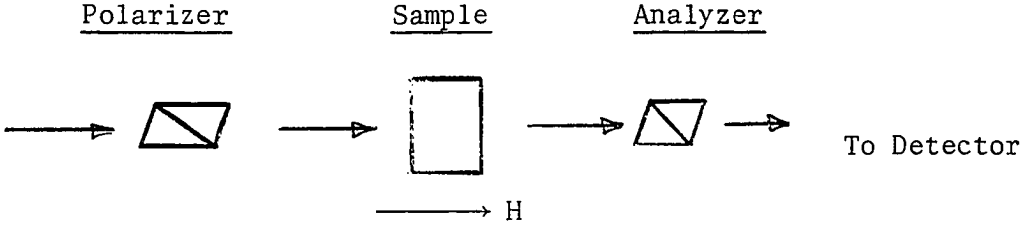

An angle measurement could be made by first "crossing" the polarizer and analyzer at H = 0. Then switching on the field one would again find the position at which the polarizer and analyzer were "crossed". The difference between this angle and the one at H = 0 is the Faraday rotation - FR for short.

The FR is a very general phenomenon, it is observed in all matter and at nearly all wavelengths in the electromagnetic spectrum.[2] In the present study the FR was observed through the range of visible wavelengths and somewhat into the UV. The shortest wavelength used was 365 millimicrons.

Most of the older FR measurements were made with the sodium D-line. Much of this work involved the study of the field dependence. The observation that the FR is often a linear function of H was first made by Verdet. In this case the FR - expressed in degrees or minutes - is given by Θ where

$$\Theta = VH\ell,$$

and V is called the Verdet constant and "ℓ" is the length of the sample. Most gases and many liquids have this linear field dependence. The second significant study of the field dependence was made by Becquerel and associates.[3] These were made at liquid helium temperature and the dependence of Θ on the magnetic field was found to obey the formula.

$$\Theta = A\ell B_J\left(\frac{g\mu_B H}{kT}\right),$$

where

ℓ = sample length
B_J = Brillouin function
g = spectroscopic splitting factor
μ_B = Bohr magneton = - 0.927 x 10^{-20} ergs/gauss
k = Boltzmann constant = 1.38 x 10^{-16} erg/deg.
T = absolute temperature

The dependence of Θ on the Brillouin function is such that Θ is approximately linear in H for small values of the argument but reaches a maximum, "saturation", at large values of H.[4]

More explicitly

$$B_J(x) \rightarrow \begin{cases} (J+1)g\mu_B/3kT & \text{as } x \rightarrow 0 \\ 1 & \text{as } x \rightarrow \infty \end{cases}$$

where N is the number of magnetic moments per unit volume. At intermediate temperatures Becquerel found that the FR could be represented by the sum of terms i.e.,

$$\phi(4^\circ<T<300^\circ) = [a\, B_J(\frac{g\mu_B H}{kT}) + bH]\ell$$

At about the time of Becquerel's work theoretical expressions for the FR were published. The most notable are those of Kramers',[4] Rosenfeld[5] and Serber.[6] All of the theories were strictly valid at wavelengths well removed from an absorption line, or band, of the sample.

About 1959 new measurements of the magneto-optic rotary dispersion - MORD - for the transition metal complexes in the visible and UV began to appear. Most of these were done at room temperature. The availability of interference filters, monochromators and excellent photo-multiplier tubes made the task of measurement at many different wavelengths and magnetic fields much easier than with the older visual observation methods. Also the range of measurements was extended to the ultraviolet region of the spectrum. Regions of strong sample

absorption could be investigated now. And of course, the data obtained near an absorption line are most sensitive to the properties of the excited states of the atom or molecules under investigation. The ground state properties can be inferred by the magnetic field dependence of the FR.[7]

The instrument used for all these measurements is given in the schematic below.

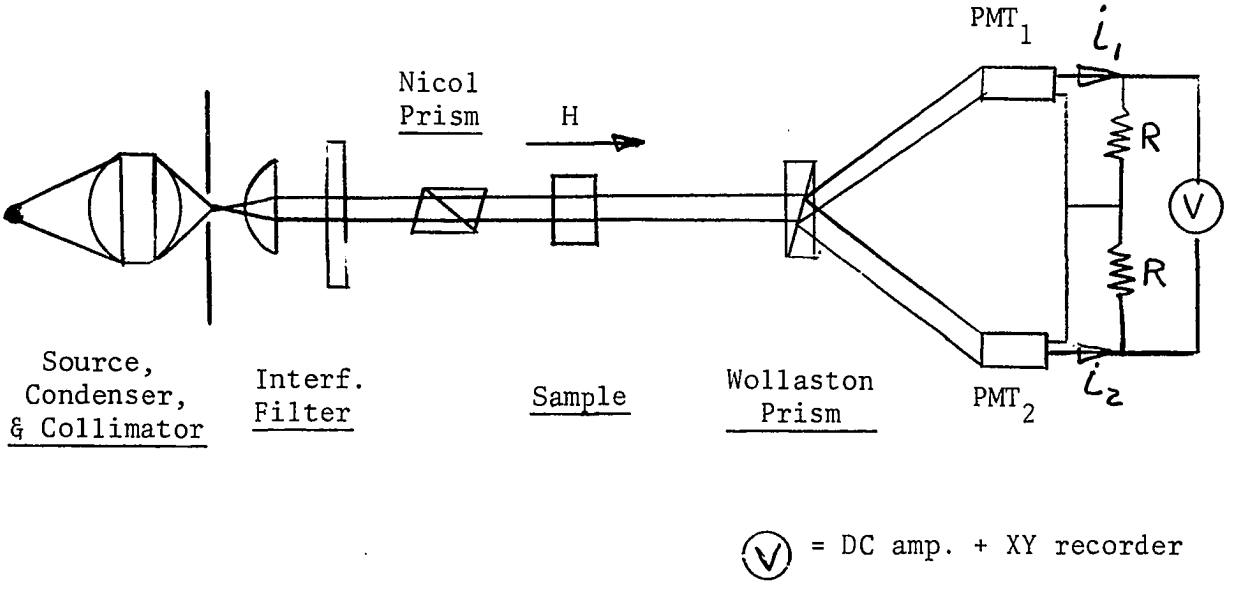

The original equipment has already been described in Ref. (1) of Chapter 1. We modified the instrument by introducing new lenses for UV work, new short - 1 mm cells and a DC amplifier in the measuring circuit.

The source - a tungsten lamp or a mercury arc - supplies a collimated beam to the interference filter which very selectively passes a narrow band of wavelengths centered at some known wavelength. This essentially monochromatic beam passes through the polarizer after which a plane polarized monochromatic beam can traverse the sample. Thereafter the beam is decomposed by an analyzer into two separate beams which strike different photomultiplier tubes - PMT's. Thus we have two currents i_1 and i_2 in the external circuit of the PMT's. These in turn produce the voltages, V_1 and V_2, across the two equal load resistors R. The voltage difference $V_1 - V_2$ across these resistors is fed to a DC amplifier and then to the Y-axis of an XY recorder. The Y-axis deflection is used to measure the Faraday rotation of the sample.

When the plane polarized beam of intensity I_o passes the Wollaston-type analyzer the two emerging beams have intensities of

$$(I_t/I_o)_1 = \cos^2\Theta$$

$$(I_t/I_o)_2 = \sin^2\Theta$$

where Θ is the angle between the polarizer and the analyzer. If one includes the effect of absorption of the sample and lens system then

$$(I_t/I_o)_1 = \alpha \cos^2\Theta$$

$$(I_t/I_o)_2 = \alpha \sin^2\Theta$$

where α is the absorption coefficient of the system at the particular wavelengths used. The voltage difference produced by these currents

is given by

$$(V_1-V_2) = (i_1-i_2)R = \alpha RSI_o(\cos^2\Theta - \sin^2\Theta)$$

$$= \alpha RSI_o \cos(2\Theta) ,$$

where S is the PMT sensitivity.

The output on the Y-axis of the XY recorder then is

$$V_o = G(V_1-V_2) = \alpha\, GRSI_o \cos 2\Theta ,$$

where G is the gain of the DC amplifier and the XY recorder. Now the sensitivity of V_o to a rotation of the plane of polarization is as follows

$$dV_o/d\Theta = -\, 2\,\alpha GRSI_o \sin(2\Theta) . \qquad (1)$$

For zero magnetic field the polarizer is set so that $\Theta = 45°$. In that case it is seen that $V_o = 0$ and that $(dV_o/d\Theta)$ reaches its maximum value of $2\,\alpha\, GRSI_o$. For changes of ± 1 degree about $\Theta = 45°$ this sensitivity is a constant so that the incremental change ΔV_o is linear with rotation $\Delta\Theta$. Thus the coefficients $\alpha\, GRSI_o$ can be experimentally determined, and the Y-axis calibrated.

The X-axis of the XY recorder is driven by either a time-base generator or by a voltage produced by the magnet current. First a record was made of the rotation versus the field H. Then the deflection ΔV_o was marked in by rotating the polarizer head at H = 0 in steps usually of 0.1°. The polarizer scale itself is calibrated in 0.01 degrees. The unit includes a high quality Nicol which permits accurate small angle measurements.

Determinations of the FR were made at each wavelength λ_o with the magnetic field along as well as opposite to the direction of the light beam. This was done to decrease systematic errors due to hysteresis of the XY recorder and magnet as well as to eliminate effects caused by small birefringence of the end windows of the cells.[8]

All data for the FR reported here concern solutions of the SFO in distilled water. We believe that the rotation in solution will be nearly equal to that observed in solid-(dried)-condition, viz., because of the preparation of the SFO's. Since the ferric complex is stabilized by the organic polymers we do not expect or observe any chemical changes of the complexes on dissolving. There is a slow precipitation as the colloidal particles tend to form larger particles. The water molecules penetrate into and around the glucose polymer so that the SFO's can go into solution. However, the water is excluded from the ferric complexes which are responsible for the magneto-optic rotation of the SFO's. Hence, the electrostatic field of the free water is only strong near the surface atoms of the ferric complex.

The cells used in measuring the FR of the SFO's and $FeCl_3 \cdot 6H_2O$ are similar in design, only the length and material is varied. Figure 1 gives the construction of these cells in detail.

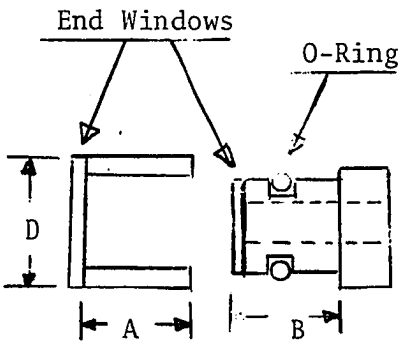

	CELL #1	CELL #2
A	9.880 mm	7.86 mm
B	8.915	7.52
1 = A-B	0.965	0.34
D	20.3	20.3
MAT'L.	Alumn. body & Brass plug	Plexiglass

Figure 1. Cells used in measuring the Faraday rotation.

These cells were also used to calibrate the magnetic field H at the position of the cells. The rotation of water was measured and then H calculated by using the known Verdet constant of water. Table 1 gives the magnetic field calibration used in this chapter.

Table 1. Magnet Current "I" and Field

I(AMPS.)	(KILOGAUSS)
2.0	1.20
5.0	2.85
9.0	5.00
14.0	7.20
22.0	10.10

Commercially available[9] interference filters were used to obtain a monochromatic beam. They have the advantage of a large transmission coefficient. This is important since the samples are highly absorbing at the shorter wavelengths. The large size of the filters allows use of a large cross section beam which insures stability of the output V_o to small vibrations or displacements of the polarizer head. The peak wavelengths λ_o of the filters used are listed below in Table 2.

The electronics of the instrument are relatively simple. The voltage difference across the resistors R is fed into a Houston Instrument Corporation DC amplifier. The main purpose of this amplifier is to match the impedance of resistors R(100 kΩ) to the input impedance resistance (10 kΩ) of the XY recorder. The voltage gain is about 10. Additional gain control is provided by the recorder input.

Table 2. Summary of Data for Interference Filters Used.

λ_o	$1/\lambda_o$	Peak Trans
800 mμ	12,500 cm^{-1}	46 %
685 mμ	14,600 cm^{-1}	40 %
661 mμ	15,100 cm^{-1}	42 %
585 mμ	17,100 cm^{-1}	47 %
546 mμ	18,300 cm^{-1}	58 %
515 mμ	19,400 cm^{-1}	42 %
478 mμ	20,900 cm^{-1}	48 %
436 mμ	22,950 cm^{-1}	44 %
400 mμ	25,000 cm^{-1}	40 %
368 mμ	27,400 cm^{-1}	32 %

The light intensity was adjusted so as to produce a 5 microamp current in the PMT's output. For highly transmitting samples the current was as high as 8 microamp using the 661 millimicron filter. It is better to operate under similar conditions. There exists a small coupling between the magnetic field and the PMT's even though magnetic shielding material is used on the PMT's. This manifests itself by a small change in V_o. Its effect is always less than that due to 5 per cent of the observed rotation. Actually, since the FR rotation due to the solute is always obtained by taking the difference between the FR observed for the solution and that observed for the solvent these effects on the PMT tend to subtract out. This also applies to the rotation caused by the windows.

When the magnetic field is calibrated by measuring the FR for the sodium D-lines we subtract the rotation by the empty cell from the rotation of the water filled cell. The FR of air is negligible in our experiments.

In the measurements of $CoSO_4 \cdot 7H_2O$ the large solute concentration used required some correction. Here the solvent molecules are displaced by the solute.

Theory

Recently a quite general theory for predicting the magnitude of the FR has been proposed by Buckingham and Stephens.[10] This theory can be shown to explain from basic quantum mechanical considerations all of the results obtained by previous experiments. It also encompasses the earlier theories of Kramers, Rosenfeld, and Serber. The most

significant advance of this theory is that optical absorption is taken into account whereas all the earlier theories were strictly valid only for wavelengths far removed from the wavelength corresponding to an absorption maximum.

All of the SFO's have a large optical absorption and correspondingly large extinction coefficients in the visible and UV. Thus it is to be expected that the theory of Buckingham and Stephens should afford a good comparison to my experimental data. Since the complete derivation of the theoretical expressions for the FR are given by the references above, only their results will be given here.

It is shown that the rotation per unit length can be written as Θ where

$$\Theta = \sum_{a,j} \Theta(a \rightarrow j) \ , \tag{2}$$

where $\Theta(a \rightarrow j)$ is the contribution to the total rotation by transitions from the lower electronic state "a" to the upper state "j".

The expressions for $\Theta(a \rightarrow j)$ depend on the relative magnitudes of the circular frequency ω of the incident light, the resonant frequency ω_{ja}, the absorption band half width Γ_{ja}, the Boltzmann energy kT, and the Zeeman splitting $\omega_{ja}^{(1)}H$. However, the form of $\Theta(a \rightarrow j)$ that is applicable to the samples studied can be written as[11]

$$\begin{aligned}\Theta(a \rightarrow j) = + \frac{4\pi N_o}{\hbar c} \ & [f_1(\omega,\omega_{ja})A(a \rightarrow j) + f_2(\omega,\omega_{ja})B(a \rightarrow j)]H \\ & + [f_1(\omega,\omega_{ja})Q_\alpha^{(o)}\tanh(g\mu_B H/2kT)] \ X \ \frac{\exp(-E_a^{(o)}/kT)}{\Sigma_a \exp(-E_a^{(o)}/kT)} \ ,\end{aligned} \tag{3}$$

where

N_o is the number of molecules /cm^3,

$E_a^{(o)}$ is the energy of the state "a" at H = 0, such that the ground state corresponds to E = 0,

$$f_1 = \frac{2\omega_{ja}\omega^2[(\omega_{ja}^2 - \omega^2)^2 - \omega^2\Gamma_{ja}^2]}{\hbar[(\omega_{ja}^2 - \omega^2)^2 + \omega^2\Gamma_{ja}^2]^2} \quad , \tag{4}$$

$$f_2 = \frac{\omega^2(\omega_{ja}^2 - \omega^2)}{(\omega_{ja}^2 - \omega^2) + \omega^2\Gamma_{ja}^2} \quad , \tag{5}$$

$$A(a \to j) = [(\mu_z)_{jj} - (\mu_z)_{aa}] \ \mathrm{Im}\{(m_x)_{aj}(m_y)_{ja}\} \ , \tag{6}$$

$$B(a \to j) = \mathrm{Im}\left\{ \sum_{k \neq a} \frac{(\mu_z)_{ka}}{\hbar\omega_{ka}} [(m_x)_{aj}(m_y)_{jk} - (m_y)_{aj}(m_x)_{jk}] + \right. \tag{7}$$

$$\left. + \sum_{k \neq j} \frac{(\mu_z)_{jk}}{\hbar\omega_{kj}} [(m_x)_{aj}(m_y)_{ka} - (m_y)_{aj}(m_x)_{ka}] \right\} \ ,$$

$$Q_\alpha^{(o)} = \mathrm{Im}\{(m_x)_{aj}(m_y)_{ja}\} \ . \tag{8}$$

Here m_x and m_y are the electric dipole moment operators along the x and y directions respectively, while μ_z is the magnetic moment operator along the z axis, H is taken along the z-axis. All matrix elements

are to be evaluated using the wavefunctions at H = 0 and all ω_{ja}, Γ_{ja} are to be taken likewise.

When $g\mu_B H/kT \ll 1$ then

$$Q_\alpha^{(o)} \tanh \frac{g\mu_B H}{2kT} \simeq (\mu_z)_{aa} \mathrm{Im}\{(m_x)_{aj}(m_y)_{ja}\} \equiv \frac{C(a \to j)}{kT} . \qquad (9)$$

The A and C terms have been called the "diamagnetic" and "paramagnetic" terms because of their analogy to terms occurring in magnetic susceptibility measurements.

The A term which is always linear in H arises from the small frequency shifts of the absorption frequencies ω_{ja} due to Zeeman splitting. The B terms are caused by changes in the transition probabilities due to the external field H. Finally the C terms are related to changes of the populations of the ground states induced by the Zeeman splitting. Thus if one can decompose the FR spectra into these A, B, and C terms, then the magnitude of each can give the relative importance of the mechanisms giving rise to the A, B, and C terms. For instance, ionic solutions of the salts of the iron group elements have large A terms but the B and C terms are considerably smaller.[12]

For an atomic state characterized by a total angular momentum J the A term has the Brillouin function dependence on the field H. This was found to be important in studies of the FR at low temperature and/or high fields.[13]

In the study of the SFO's we have encountered the unique case that the C terms are large and of comparable magnitude to the A terms. There exists a component of the FR for the SFO's that tends to "saturate" at the fields used. And this occurs for the SFO's in water solution and at room temperature!

MORD for $Co(SO)_4 \cdot 7H_2O$

We have made measurements of the FR for nine different SFO's and for $CoSO_4 \cdot 7H_2O$. The experimental results are depicted as FR in degrees per cm per concentration of iron (gm per liter) versus either the magnetic field or the wavenumber. These curves are fitted with the functions given above in Eqs. (2) through (9).

To check the method and fitting procedure to be used we initially started with a solution of $CoSO_4 \cdot 7H_2O$ in water. Its optical absorption has been shown to be due to the cobaltous ion, or possibly to $[Co(H_2O)_6]^{2+}$ as stated by Jörgenson.[14] The positions of the absorption peaks λ_o and the widths at half height Γ are given by Jörgenson, viz.,

$$(\lambda_o)_1 = 21{,}500 \text{ cm}^{-1}. \qquad \Gamma_1 = 2{,}250 \text{ cm}^{-1}.$$

$$(\lambda_o)_2 \doteq 19{,}400 \text{ cm}^{-1}. \qquad \Gamma_2 = 2{,}250 \text{ cm}^{-1}.$$

These parameters were used by Jörgenson to fit the optical absorption spectra.

Using the methods given in sections 2 and 3 of this chapter we measured the FR of the $CoSO_4$. It was indeed linear with H within experimental error. Thereafter we fitted the experimental data using the $f_1(\omega,\omega_{ja})$ and $f_2(\omega,\omega_{ja})$ functions of Eqs. (4) and (5).

A first order fit was obtained by assuming that the FR is the sum of f_1 and f_2 terms centered about 19,500 cm^{-1}, with a width of 2,000 cm^{-1}. The equation fitting the experimental data then is

$$[\Theta/\ell C]_{CoSO_4\cdot 7H_2O} = [(1.5\times10^{-15}\ \hbar)f_1(19.5,2.0) + 3.8\times10^{-2}\ f_2(19.5,2.0)]H \qquad (10)$$

with H in kilogauss. The shapes of f_1 and f_2 are shown in Fig. 2. These functions are used throughout this next section.

In Eq. (10) it is to be understood that the functions f_1 and f_2 are to be calculated using the circular frequency $\omega = 2\Pi\nu = 2\pi c\bar{\nu}$. The two numbers in the brackets of f_1 and f_2 signify the center $\bar{\nu}_o$ and half width Γ of the frequency functions. These units are $\bar{\nu}_o\ (cm^{-1})\times10^{-3}$ and $\Gamma(cm^{-1})\times10^{-3}$. Figure 2 shows both these functions and their sum plotted as a function of $\bar{\nu}$, as well as the experimental data. It is seen that the "fit" is within experimental error for frequencies below 20,000 cm^{-1}. Above 20,000 cm^{-1}, the fit can be considerably improved by using two frequency functions.

Several things can be pointed out with regard to Fig. 2. First the FR of Co(2+) is so small that very concentrated solutions were required. Therefore, the FR results had to be corrected for displacement

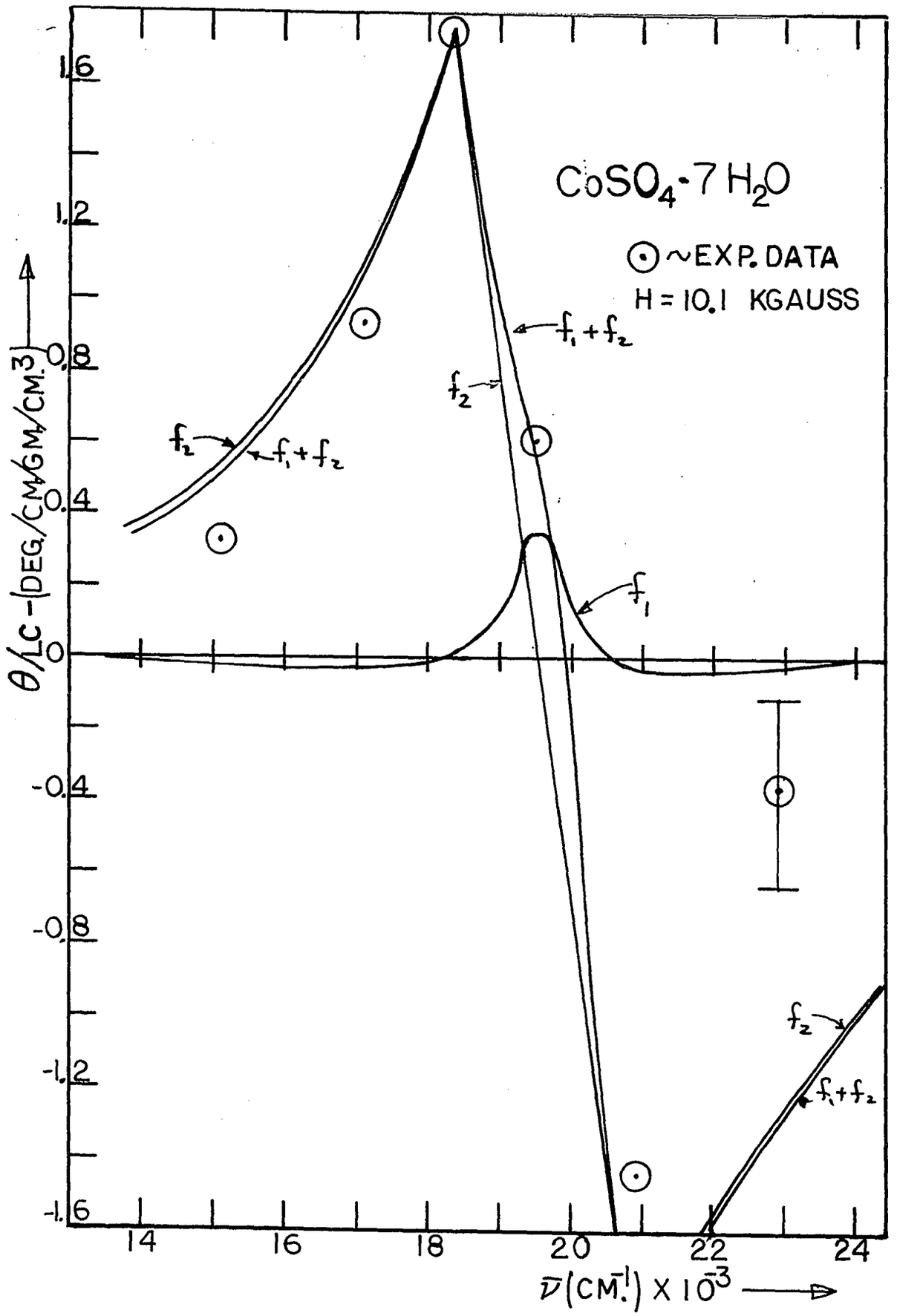

Figure 2. MORD for $CoSO_4 \cdot 7H_2O$

of the solvent (H_2O) molecules by the Co(2+) and SO_4(2-). This was done by means of the formula

$$\Theta_{Co(2+)SO_4(2-)\cdot 7H_2O} = \Theta_s - \left(\frac{d_s - C}{d_o}\right)\Theta_o \,, \qquad (11)$$

where Θ_s is the observed rotation of the solution, Θ_o is the rotation of water and d_s, d_o are the densities of the solution and solvent resp. C is the solute concentration. In this particular experiment, the value of $[(d_s - C)/d_o] = 0.81$.

Next it should be pointed out that the relatively large experimental error in $\Theta/\ell C$ corresponds to an error in the angle of only ±0.005!

The coefficients of f_1 and f_2 in Eq. (10) are a measure of the magnitude of the A and C terms. Their relative importance is not readily apparent because the units of f_1 and f_2 are not the same. Whereas f_2 is dimensionless, f_1 has the units of $(\omega^{-1}/\hbar)$. This can be checked with Eqs. (4) and (5). From Fig. 2 one can see that the contribution to the FR of Co(2+) by the A term is almost negligible, except near 19,500 cm^{-1}. The rotation is normalized to the number of grams of $CoSO_4\cdot 7H_2O$ even though the total rotation near resonance is due mostly to the cobalt.[15]

Now the SFO's shall be discussed. Similar to $Co(SO_4)\cdot 7H_2O$, the SFO's are measured in aqueous solution at a temperature of 23±2 °C. The FR is normalized to the iron content in gm/liter while the results are again displayed as two separate plots. First is a plot of the

normalized rotation ($\Theta/\ell C$) in degrees per cm per gram iron per liter versus the magnetic field strength H in gauss and second is a plot of the normalized rotation $\Theta/\ell C$ versus the frequency $\bar{\nu}$ in wavenumbers.

Discussion of SFO #5

In this section two fractions of SFO #5 will be discussed. This sample was obtained from Poly-Meros Co.. The sample was fractionated by means of a Sephadex column.[16] A high fraction SFO #5C-1 and a low fraction SFO #5B-6 were chosen. The iron content is 45.2 per cent and 4.6 per cent by mass respectively.

Some of the experimental data obtained is shown in Figs. 3 through 6. Evidently, the magnetic field dependence is not linear. In fact, it can be seen that the data reveals a partial "saturation" with field. Superimposed on this saturation is a linear dependence which dominates at higher fields.

The theory outlined above does encompass this type FR but it is possible, that this is the first time that this type FR has been observed at room temperatures. With regard to the frequency dependence the theory shows that a saturation type rotation has the shape of $f_2(\omega,\omega_{ja})$ whereas the linear term can have either an $f_1(\omega,\omega_{ja})$ or an $f_2(\omega,\omega_{ja})$ dependence. The total FR is of course the sum of these functions along with their particular H dependence.

For SFO 5C-1 the absorption spectra show the strong UV absorption as well as two lesser absorption band maxima closer to the visible. They are centered as $22{,}500\pm1{,}000$ cm^{-1}, and $32{,}000\pm2{,}000$ cm^{-1}. The experimental data were fitted by using four functions centered around

these wavenumbers. The procedure is just like that in section "MORD for $Co(SO)_4 \cdot 7H_2O$" except that more functions are used while we must also produce a non-linear field dependence.

The equation describing a best fit to the experimental data is

$$[\theta/\ell C]_{5C-1} = [-\ (3.9\times10^{-14}\ \hbar) f_1(23,3.4) - (5.6\times10^{-12}\ \hbar) f_1(32,10)]H$$
$$+ 0.67\ f_2(23,3.4)\tanh(1.0H) \qquad (12)$$
$$- 16.5\ f_2(32,10)\tanh(0.1H).$$

where H is in kilogauss.

First the experimental points at the highest field are made to fit. As can be seen from Fig. 4 this is usually quite satisfactory. The real test then becomes the fit of the field dependence such as in Fig. 3. It can be seen that this could be improved, however, the fit is commensurate with the experimental error and sample definition in particular. No significant gain in physical information can be expected.

The second fraction of SFO #5 was SFO #5B-6. This is a low fraction with an iron content of only 4.6 per cent. It has absorption maxima at 16,500±1000 cm^{-1}, 22,500±1,000 cm^{-1}, 26,500±1,000 cm^{-1}, and at 32,000±2000cm^{-1}. A reasonable fit to the experimental data could be obtained using again four frequency functions centered at 23,750 cm^{-1} and 30,000 cm^{-1}. Figures 5 and 6 show the field and frequency dependence of the experimental data and fitted curves. The equation used to fit the experimental points is

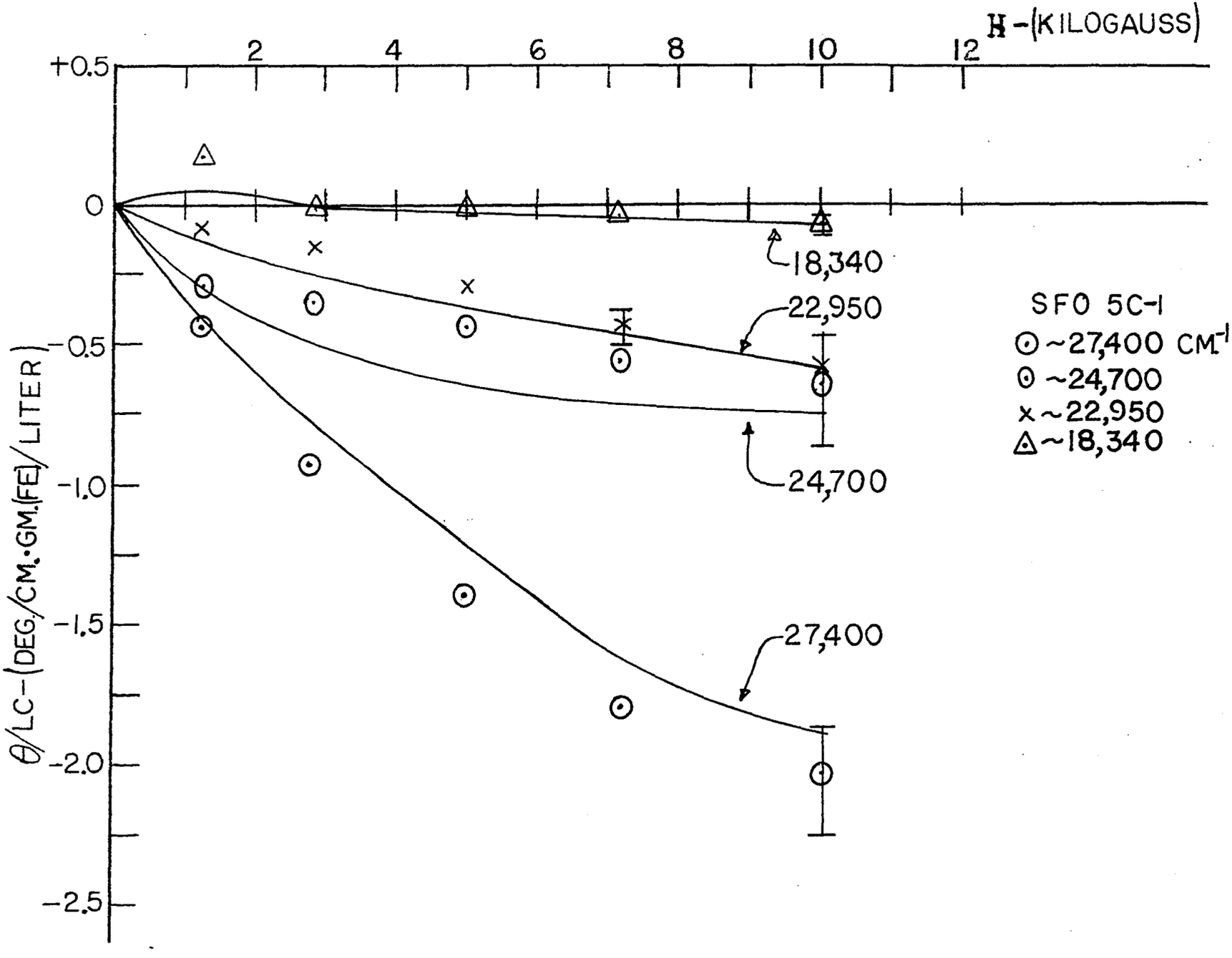

Figure 3. Magnetic field dependence of the FR for SFO #5C-1

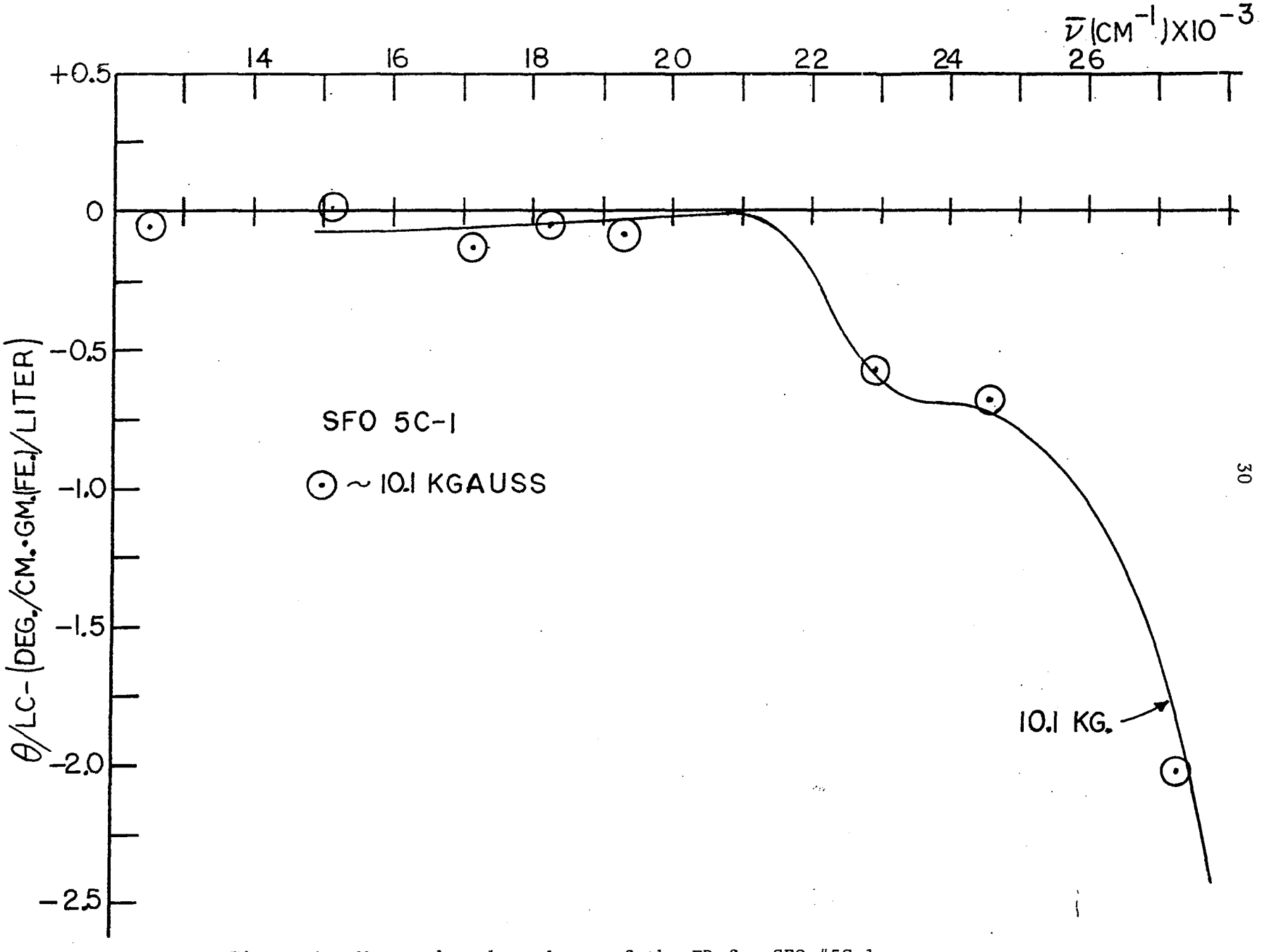

Figure 4. Wavenumber dependence of the FR for SFO #5C-1

$$[\theta/\ell C]_{5B-6} = [(-6.6\times10^{-15}\ \hbar)f_1(23.75,3.0) - (2.9\times10^{-12}\ \hbar)f_1(30,12)]H + [-0.025\ f_2(23.75,3.0) - 0.5\ f_2(32,10)]\tanh(0.4H) \quad (13)$$

where H is again in kilogauss.

Several comments can be made by considering these two samples. First, when the rotation is normalized with the concentration of the iron both rotations are of the same magnitude viz., -1.58 and -2.05 deg./g(Fe)/liter for 5B-6 and 5C-1, respectively, at 27,400 cm^{-1} and H = 10.1 kilogauss. Secondly, two different values of α are needed in Eqs. (12) and (13). The shape of the field dependence necessitates this. It is especially evident for SFO #6A-1 which will be discussed below. A possible explanation is that several different particle sizes are contained in the ferric oxide. Another possibility is that there exists two different crystal structures within the ferric oxides e.g. ferrimagnetic γFe_2O_3 and antiferromagnetic αFe_2O_3. We also note that the shapes of the curves, both the frequency dependence and the field dependence, are quite similar for both SFO's.

Discussion of SFO #6

In this section the high fraction SFO #6A-1 and the lowest fraction SFO #6'-8 will be discussed. SFO #6 was also obtained from Poly-Meros. It has been one of the most interesting samples because of the large effects shown in all the phenomena. Most notable is the value of the magnetic susceptibility χ(6A-1) which is 51,000 cgs/g(Fe).

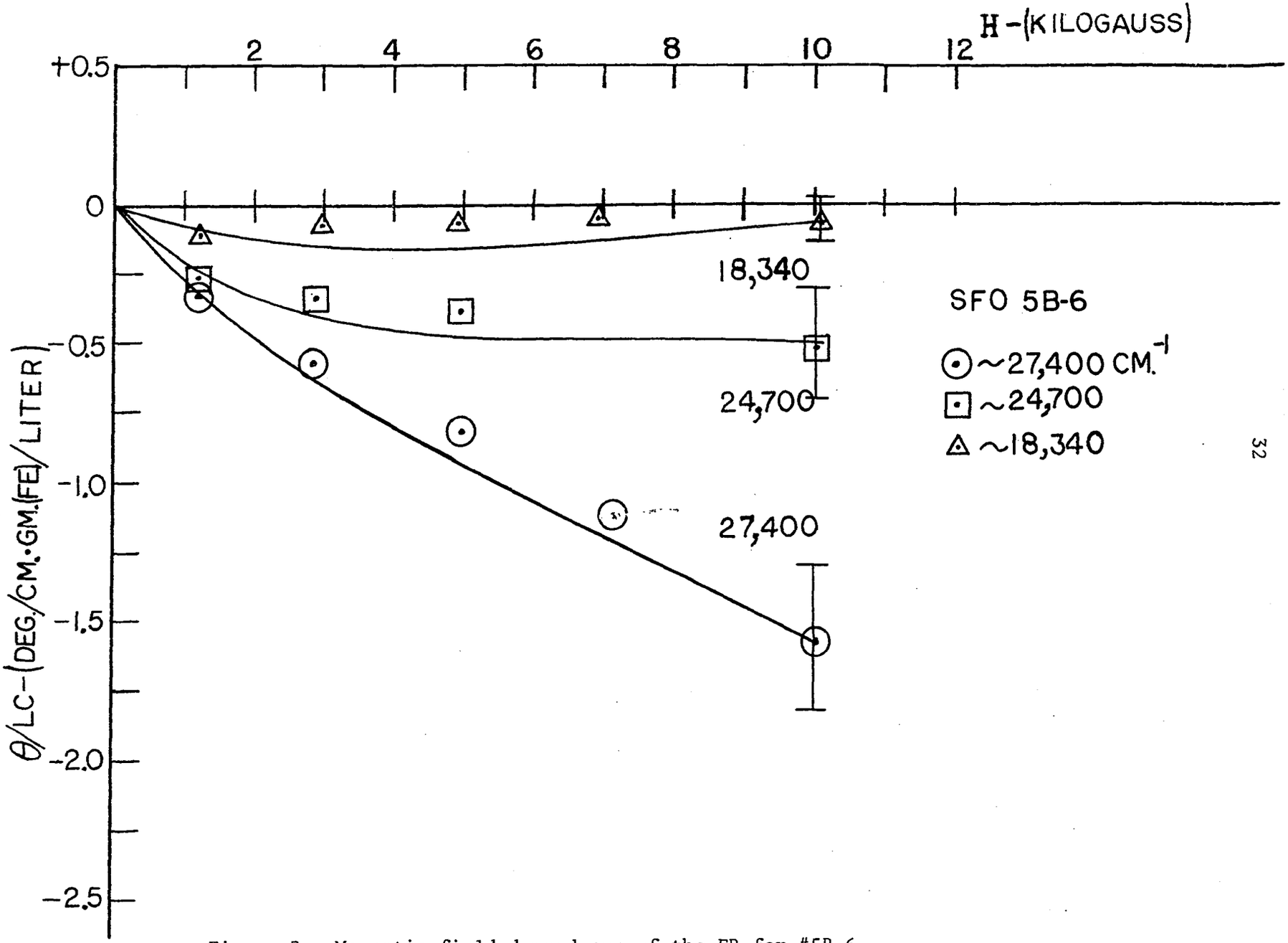

Figure 5. Magnetic field dependence of the FR for #5B-6

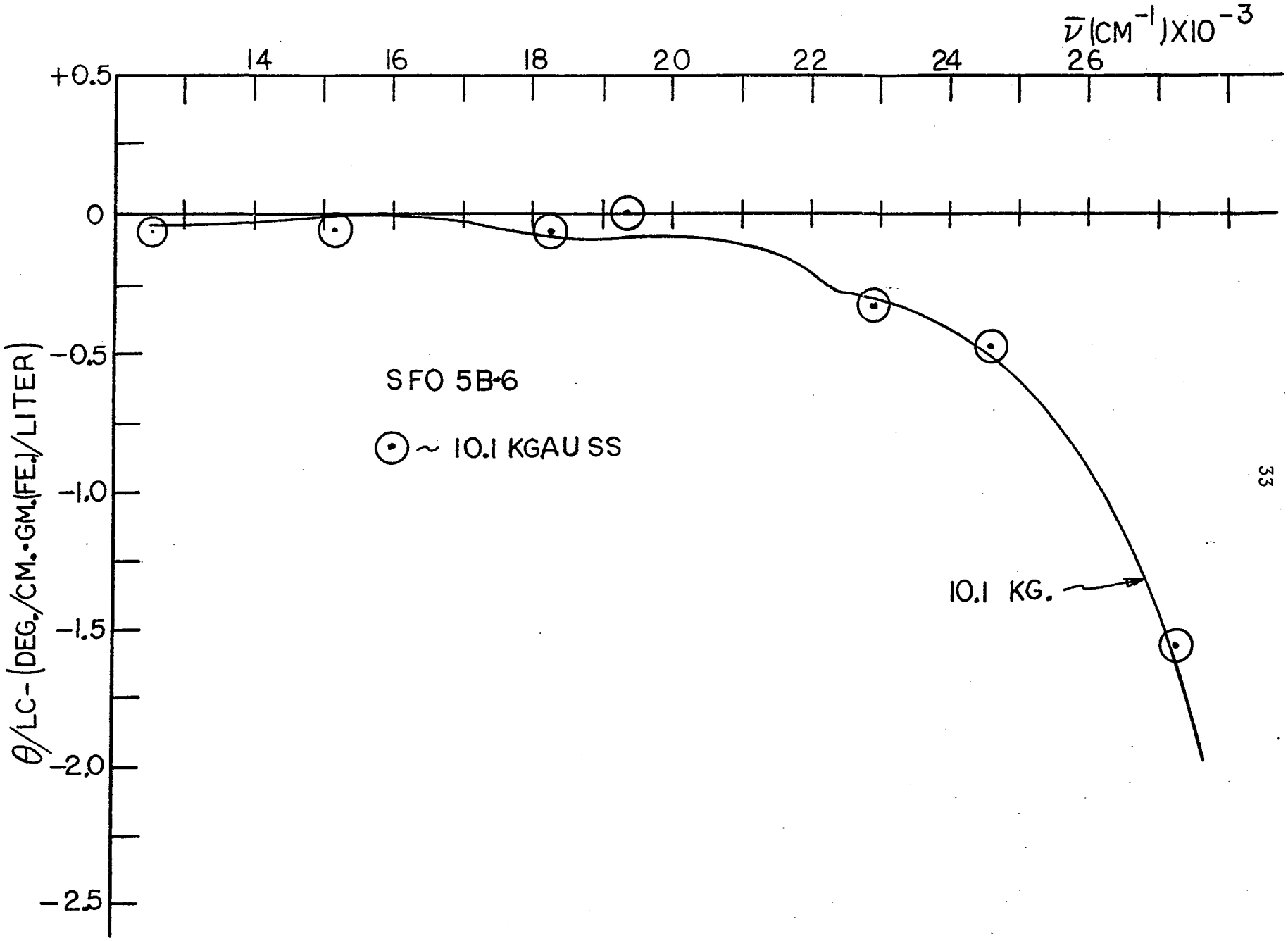

Figure 6. Wavenumber dependence of the FR for SFO #5B-6

Likewise, the largest values of the FR were observed in 6A-1. Inspection of the field dependence of the FR show that a definite saturation occurs. Superposed on this is the linear field dependence.

The field and frequency dependence of SFO #6A-1 has been fitted with eight frequency functions centered at 17,000 cm^{-1}, 22,500 cm^{-1}, 27,400 cm^{-1}, and 32,000 cm^{-1}. These correspond to positions of absorption maxima observed in optical absorption spectra. The equation used to fit the experimental data is

$$\begin{aligned}[\Theta/\ell C]_{6A\text{-}1} = [&-0.125\ f_2(17.0,2.0) - 0.20\ f_2(22.5,2.0) \\ &- 1.1\ f_2(27.4,6.0) - (5.5\times10^{-11}\ \hbar) f_1(32,22)]H \\ &+ [4.8\times10^{-2}\ f_2(22.5,2.0) - 0.5\ f_2(27.4,6.0) \\ &- 2.8\ f_2(32,20)]H + 4.0\ f_2(36,2.0)\tanh(0.2\ H)] \ . \end{aligned} \tag{14}$$

An inspection of the field dependence shows that the data again are to be fitted by the sum of a tanh(αH) term and a term linear in H. Moreover, because the experimental data contain a region between 2 and 7 kilogauss where the slope is zero another tanh(αH) is needed. This should be of opposite sign and of different α. Evidently, different particle sizes occur or different crystal structures or both.

For this particular SFO the linear H dependence is best described with an $f_2(\omega,\omega_{ja})$. This corresponds to the B terms which arise from wave function "mixing" or to changes in the transition probability on applying the field. In all SFO's except SFO #6A-1 and SFO #6'-8, the linear H terms can be adequately described by $f_1(\omega,\omega_{ja})H$.

The lowest fraction SFO #6'-8 has an iron content of 3.15 per cent. Figures 9 and 10 give the frequency and field dependence for this sample. The fitted curves are in good agreement with the experimental data. Both the curve shape and magnitude of the rotation can be reproduced. The equation used is

$$\begin{aligned}[\theta/\ell C]_{6'-8} = [&-0.058\ f_2(27.5,2.0) - (2.4\times10^{-3}\ \hbar) f_1(27.4,2.0) \\ &- (4.2\times10^{-12}\ \hbar) f_1(23.0,2.0)]H \\ &+ 0.055\ f_2(23.0,2.0)\tanh(1.0H) \\ &- 0.1\ f_2(27.4,2.0)\tanh(0.4H) \\ &+ 1.03\ f_2(32,8.0)\tanh(0.2H)\ .\end{aligned} \tag{15}$$

Here six frequency functions are used. Three of these are f_2 type with a $\tanh(\alpha H)$ field dependence. Another f_2 function has a linear dependence and the other two are f_1 functions with a linear dependence on H. Furthermore, three different α's are used here. The ultimate fit can be seen in Fig. 9.

Discussion of SFO #10

SFO #10 was obtained from Poly-Meros and separated by a Sephadex column. One heavy fraction, SFO #10B-2 was measured. Three light fractions were mixed to form SFO #10'-7+8+9. This mixture was of sufficient quantity to determine the FR. It should be understood that some fractions are only available in small quantity.

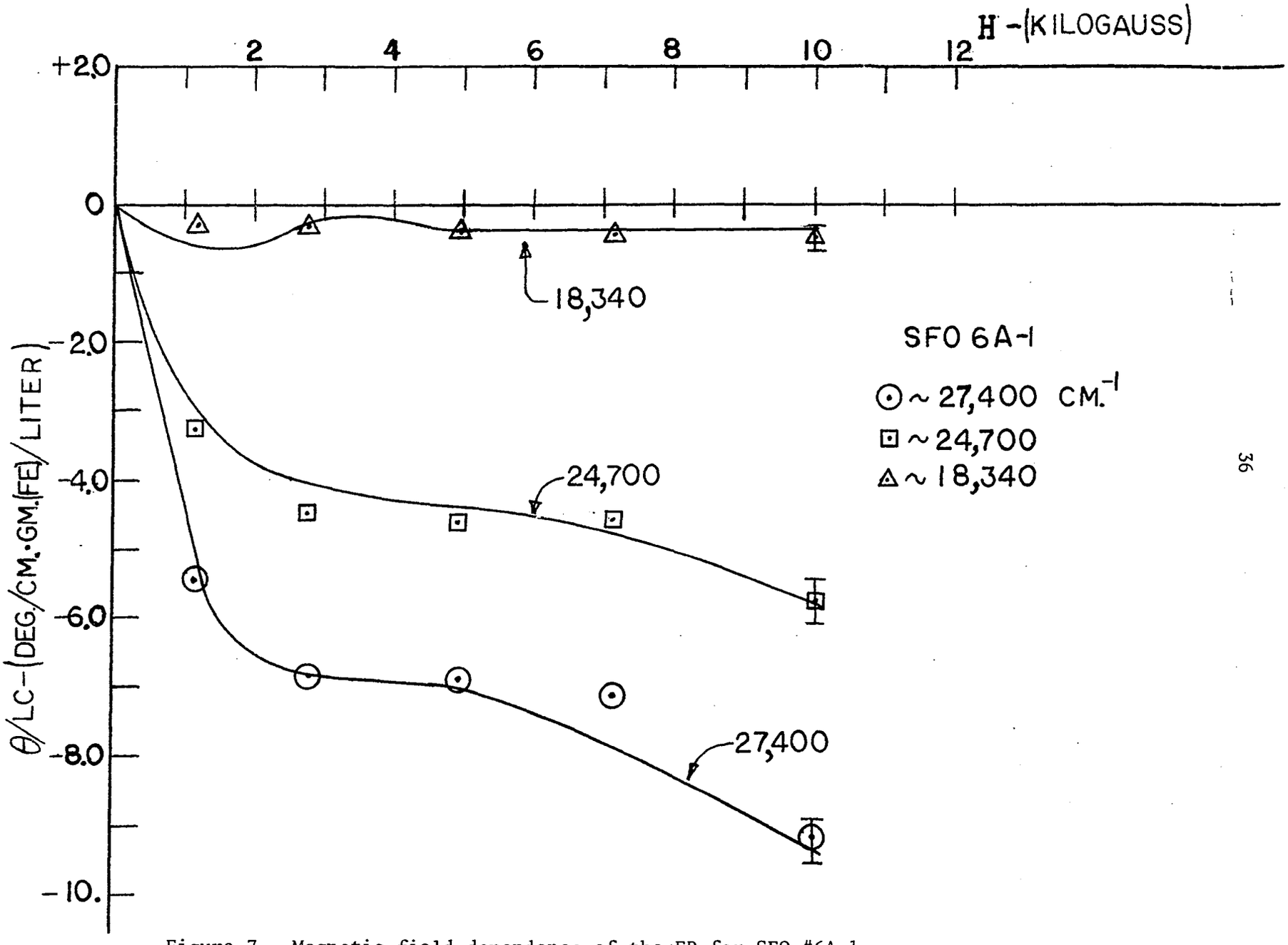

Figure 7. Magnetic field dependence of the FR for SFO #6A-1

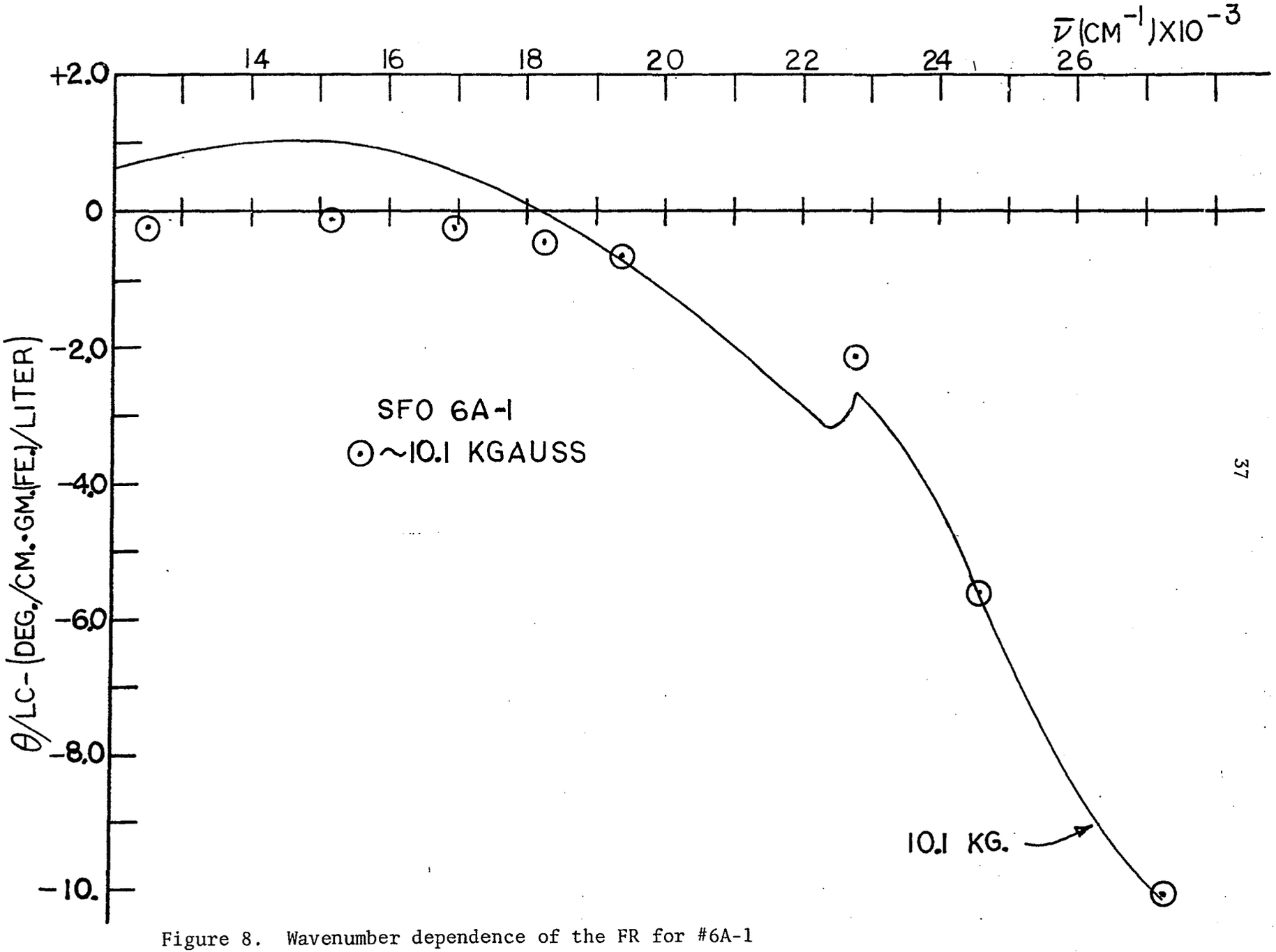

Figure 8. Wavenumber dependence of the FR for #6A-1

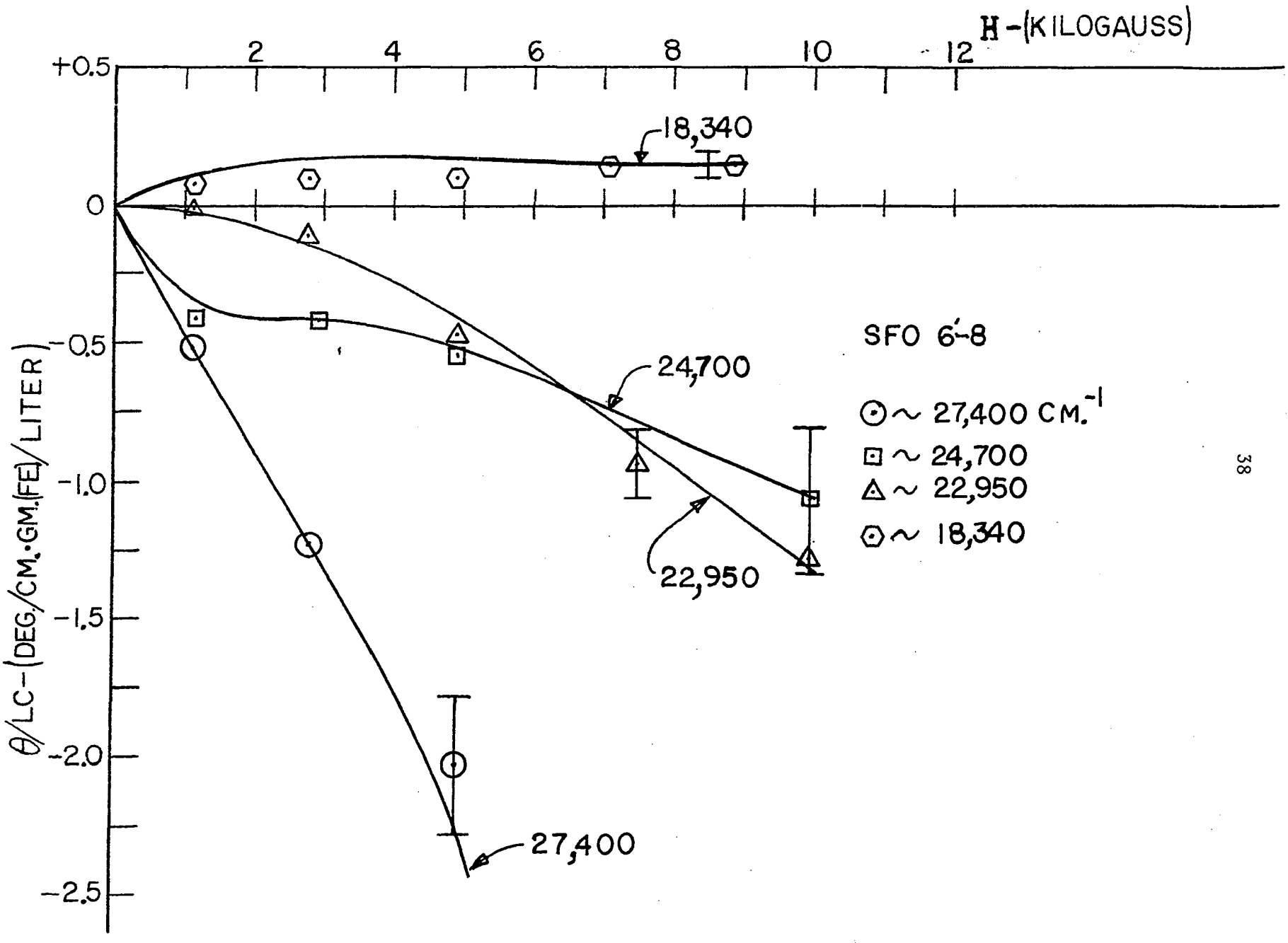

Figure 9. Magnetic field dependence of the FR for SFO #6'-8

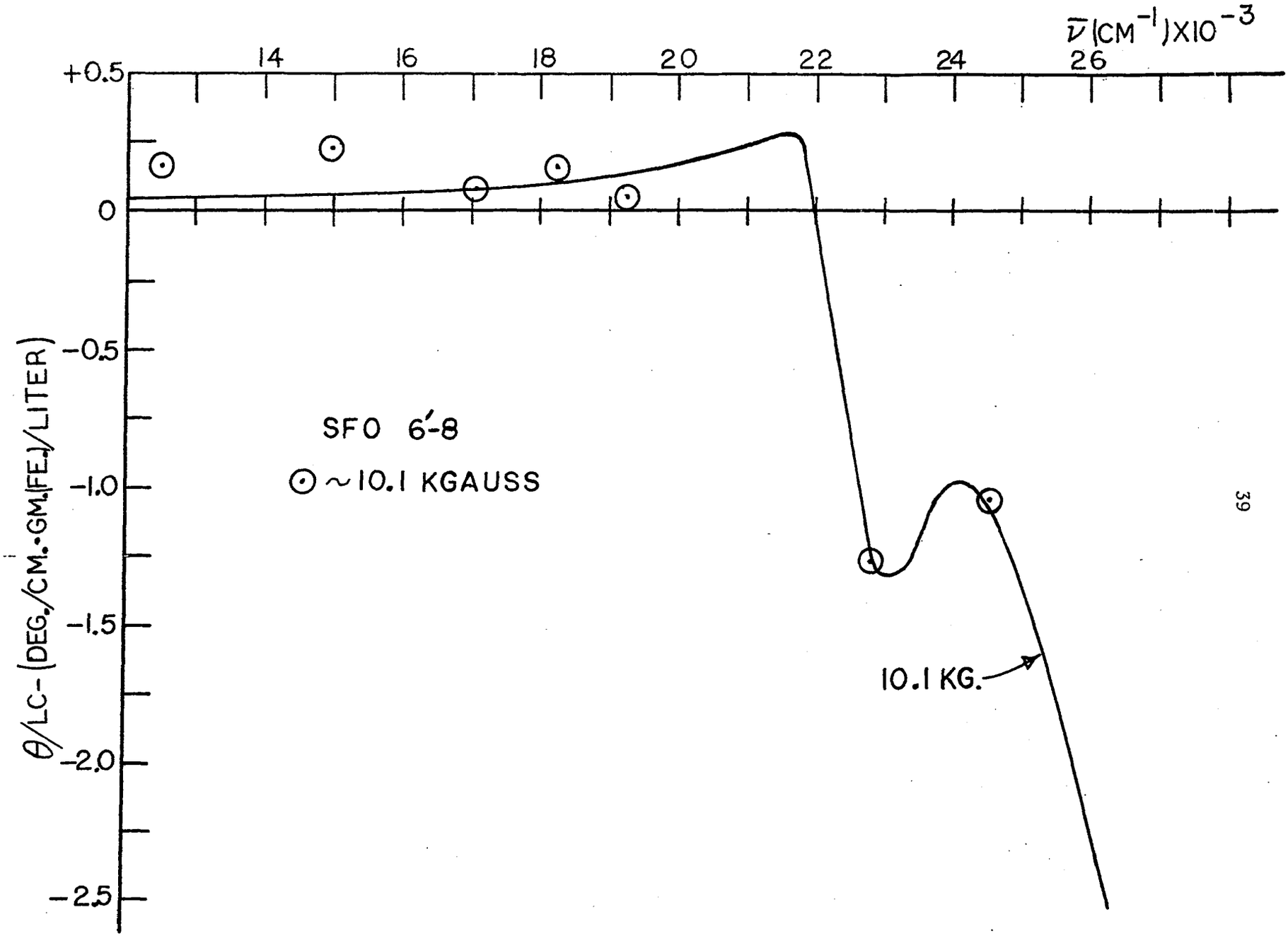

Figure 10. Wavenumber dependence of the FR for SFO #6'-8

SFO #10B-2 has an iron content of 44.8 per cent and an absorption spectra nearly identical to SFO #6A-1. Positions of the absorption maxima are at 22,500±1000cm^{-1}, 26,500±1,000 cm^{-1}, and 32,000±2,000 cm^{-1}.

The rotation data for SFO #10B-2 are similar in shape to those of 6A-1 but the magnitudes are smaller. As Fig. 11 shows the data for 27,400 cm^{-1} show a definite saturation at a value about one third that of 6A-1 at the same frequency. A good fit to the experimental data is obtained by using only four frequency terms. The equation fitting the experimental data is

$$[\Theta/\ell C]_{10B-2} = [-(4.0\times10^{-13}\hbar)f_1(23.75,4.0)-(2.0\times10^{-13}h)f_1(18.5,5.0)]H + 0.5\, f_2(26.5,4.0)\tanh(1.0\ H) - 1.25\, f_2(32,0.9)\tanh(0.5\ H) \quad (16)$$

Inspection of Figs. 11 and 12 show that both the frequency and field dependence are fairly well fitted.

The experimental data for the light fraction was most difficult to fit. This can be seen by comparing the experimental and fitted data for 22,950 cm^{-1} and 27,400 cm^{-1} in Fig. 13. The frequency curve in Fig. 14 on the other hand is an excellent fit.

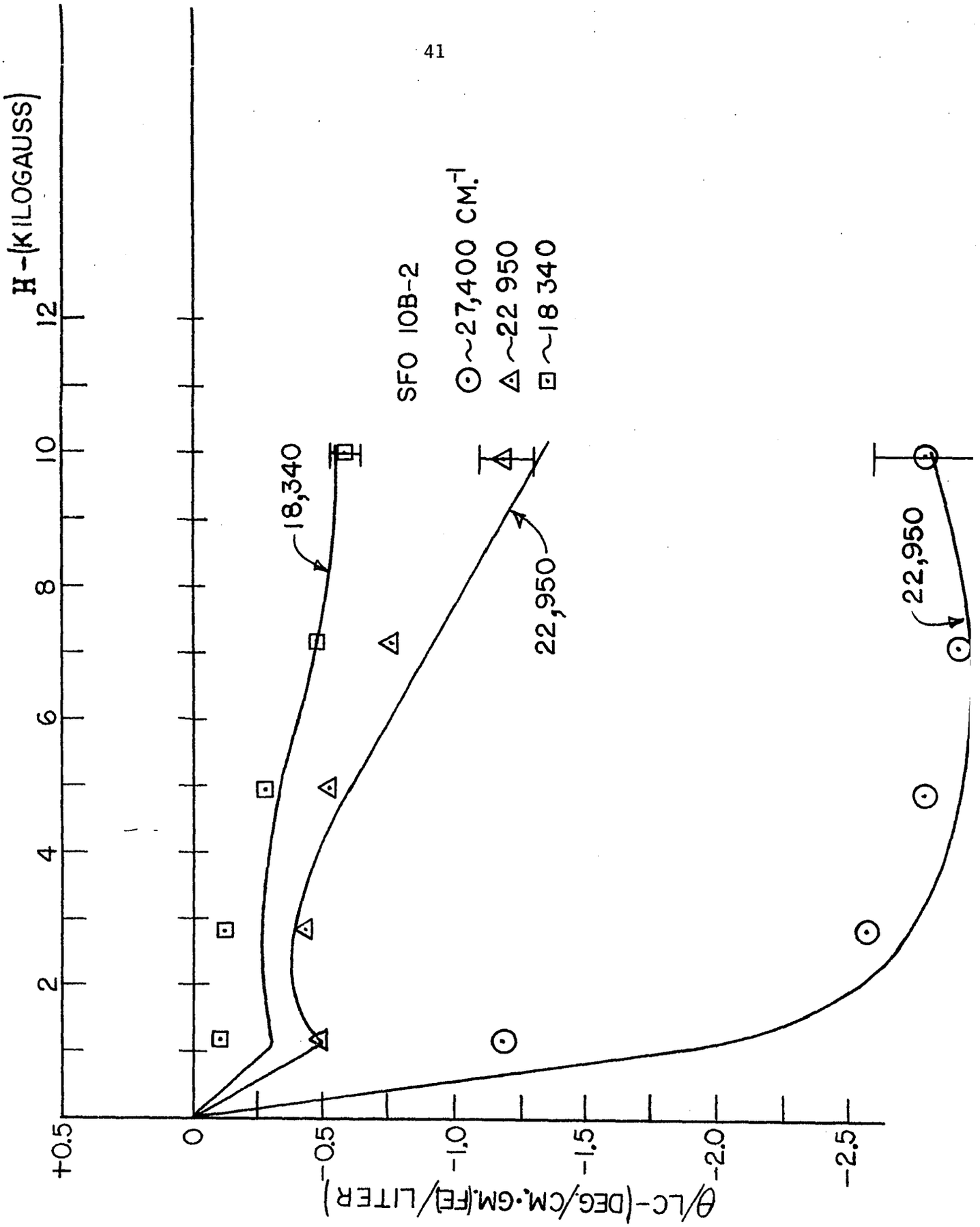

Figure 11. Magnetic field dependence of the FR for SFO #10B-2

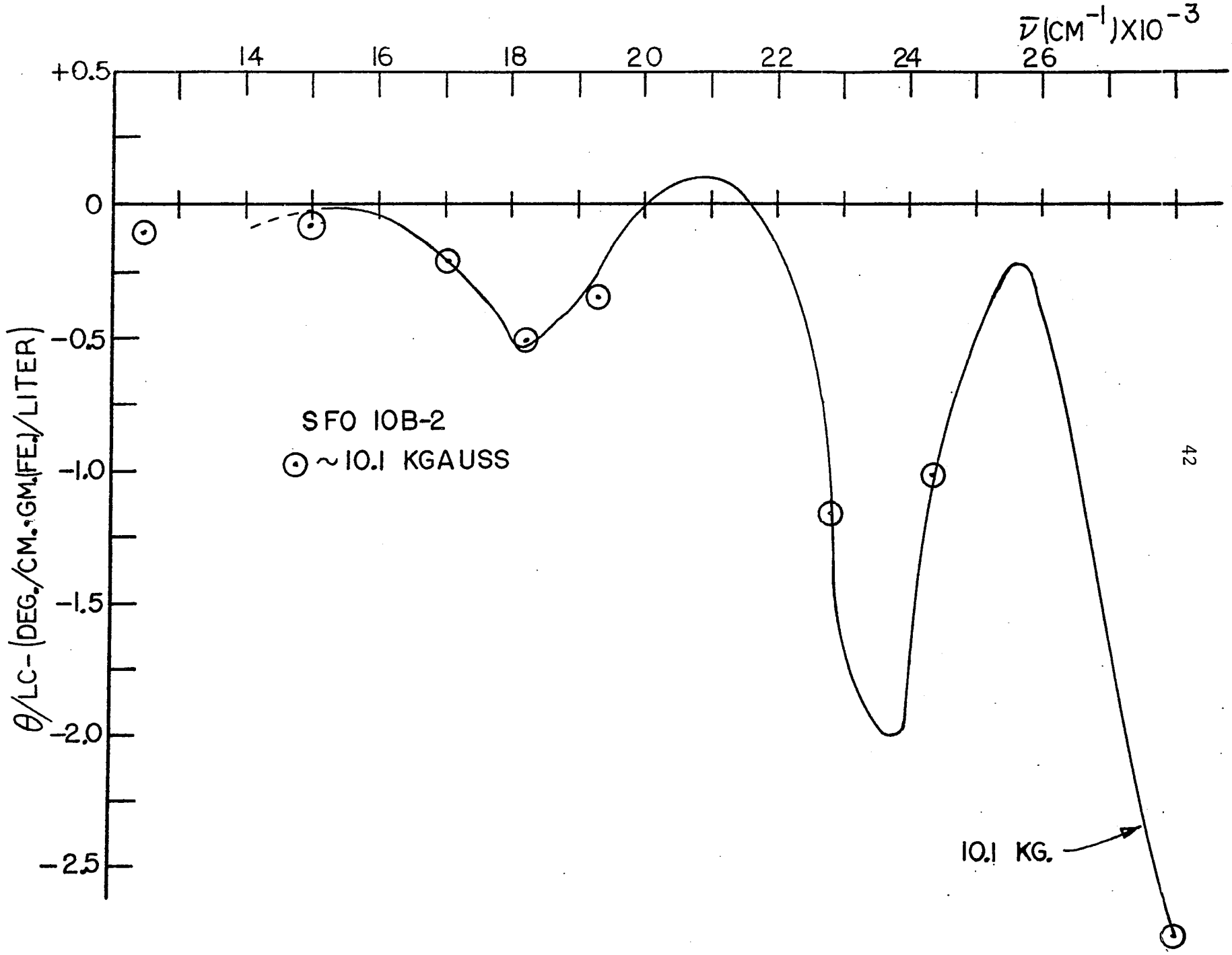

Figure 12. Wavenumber dependence of the FR for SFO #10B-2

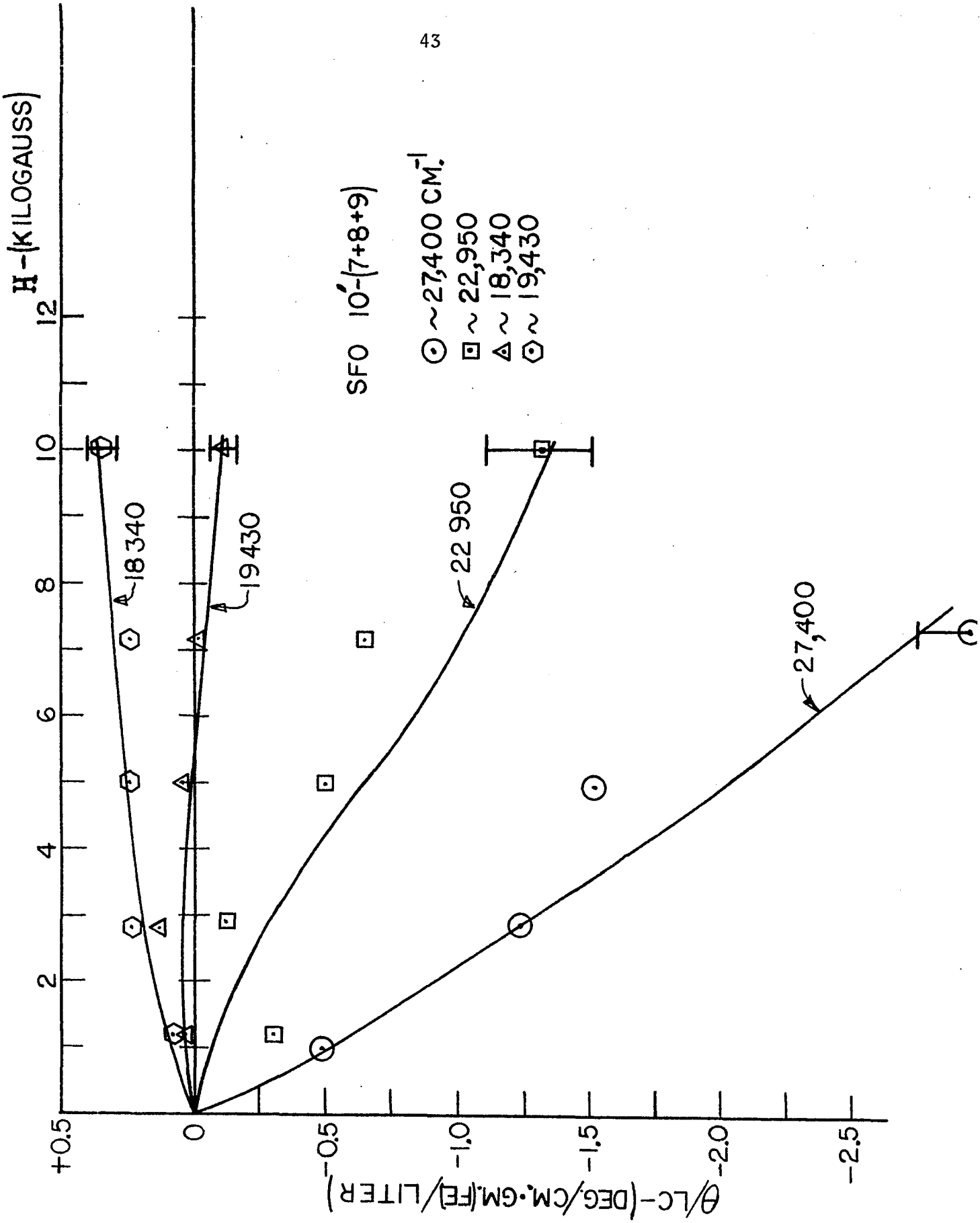

Figure 13. Magnetic field dependence of the FR for SFO #10'-(7+8+9)

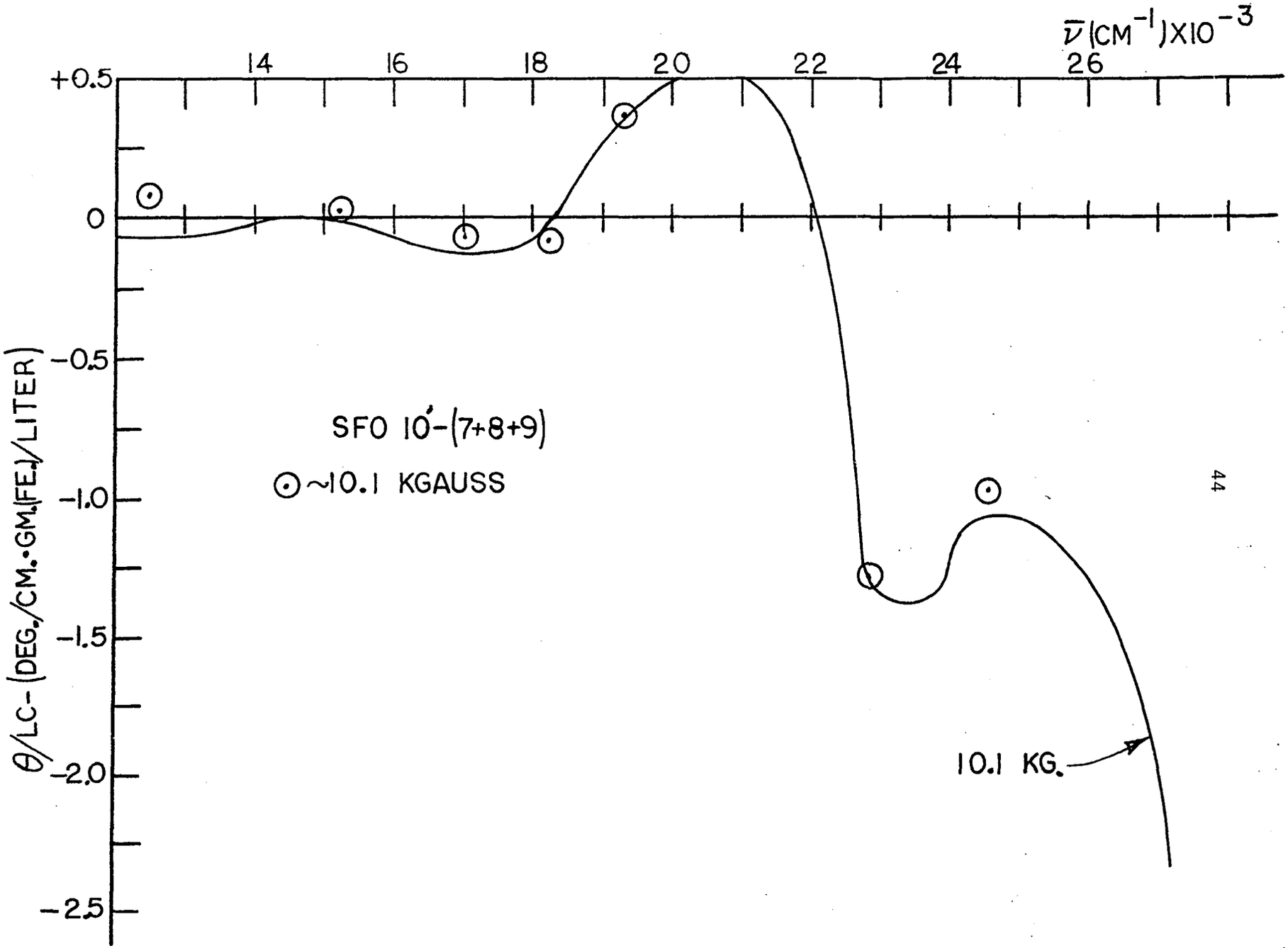

Figure 14. Wavenumber dependence of the FR for SFO #10'-(7+8+9)

The equation used to fit the experimental data is

$$
\begin{aligned}
[\Theta/\ell C]_{10'-7+8+9} = [&-(5.3\times10^{-14}\ \hbar) f_1(17.75,3.25) \\
&- (2.2\times10^{-13}\ \hbar) f_1(23,4.0) \\
&-(3.2\times10^{-13}\ \hbar) f_1(27.5\times4.0)]H \\
&+ [0.37\ f_2(23,4.0)-2.20\ f_2(32,24)]\tanh(0.15H) \\
&+ 0.28\ f_2(27.5,4.0)\tanh(0.3\ H).
\end{aligned}
\tag{17}
$$

Discussion of SFO #11

SFO #11 was obtained from Diamond Laboratories. After fractionation the heavy fraction chosen was 11A-3, having an iron content of 41 per cent. The lightest fraction #11-C chosen has an iron content of 11.2 per cent. They have similar absorption spectra with peak absorptions at 22,500±1000cm^{-1}, 26,500±1000cm^{-1} and 32,000±2,000 cm^{-1}. (In general the commercially successful laboratories produced uniform products.)

Likewise, the FR of these two samples is very similar. Figures 15 through 18 give the field and frequency dependence for these two SFO's.

The equations used to fit the experimental data are

$$
\begin{aligned}
[\Theta/\ell C]_{11A-3} = [&-(3.8\times10^{-14}\ \hbar) f_1(23,2.0) \\
&- (1.3\times10^{-12}\ \hbar) f_1(26.75,6.0)]H - \\
&- 0.33\ f_2(26.75,6.0)\tanh(0.4\ H) \\
&+ 0.44\ f_2(32,4.0)\tanh(0.1\ H)
\end{aligned}
\tag{18}
$$

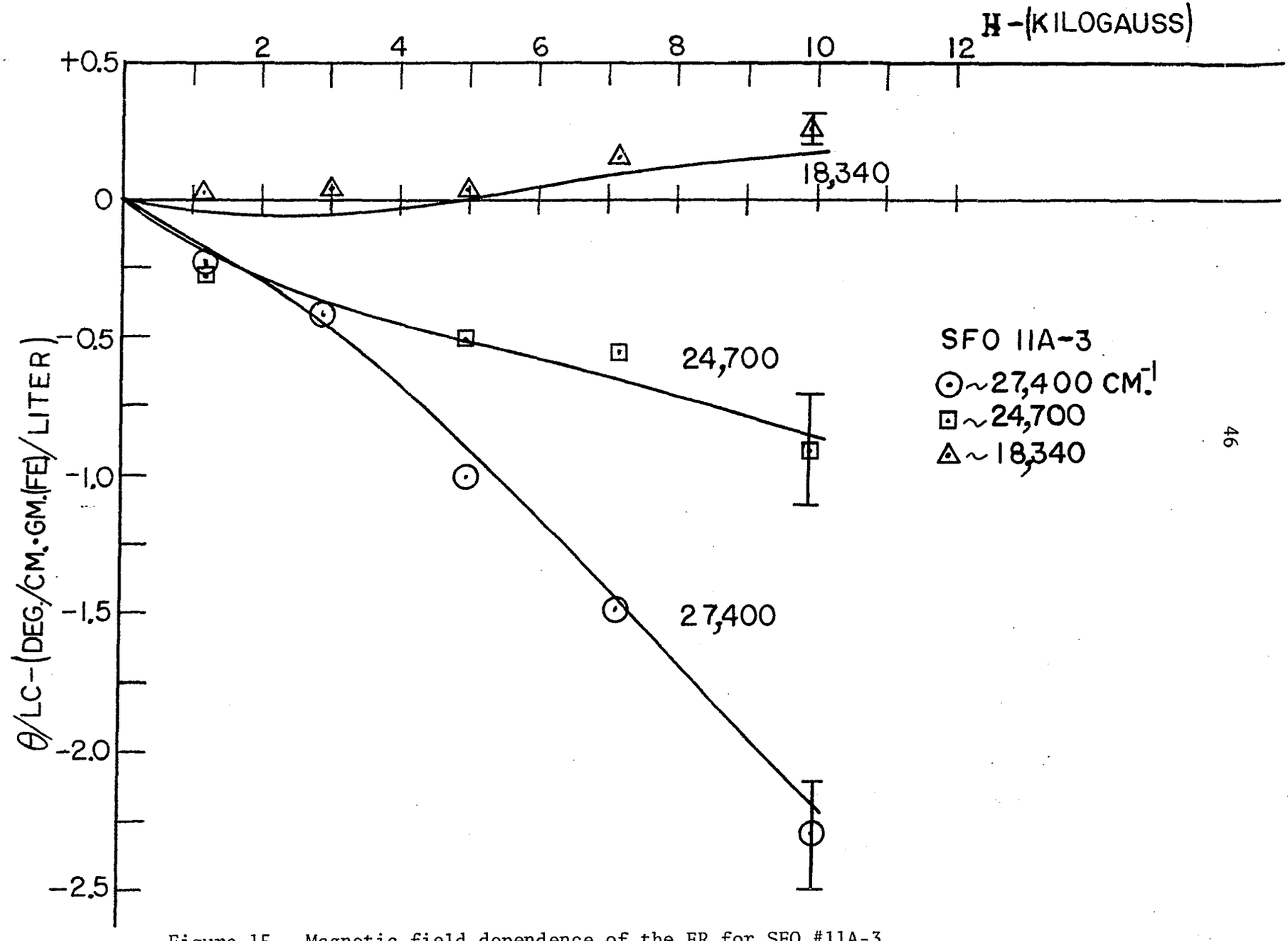

Figure 15. Magnetic field dependence of the FR for SFO #11A-3

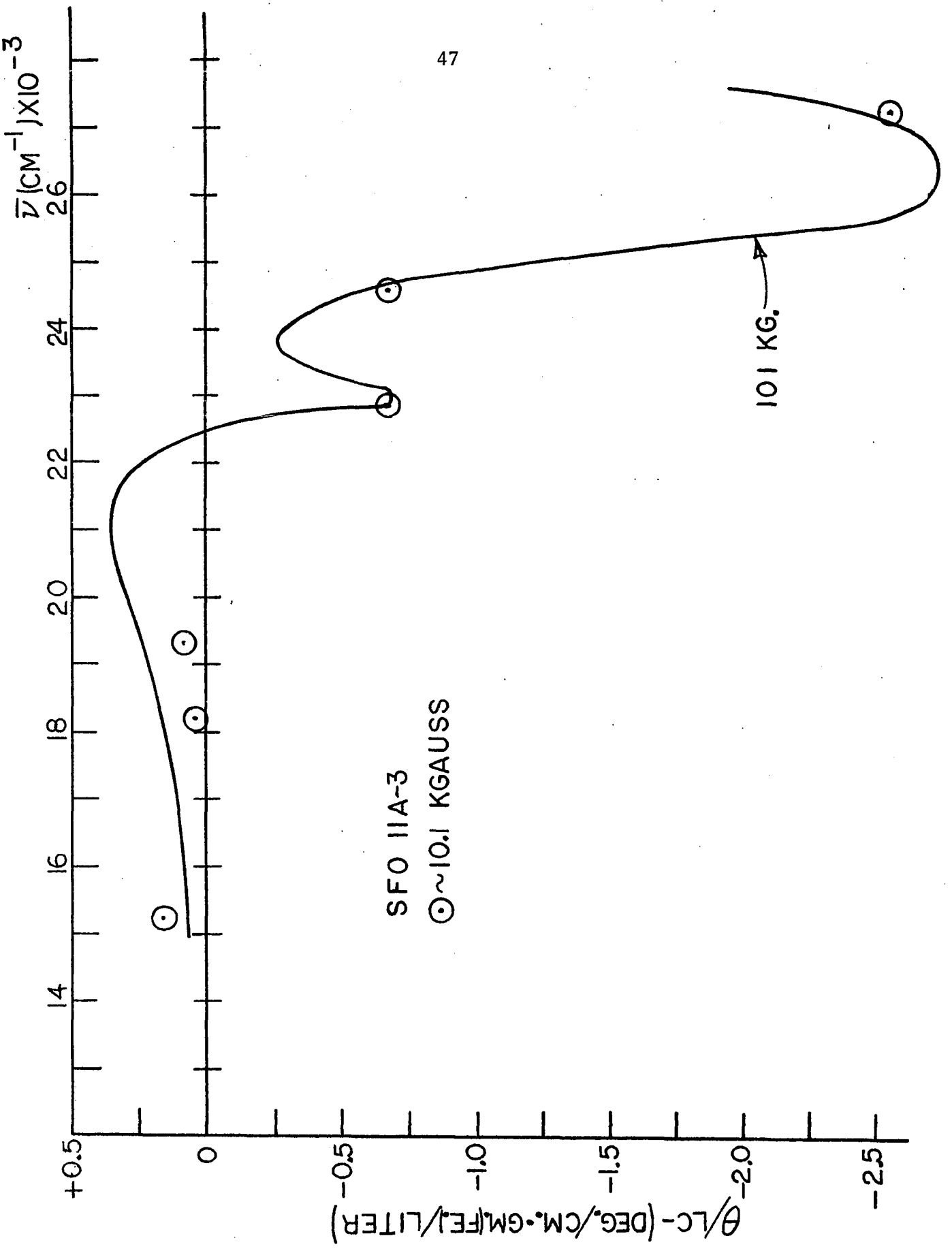

Figure 16. Wavenumber dependence of the FR for SFO #11A-3.

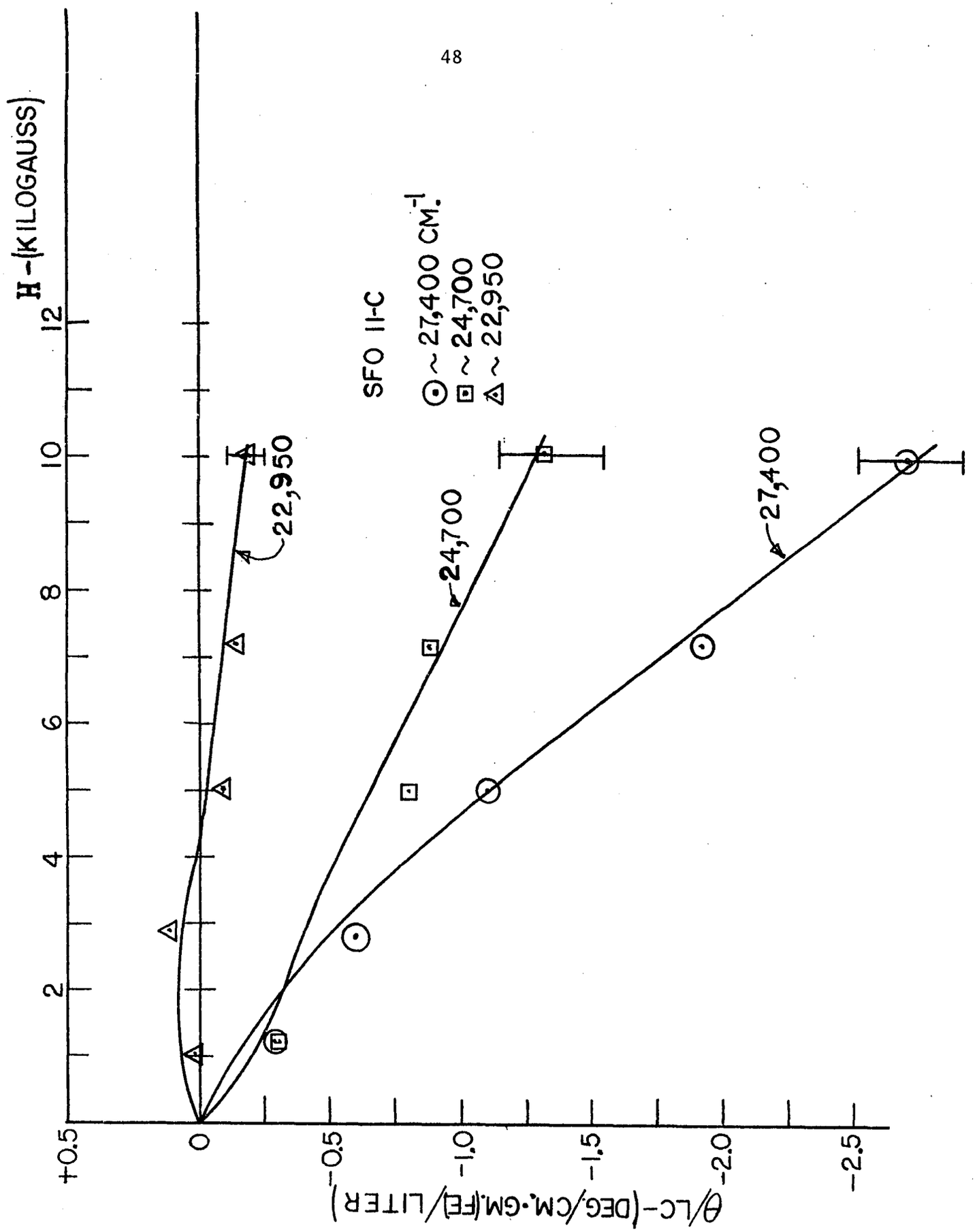

Figure 17. Magnetic field dependence of the FR for SFO #11-C

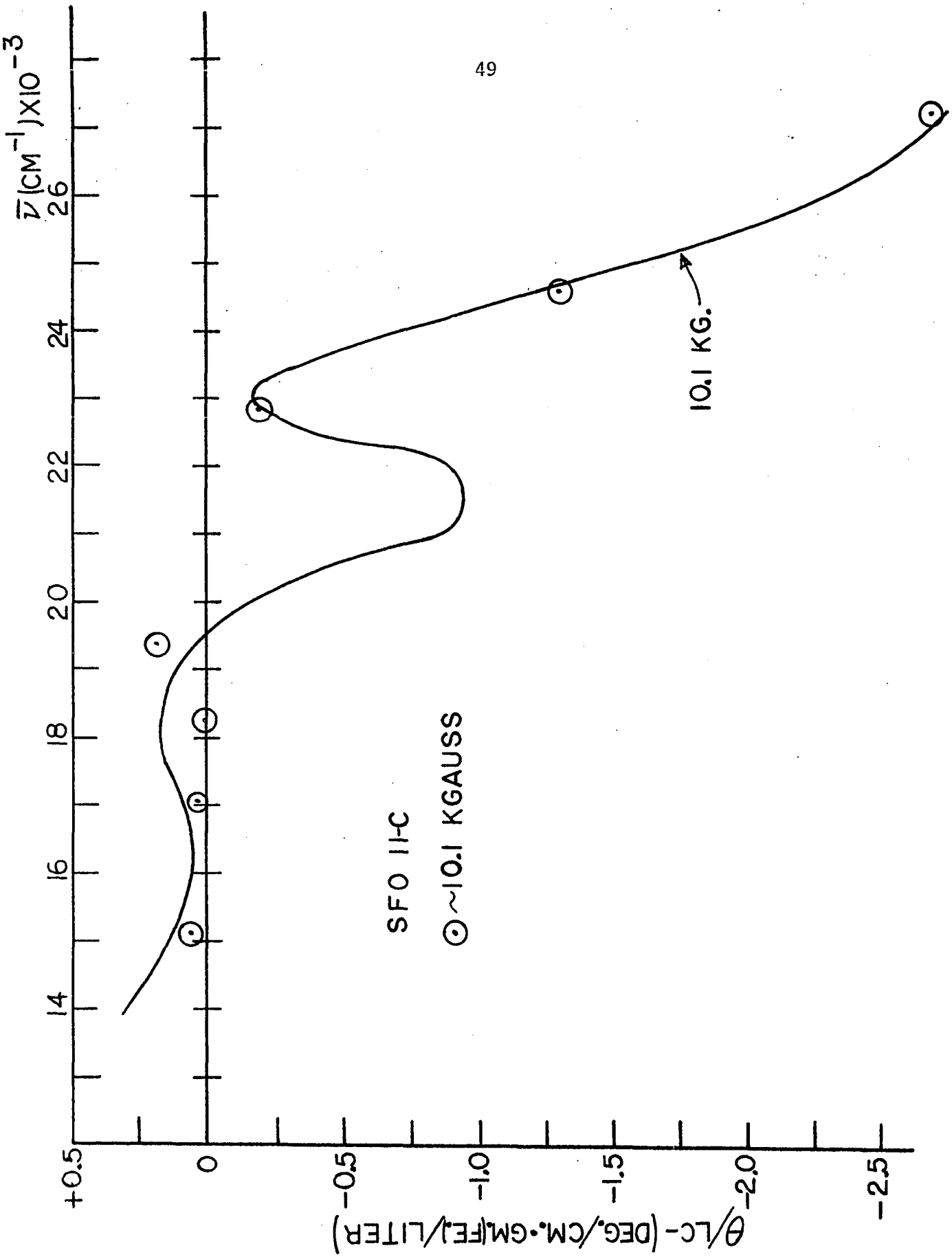

Figure 18. Wavenumber dependence of the FR for SFO #11-C

and

$$[\theta/\ell C]_{11-C} = [-1.5\times10^{-13}\,\hbar)f_1(16.5,4.5) - (2.7\times10^{-11}\,\hbar)f_1(32,24)]H - 0.14\,f_2(22.5,2.0)\tanh(0.35H) - 0.22\,f_2(27,4.5)\tanh(0.3\,H)\,, \tag{19}$$

where H is again in kilogauss.

The fit is generally satisfactory except possibly for the field dependence at 24,700 cm^{-1}. Of course, taking more frequency functions might improve this.

Discussion of SFO #14

The last SFO to be discussed is #14. This was obtained from Cyanamid Laboratories. Its iron content is 10.7 per cent. Electron microscope data show that the ferric oxide particles are very uniform with a size of 150 by 20 Angstroms. This sample was very uniform and did not fractionate in the Sephadex column.

The FR is interesting, it is dominated by the f_1 dependence especially near 26,000 cm^{-1}. Furthermore, the field dependence is essentially linear with H. Figure 20 shows this linear dependence as well as the deviations of the experimental data. The experimental error, 0.005 degrees, is indicated with the field dependence data.

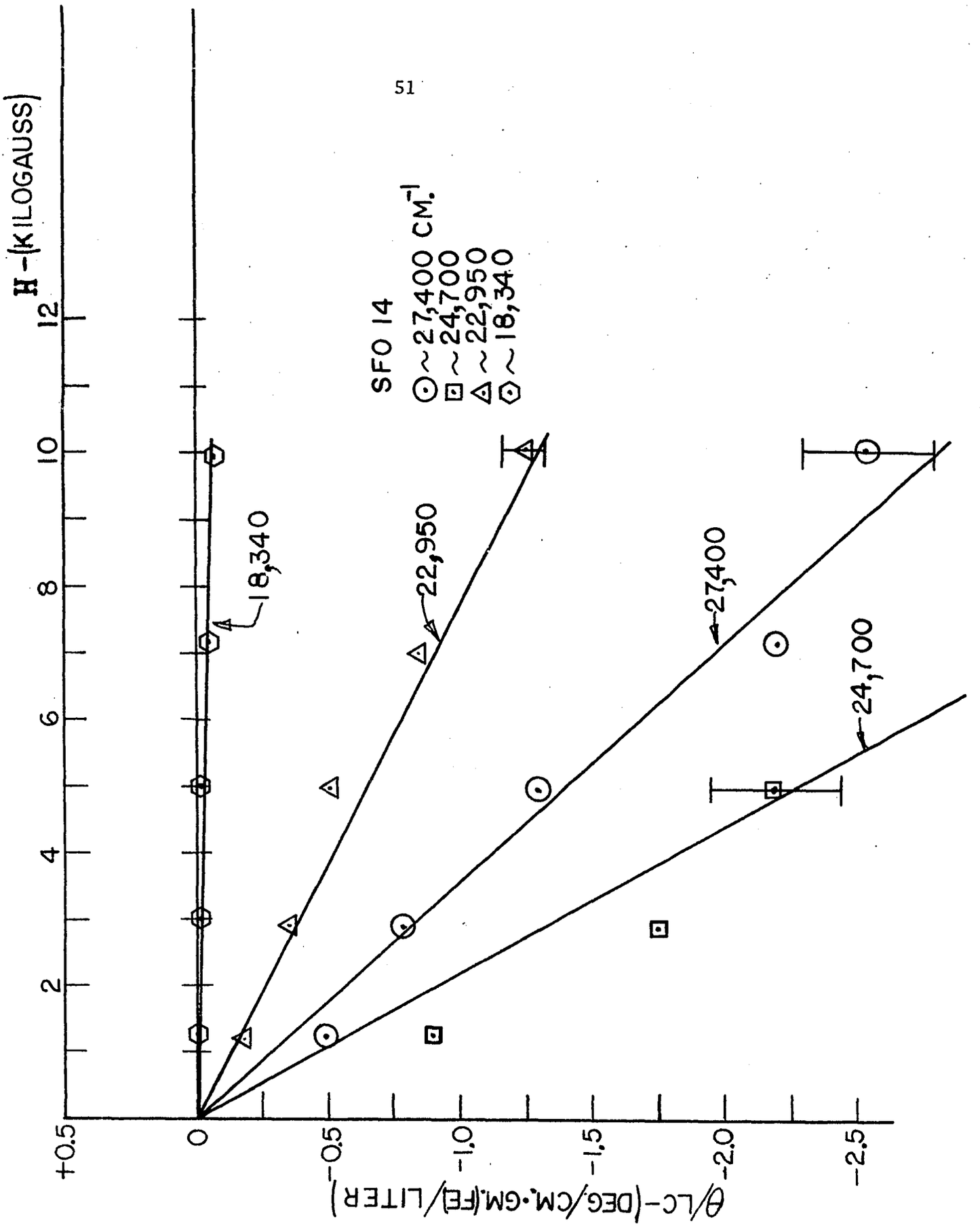

Figure 19. Magnetic field dependence of the FR for SFO #14

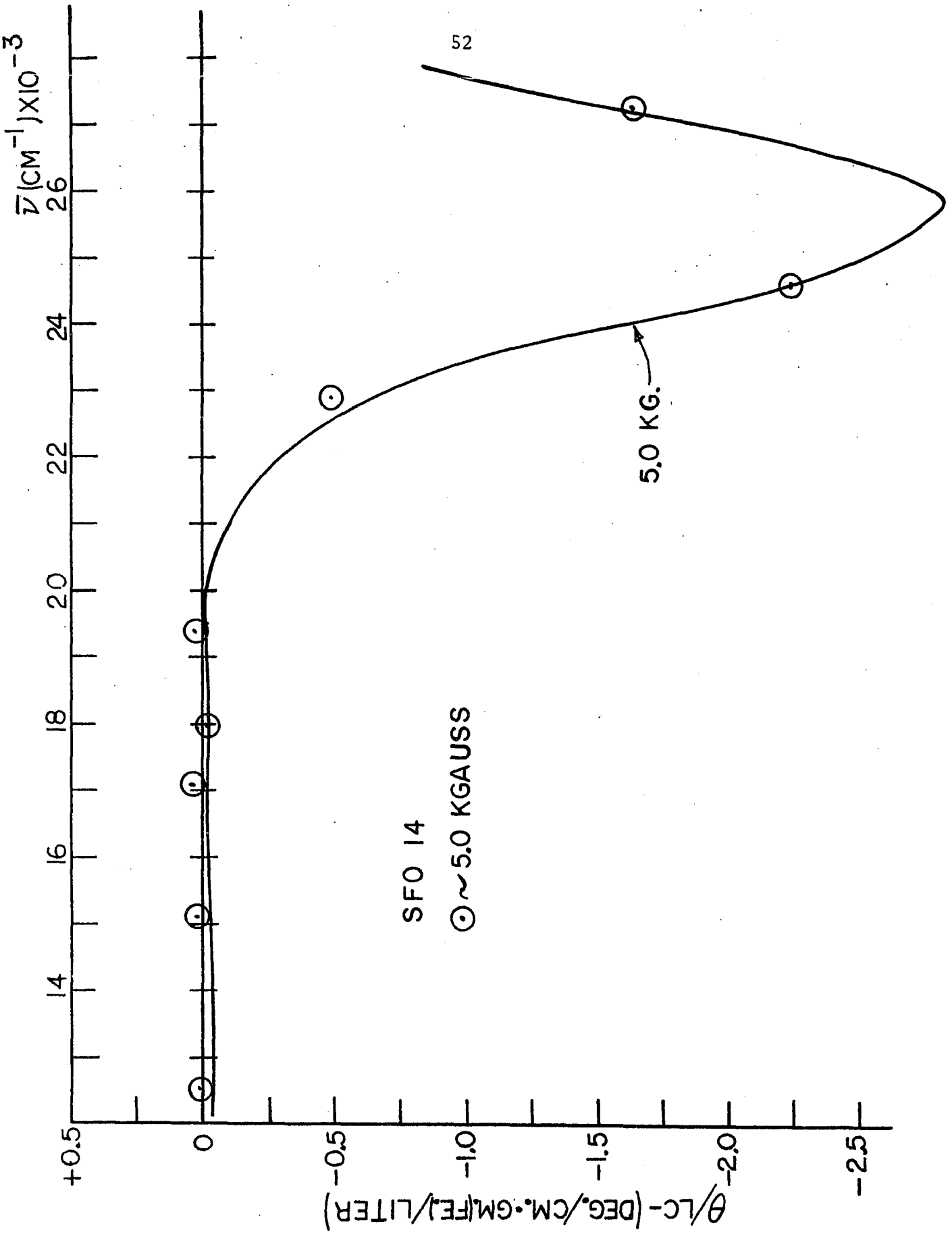

Figure 20. Wavenumber dependence of the FR for SFO #14

The equation used to fit to experimental data is

$$[\Theta/\ell C]_{14} = [-(2.8\times10^{-12}\ \hbar) f_1(26,7.0) - 0.33\ f_2(26,7.0)]H \qquad (20)$$

where H is in kilogauss. Both f_1 and f_2 frequency functions must be used. In this case they correspond to the A and C terms of Eqs. (6) and (9) respectively.

Summary

In this section the results of experimental data and the fitted curves will be summarized and some comparison between the different SFO's will be made.

Evidently, the general formula given in Eq. (3) is able to fit the data. The theory of Buckingham and Stephens and earlier similar theories can therefore be used as a basis of discussion. The former theory does predict the field and frequency dependence in regions of large absorption as well as in regions far from this.

The signs of the A, B and C (or Q_α for the SFO's) terms which arise from the fitted equations are summarized in Table 3.

Table 3. Summary of the Signs of the A, B and C Terms for the SFO's

$\bar{\nu}_o(cm^{-1})$	A	B	C(or Q_α)
17,000±1,000	negative	positive	n.a.
22,500±1,000	negative	negative	positive (except 11-C)
26,500±1,000	negative	negative	positive and negative
32,000±2,000	negative	n.a.	positive and negative
36,000±2,000	n.a.	n.a.	positive (6A-1 only)

The sign of the Q_α term is interesting because it depends only upon the matrix elements of the electric dipole moment. Thus from Eq. (8) it is seen that

$$\text{Im}\{(m_x)_{aj}(m_y)_{ja}\} = \begin{cases} >0 \text{ for sign of } Q_\alpha > 0 \\ <0 \text{ for sign of } Q_\alpha < 0 \end{cases} \tag{21}$$

For the transition $a \rightarrow j$ corresponding to 22,500±1,000 cm^{-1} the sign is always positive, except in the case of SFO 11-C. Furthermore, since the sign of the A terms is negative for all $a \rightarrow j$ transitions is followed from the expression for the A terms in Eq. (6) then

$$[(\mu_z)_{jj} - (\mu_z)_{aa}] = \begin{cases} >0 \text{ for sign of } Q_\alpha < 0 \\ <0 \text{ for sign of } Q_\alpha > 0 \end{cases} \tag{22}$$

The sign of the B terms cannot be designated as due to either the magnetic or the electric dipole terms. This is readily apparent on examining the expression for B in Eq. (7).

Although no special attempt has been made to prove that the total rotation is proportional to the iron content I believe that the results make this plausible. Note that the heavy and light fractions have iron contents differing by a factor of 10 usually. However, the normalized FR is of the same order of magnitude. This is especially apparent in SFO #11. In the other SFO's differences in shape and magnitude of the FR between the heavy and light fractions can be due to a further developed crystal structure in the heavy fraction.

The SFO's exhibit a field dependent FR which is very similar to the superparamagnetism observed for fine particles.[17] In this the magnetization of most all of a domain acts as an aligned magnetic moment. The magnitude of the α term in $\tanh(\alpha H)$ fits this picture. Thus for a paramagnetic substance at room temperature, one has[18]

$$|\alpha| = \frac{|\mu|}{kT} = 10^{-6}/\text{gauss} ,$$

But the α's used for the SFO's are in the range of 10^{-4}/gauss to 10^{-3}/gauss. Hence, we are observing alignments of domains containing 10^2 to 10^3 magnetic atoms. The electron microscope and X-ray data show that the largest particles are about 50 Angstroms in diameter. Assuming that these have a ferrite structure[16] similar to Fe_3O_4 the total number of iron atoms is about 5×10^3. A summary of the α's for the SFO's used in the fitting equations as given in Table 4.

Table 4. Summary of the α's for the SFO's

SFO	α_1(in kilogauss^{-1}) for $\bar{\nu}_1$(22,500±1,000)	$\bar{\nu}_2$=(26,000±1,000)	$\bar{\nu}_3$=(32,000±2,000)	36,000
5C-1	1.0	-	0.1	-
5B-6	0.4	-	-	-
6A-1	1.0	1.0	1.0	0.2
6'-8	1.0	0.4	0.2	-
10B-2	-	1.0	0.5	-
10'-(7+8+9)	-	0.3	0.15	-
11A-3	-	0.4	0.1	-
11-C	-	0.3	-	-

There α's seen to group rather well into two groups i.e.

$$\text{Group I } (|\alpha|_{max}=1.0) \sim \begin{matrix} \text{5C-1} \\ \text{6A-1} \\ \text{6'-8} \\ \text{10B-2} \end{matrix}$$

$$\text{Group II } (|\alpha|_{max}<1.0) \sim \begin{matrix} \text{5B-6} \\ \text{10'-7+8+9} \\ \text{11A-3} \\ \text{11-C} \end{matrix}$$

As was mentioned before the experimental data demand that the fitting equation include at least two tanh(αH) terms with different α's. It is possible that the magnetic iron atoms exist in different crystal structures within a particular SFO. Also the uncoordinated surface atoms might be associated with a different α's than the interior atoms. Of course, a difference in magnitude of α can be explained on the basis of a variation in size of the crystallites of a particular SFO. This does not necessarily explain the sign reversal of the tanh αH terms, however. The greatest difference in α occurs in Eq. (12) for 5C-1 as it contains α's of both 1.0/kilogauss and 0.1/kilogauss. This factor of 10 can be accounted for by a factor of 2.2 in the crystallite diameter. This fits the electron microscope and x-ray data.

For thin ferromagnetic films it has been shown that the FR/gauss/cm is proportional to the magnetization.[2] This is referred to as Kundt's law and a variation of this is utilized by Van Vleck and Hebb[19] to increase the usefulness of FR data. The SFO's especially those with a large C(or Q_α) term should display this same effect. In particular SFO#6A-1 and SFO #10B-2 should follow Kundt's law. Thus, for $\bar{\nu}$ = 27,400 cm^{-1} we can write

$$\frac{[\Theta/\ell C]_{6A-1}}{[\Theta/\ell C]_{10B-2}} = \frac{[-7.39\tanh(1.0H) + 5.30\tanh(0.2H) - 0.14\tanh 1.0H]/H}{[-1.89\tanh(1.0H) - 1.27\tanh(0.5H)]/H} \qquad (23)$$

which reduces for small values of H to

$$\simeq \frac{[-7.39(1.0) + 5.30(0.2) - 0.14(1)]}{[-1.89(1.0) - 1.27(0.5)]}$$

or finally

$$\frac{[\Theta/\ell CH]_{6A-1}}{[\Theta/\ell CH]_{10B-2}} \xrightarrow{H \to 0} 2.56 \quad . \tag{24}$$

The susceptibility χ of these samples have been measured[16] and their ratio at room temperature is

$$\frac{\chi(6A-1)}{\chi(10B-2)} = \frac{30,500}{11,000} \times \frac{0.45}{0.60} = 2.1 \tag{25}$$

The factor of 0.45/0.60 was the normalization factor for the iron content. The uncertainty in the experimental numbers of Eq. (24) is ± 0.25. Comparison of Eqs. (24) and (25) does tend to support the contention that the tanh term of the SFO's follows Kundt's law.

Experimental Error

This section is reserved for a description of the error in the experimental data and the precision of the angle of rotation. In the section on "Experiment" it was mentioned that

$$\left(\frac{\Theta}{\ell C}\right)_{SFO} = \frac{1}{\ell C}\left[\Theta_s - \Theta_o\right] \tag{26}$$

where Θ_s is the rotation observed for the solution of the SFO in water and Θ_o is the rotation of pure water. An error in the parameters on the right side of Eq. 26 will cause an enlarged inaccuracy in $[\Theta/\ell C]$. The major error is in the angle. Because of the large optical absorption of the SFO's one must keep the iron concentration

relatively small. As a result Θ_s comes very close to Θ_o. Using a short optical path, and larger concentration, one can reduce this error. Our cells were about 1 mm wide.

In measurements of the rotation of water at a particular field and wavelength the error was as small as 0.0025° at H = 10.1 kilogauss. This results in an uncertainty in $[\Theta/\ell C]$ of

$$\Delta[\Theta/\ell C] = \pm \frac{0.005^\circ}{\ell C} \qquad (27)$$

This error depends upon the size of $[1/\ell C]$ and is given for each wavelength on the field dependence curves. This uncertainty is as large as 20 per cent of $[\Theta/\ell C]$ at H = 10.1 kilogauss.

The error in the path length is

$$\ell = 0.965 \pm .010 \text{ mm.}$$

Errors in C caused by the analysis of the iron content and on diluting the solution, are probably of lesser importance. The measurement cell was sealed to prevent evaporation during a measurement of the FR. The results available on the reproducibility of the chemical analysis show that the analysis reproduced to 10 per cent.

Of course, the uncertainty in ℓ and C results in a scale factor uncertainty for $\Theta/\ell C$ so that all numbers at a particular wavelength are uniformly high or low. "Scatter" is caused by errors in the angle measurements.

The reproducibility of the rotation measurements is illustrated by SFO #6A-1. This was measured in two different cells (of the same path length) one month apart. The shapes of the field dependent curves were found to reproduce considerably better than the error Eq. (27) indicates. The magnitudes of the rotation reproduced to 10 per cent.

REFERENCES

1. Skaggs, F.L., and S. Broersma, Rev. Sci. Instr. 35, 1489 (1964).
2. For a comprehensive review of this work see: a) W. Schutz, Vol. 16, Handbuch Der Experimental Physik, (Akademische Verlagsgesellschaft, Leipzig, 1936) pgs. 1-316.
3. For example see Becquerel, J., W. T. DeHaas and J. Van Den Handel, Physica 3, 1133 (1936).
4. Kramers, H.A., Proc. Acad. Sci. Amsterdam 33, 959 (1930).
5. Rosenfeld, L., Z. Physik 57, 835 (1929).
6. Serber, R., Phys. Rev. 41, 439 (1932).
7. For a comprehensive review see for example Buckingham, A.D. and P. J. Stephens, Ann. Revs. Phys. Chem. 17, 399 (1966).
8. Ramachandran, G.N., and S. Ramaseshan, J. Opt. Soc. 42, 49 (1952).
9. Bausch & Lomb, Inc., Rochester, New York, 2nd order interference filters, standard series.
10. Buckingham, A.D., and P. J. Stephens, *loc. cit.*; Stephens, P.J., "Theoretical Studies of Magneto-Optical Phenomena", (Doctoral Thesis, Oxford University, Oxford 1964).
11. *Ibid.*, however, note that the symbol of Θ for the FR has been retained here. Also the designation of the sign of the FR is such so that H_2O has a positive rotation. This agrees with the usual experimental terminology.
12. Schatz, P.N., *et al.*, J. Chem. Phys. 15, 722 (1966).
13. See for example Becquerel, J., and J. van den Handel, Physica 7, 705 (1940).

14. Jorgenson, C.K., Acta Chem. Scand. 8, 1495 (1954).

15. Meischer, E., Helv. Phys. Acta. 3, 93 (1930).

16 Wilson, D.M., (M.S. Thesis, University of Oklahoma 1968, in preparation).

17. Bates, L.F., Modern Magnetism (Cambridge University Press, Cambridge Fourth ed. 1963), p. 293.

18. Ballhausen, C.J., Intro. to Ligand Field Theory (New York, McGraw-Hill, 1962), pp. 139-149.

19. Van Vleck, J.H., and M. H. Hebb, Phys. Rev. 46, 17 (1934).

CHAPTER III

ELECTRICAL PROPERTIES

Introduction

The electrical resistance of the stabilized ferric oxides (SFO) is very sensitive to the temperature of the sample. In fact, the dependence upon the temperature is exponential. This is analogous to the behavior of a semiconductor. In pure semiconductors this has led to an understanding of its energy structure. Therefore, we shall draw upon the large amount of information available for pure semiconductors to further our understanding of the SFO.

Experimental

The apparatus used to make measurements is shown in the Fig. 21 below. The sample is suspended from its leads inside the cell. A forepump was used to keep the pressure below 100μ mercury pressure inside the cell. This eliminates conduction effects due to moisture at the surface. The experiments were performed in the range of room temperature up to 200 °C. Initially, measurements were taken with the temperature increasing as well as decreasing. However, it was found that the data taken with the temperature decreasing were more reproducible. Therefore, all the results reported here one obtained by heating the bath to about 200 °C then allowed it to cool slowly, while the resistance was measured.

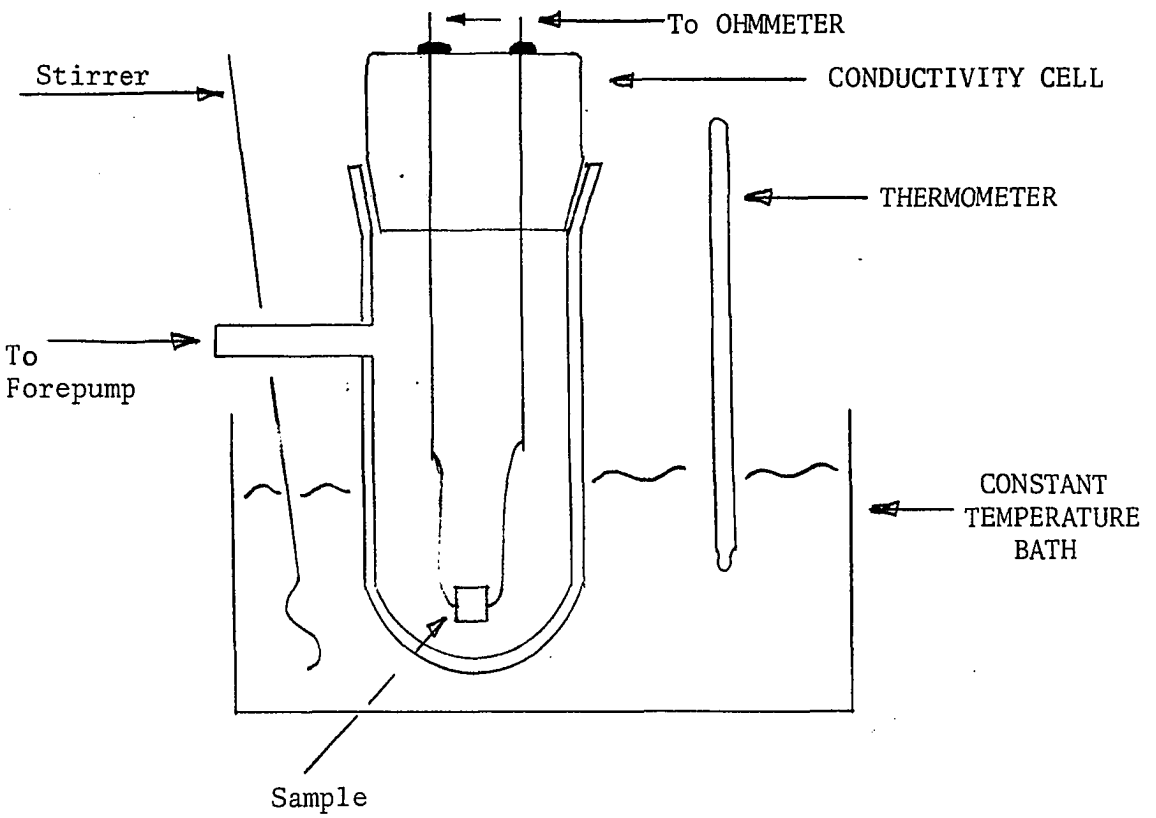

Figure 21. Schematic of apparatus used in measuring resistance values.

We used a General Radio Type 1644-A megohm bridge, which has a working range of 9×10^2 to 1×10^{15} ohms. This is quite convenient for our study: the SFO's cover this entire range. It is also possible to determine the current-voltage characteristic of the samples by using the various measuring voltages provided on the "megohm bridge". However, all the results given here are taken at 100 volts.

Two leads were attached to the samples with a commercial silver paste. This provided an excellent mechanical and electrical connection to the sample. These leads are then soldered to the output leads of the measurement cell. The "open circuit" resistance of the cell is approximately 10^{15} ohms, which is sufficiently high for all measurements reported here. All the samples were prepared by compacting them at about 2000 bar . Before the leads are attached the samples are in the shape of a "pill" having a diameter of 8.13 mm and a thickness of 1.5-6 mm.

Data and Analysis

In the present study it is found that the resistance of our samples can be described by the formula

$$R = R_o e^{+E/kT}$$

where $k = 1.38 \times 10^{-16}$ erg./deg, T is the absolute temperature, E is the activation energy and R is the sample resistance. The resistivity ρ is dependent only upon the characteristics of the sample. ρ is given by

$$\rho = RA/\ell = R_o (A/\ell) e^{E/kT}$$

$$= \rho_o e^{E/kT}$$

where A is the cross sectional area and ℓ the length.

The area of electrical contacts and hence "A" was not the same for all runs except those on SFO #14. In this case values of the resistivity are given. For all other samples the numeric value of (A/ℓ)

is in the range 0.5 cm to 2.0 cm. Of course, ρ is a constant so that all resistivity values can be ascertained from the resistance data within a factor of two. This uncertainty does not affect the interpretation of our results as we are mainly interested in the slope of the curves and only in the order of magnitude of the resistance (resistivity) itself. The range of resistance values is quite large.

It is found experimentally that the plots of resistance - 1/T have some curvature. Hence the use of an exponential is an approximation, but a reasonable one. Some of this curvature could be due to temperature dependence of the "mobility" μ of the electron within the sample. For pure, crystalline semiconductors lattice scattering gives rise to a mobility dependence of $T^{-3/2}$ at room temperature and above.[1]

Most of this curvature in the SFO data can be accounted for by assuming that conduction over the temperature region observed is due to electrons arising from two levels, E_1 and E_2 above the ground state. Figures 22 and 23 are two typical resistance - 1/T graphs in which the experimental data has been fitted with the approximation described above. Hence the resistance would be R_{EXP} where

$$\frac{1}{R_{EXP}} \simeq \frac{1}{R_1} + \frac{1}{R_2} = \frac{e^{E_{1/kT}}}{R_{0,1}} + \frac{e^{E_{2/kT}}}{R_{0,2}}$$

The fit is seen to be within the experimental error.

The mobility μ is further decreased by sample irregularity and poor microcrystalline contacts. For the pressed "powder" samples it

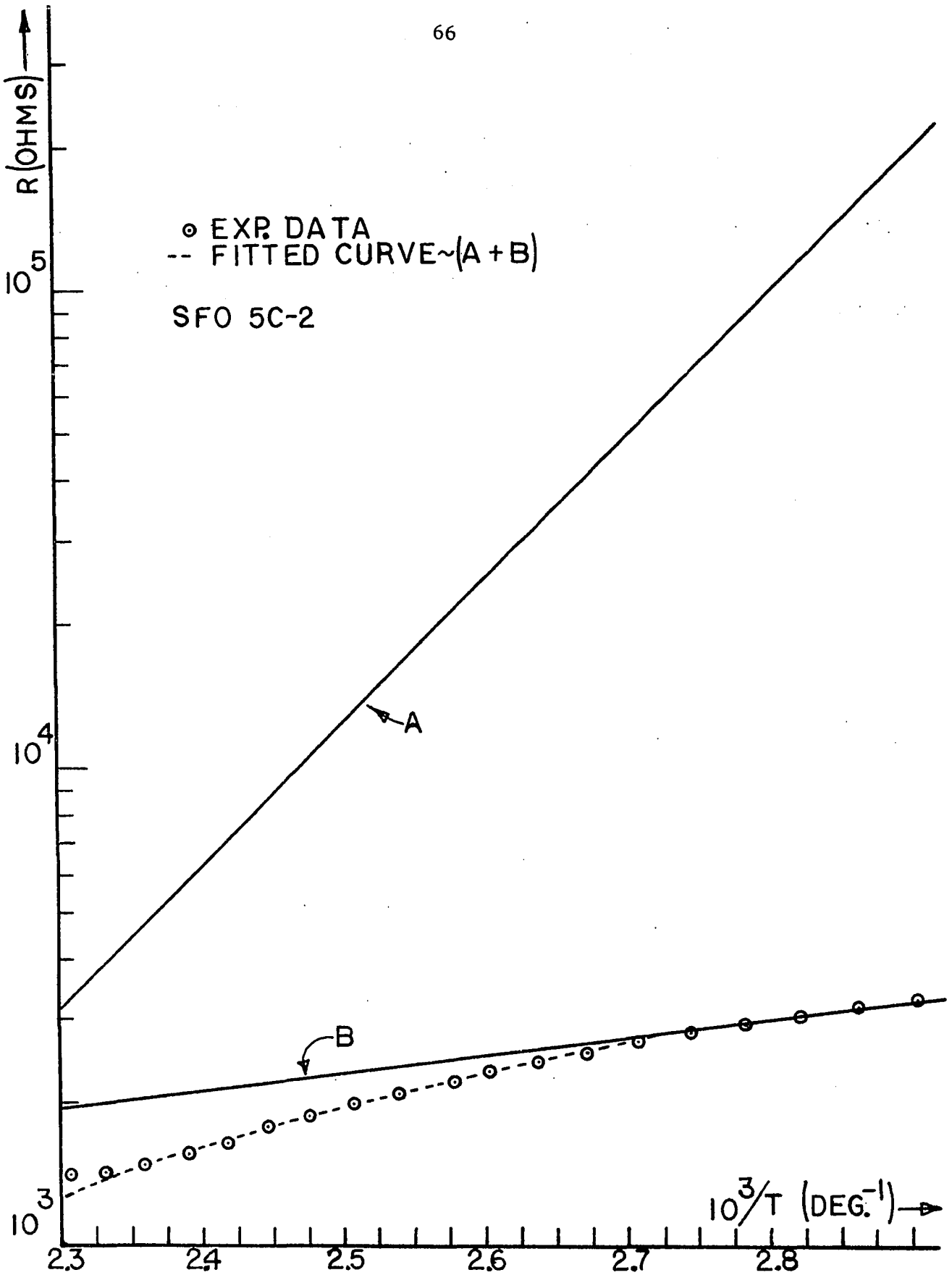

Figure 22. Temperature dependence of the resistance of SFO #5C-2.

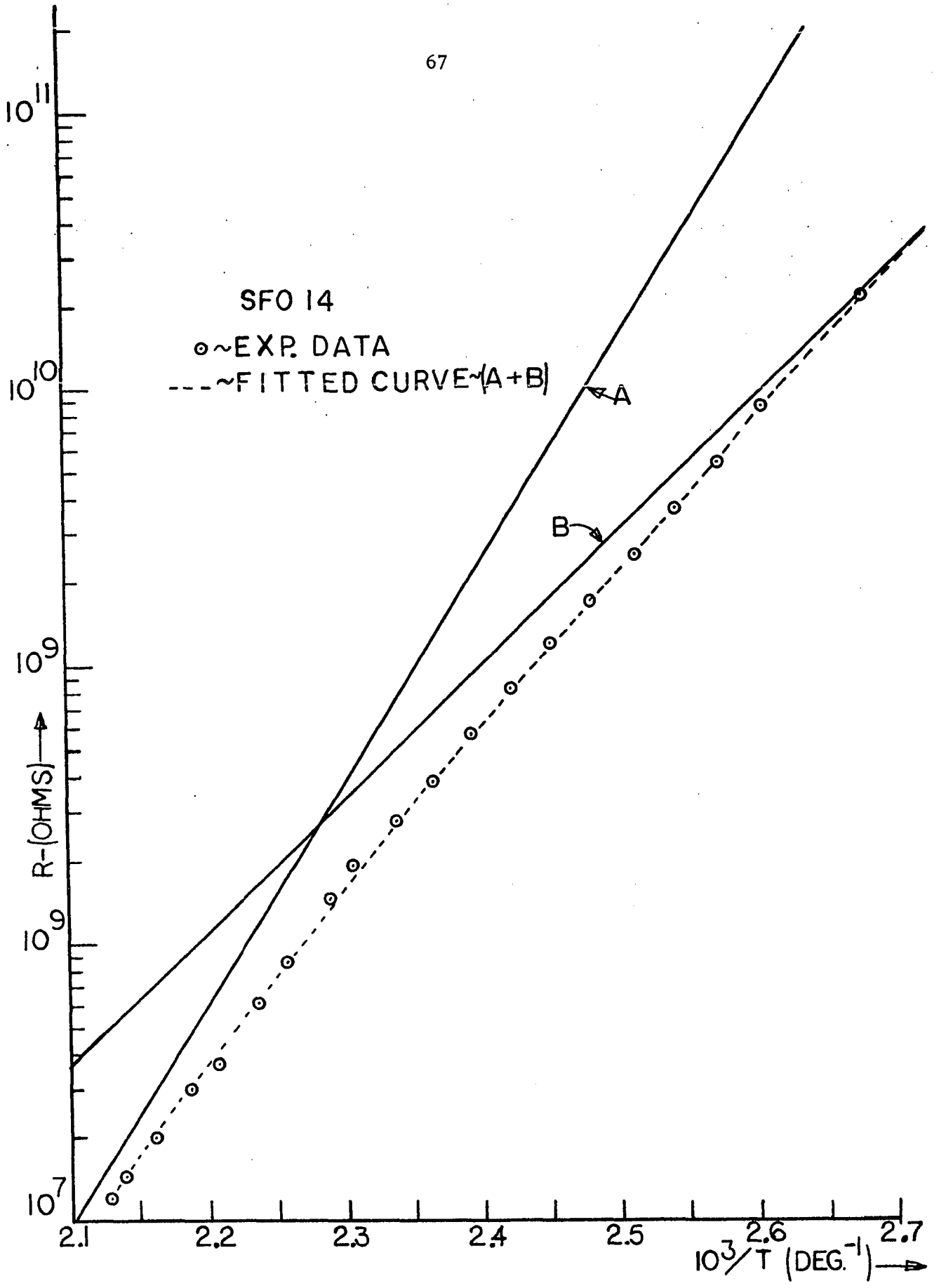

Figure 23. Temperature dependence of the resistance of SFO #14.

might be expected that electric conduction might not resemble electron flow in an extended conduction band as observed in other ions exhibiting 3d-electron conduction. It is possible that the electron must "hop" from one site to another as in a tunneling process. This, in turn should lead to a non-ohmic condition.

Figure 24 shows that the conduction is indeed non-ohmic. However, this could be caused by a semiconducting barrier between the contacts and the sample.[2] In order to examine the effect of different contact materials SFO #14 was measured with silver, platinum, gold and aluminum contacts. Table 5 lists the results in this study.

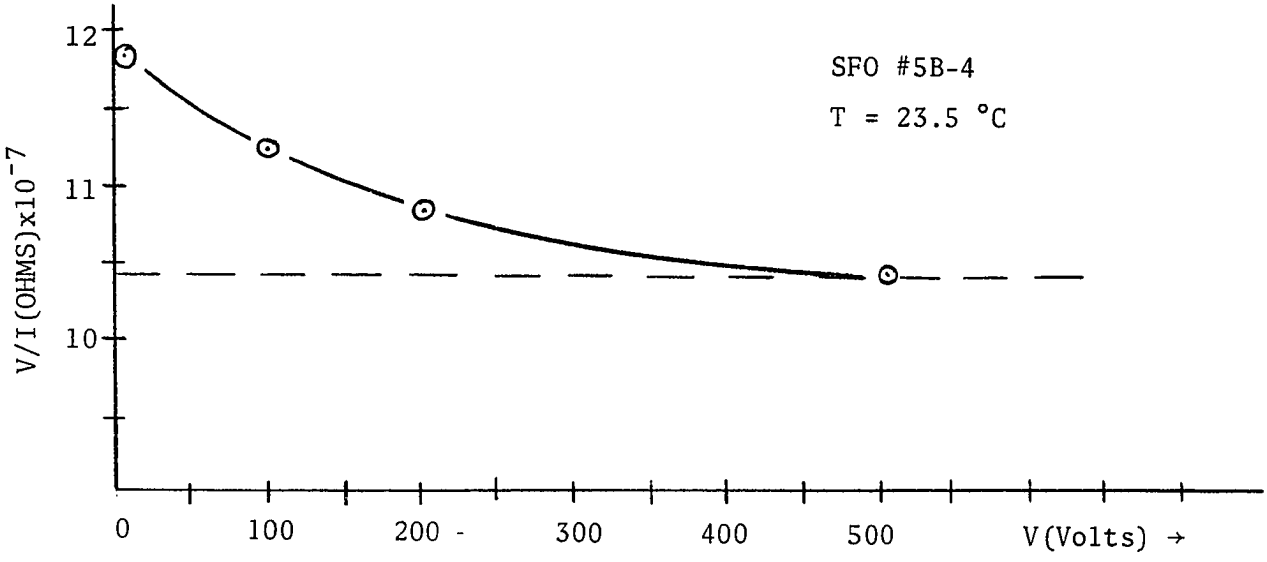

Figure 24. Resistance-voltage characteristic for a typical SFO.

The variation is small enough to conclude that the contact barrier is not dominating the conductivity. Rather, some other process, such as tunneling, which also non-ohmic must give rise to the behavior of the R vs. V graph of Fig. 24. Because of this voltage dependence all samples are measured at 100 volts. More will be said of this when the effect of the pressure on the resistance is discussed.

Table 5. Effect of the Contact Material on the Experimental Energy Levels E_i.

Contact	E_1(eV)	E_2(eV)
Silver	1.6	1.0
Gold	1.5	1.15
Aluminum	1.6	0.95
Platinum	1.6	0.8

The conductivity of a substance is given by

$$\sigma = 1/\rho = \Sigma_i n_i q_i \mu_i \ ,$$

where μ_i is the mobility of the charge q_i in the sample and where n_i is written for the Boltzmann distribution as

$$n_i = n_o e^{-E_i/kT} \ .$$

Hence

$$\sigma = n_o \Sigma_i \ e^{-E_i/kT} \ q_i \mu_i \qquad (28)$$

considering that μ is much less temperature dependent than the expotential this relationship can be used to determine the E_i's. This is especially advantageous where optical transitions are formally "forbidden" among the 3d levels. For ferric ions the 3d electrons are predominant in the electronic conductions. For Eq. (28) to apply to the SFO's it must be modified slightly. First, the mobility of the "hole" in the ground state should be much smaller than that of the excited electrons so that $q_i = e$ only. Secondly, we realize that excitation of the electron into an excited state will not produce conduction unless it can escape the ferric nucleus. This can happen by a tunneling process. Letting t_i be the percentage of electrons in state "i" which "tunnel" free, one gets finally for the conductivity

$$\sigma = (n_o e)\Sigma_i e^{-E_i/kT}(\mu_i t_i) \quad . \tag{29}$$

At low temperatures the levels near $E \sim 0$ will have the largest exponentials. Larger values of T increase the contribution to σ of the electrons in the higher levels and a change in slope of the conductivity - 1/T plot will occur. We note that t_i is some function of the level E_i since if E_i was the conduction band energy it is expected that $t \simeq 1.0$ whereas t should approach zero for an electron in the ground state.

In the region $40 \rightarrow 200$ °C usually three different slopes occur in the resistance - 1/T graphs for the SFO's. However, the data can be represented by only two straight lines for the region T = 200 °C $\rightarrow$ 40 °C. These lines must be "fitted" to the experimental data as explained

Table 6. Summary of Results from Resistance-(1/T) Data.

Sample[c]	% Iron	Resistance (185°C) Fitted	Resistance (185°C) Exp.	E_1[a]	Resistance (85°C) Fitted	Resistance (85°C) Exp.	E_2[a]
Dextrin	-	-	-	-	-	-	-
(BACT)	-	$5.9\times10^{7}\Omega$	$5.9\times10^{7}\Omega$	2.2[b] eV	$5.8\times10^{10}\Omega$	$5.8\times10^{10}\Omega$	(E_2=E_1=E)
(Corn)	-	1.9×10^{7}	1.8×10^{7}	3.5	9.2×10^{10}[d]	9.4×10^{10}[d]	2.1 eV
Fe_2O_3	69.9%	8.5×10^{6}	8.7×10^{6}	1.6	3.0×10^{9}	2.9×10^{9}	0.8
14	10.6	3.0×10^{7}	3.0×10^{7}	1.4	7.6×10^{10}	7.5×10^{10}	0.95
11A-B	<1.0	1.3×10^{9}	1.2×10^{9}	1.7	2.6	2.7×10^{12}	0.9
10 -1	35	6.7×10^{6}	6.9×10^{6}	1.7	1.5×10^{10}	1.4×10^{10}	0.9
$CoFe_2O_4$	38.1	1.2×10^{6}	1.2×10^{6}	0.54	4.1×10^{6}	4.3×10^{6}	0.47
Fe_3O_4	72.4	2.1×10^{3}	1.9×10^{3}	0.16	3.9×10^{3}	3.8×10^{3}	0.04
5C-2	33.4	1.5×10^{3}[e]	1.5×10^{3}[e]	0.6	2.9×10^{3}	2.9×10^{3}	0.07
5B-4	27.6	1.0×10^{7}[f]	1.0×10^{7}[f]	1.1	3.1×10^{8}	3.2×10^{8}	0.45
5A-5	15.4	1.8×10^{7}	1.9×10^{7}	2.4	7.1×10^{10}	7.3×10^{10}	1.1
5A-6	5.5	1.8×10^{7}	2.0×10^{7}	1.7	5.3×10^{10}	5.3×10^{10}	1.0

[a] Calculated from $\log R/R_o = E/kT$ except for dextrin where $\log R/R_o = E/2kT$.

[b] 1 eV corresponds to 1.24 micron wavelength.

[c] Samples selected on basis of availability of sufficient sample (≃ 100 mm^3).

[d] 105 °C.

[e] 150 °C.

[f] 165 °C.

above. Table 6 summarizes the results for the SFO's and several "pure" samples. Included are data concerning the iron content, R_o and resistance range observed.

Because the SFO microcrystals are stabilized, hence separated, by polysaccharide chains these can contribute to the resistance. As the entry on pure dextrin indicates its resistivity is as high as or higher than that for the pure oxides. Therefore, the magnitude and the temperature dependence of the resistivity is also a function of the structure of the specimen.

Evidently, the polysacchrides (dextrins) themselves are semiconductors. But if the conduction takes place in the conduction band, the hole in the valence band can contribute. Thus the formula for the resistance of the dextrins is likely to be

$$R = R_o e^{-E_g/2kT} \qquad (30)$$

where Eg is the band gap energy and the factor 2 reflects the fact that now the Fermi level is in between the conduction and valence band.[3] It is seen that the two values of $E_g/2$ for dextrin are also found in several of the SFO's. Hence, these values of E in the SFO's are characteristic of the dextrin and not excited levels of the ferric ion.

According to various pieces of information, in particular the X-ray data, we found that our SFO's approximate three different categories:

1. Distorted ferrites - glucose stabilized (e.g. #6A-1, #10 -1)

2. Hydrous ferric oxides - glucose complex (e.g. #11, #5)

3. β-$Fe_2O_3 \cdot H_2O$ - glucose stabilized (#14)

Therefore, a comparison of the resistance values with pure Fe_3O_4, pure Fe_2O_3 and pure dextrin is worthwhile.

According to Verway *et al.*[4] the resistance of Fe_3O_4 is low because the extra electron of Fe^{2+} is easily transferred to Fe^{3+} placed in an equivalent octahedral site. In both cases the octahedrally coordinated ions are oxygen ions. Thus the conductivity is large. The regular ionic 3d conductivity is much smaller. This is experimentally demonstrated by Verway by examining mixed ferrites Fe_3O_4 and $Mn \cdot Al_2O_4$ where Mn indicates a metal ion with valence of +2. Here Al^{3+} can take the lattice position of Fe^{3+} and thus eliminate the path of easy conduction. Likewise the resistivity of Fe_2O_3 is much larger.

The relatively small resistance of SFO #5 can be understood on this basis. For the light fractions, the iron content is low so that the particles are small. The interparticle resistance is similar to that of dextrin, while the scattering in the small iron oxide crystals themselves is considerable. For the heavy fractions the iron content is high and the particles are large. The resistivity approaches that of the pure lattice. Evidently this is closer to a ferrite than the pure Fe_2O_3 lattice. Perhaps the Fe(3+) is induced to give up another electron when $[Fe(OH)]^{2+}$ is present. In any event one would expect a loosely bound electron to be present.

REFERENCES

1. Kittel, C., Intro. to Solid State Physics, 2nd ed. (John Wiley and Sons, Inc., New York, 1961) p. 365.

2. Kittel, C., *ibid.*, p. 384.

3. Kittel, C., *ibid.*, Chapter 13.

4. Verway, E.J.W., Phillips Tech. Rev. 9, 239 (1948).

CHAPTER IV

OPTICAL ABSORPTION

General Information

Absorption spectra of most of the stabilized ferric complexes have been measured in solution in the range 200 - 800 millimicrons (mμ). In addition several have been measured to 1700 mμ and some pure compounds like $FeCl_3$ have been measured in the region 200 - 800 mμ. With the exception of measurements taken from 800 - 1700 mμ on the "DK-1"[1] all the data were obtained with a "Beckman DB".[2] Both spectrophotometers measure the transmission of a solution. They are set up as "differential" instruments and provide an output T which is given by

$$I/I_o = T = \text{transmittance of solute}$$

where I_o is the intensity transmitted by reference cell filled with solvent, and I is the intensity transmitted by sample cell filled with solvent and solute. This output is recorded on a chart which is ruled from 0 to 100 so that the transmission percentage is easily read.

All results given here are derived from such data. For the most accurate results it was found necessary to first obtain a spectrum with both "sample" and "reference" cells filled with the solvent.

Therefore, a spectrum was obtained with the "sample" cell filled with the solution and the "reference" cell filled with the solvent. A small cell mismatch (≃ 1%) and some mismatch between the "reference" and "sample" beam in the instrument necessitated this. The total correction was about 10 per cent in the region 200 - 400 mμ. For the two measurements described it follows that

$$\frac{\{I_1(\text{Water + Solute})/I_o\ (\text{Water})\}}{\{I_1(\text{Water})/I_o\}} = \frac{I_1(\text{Water + Solute})}{I_1(\text{Water})} = T\ .$$

The absorption spectrum can be given in several ways. For instance, the extinction coefficient ε can be plotted versus the wavenumber $\bar{\nu}$. The extinction coefficient is defined as

$$\varepsilon = (1/\ell C)\cdot\log(1/T)$$

where ℓ is the cell length in cm and C is the concentration of solute in moles/liter. Sometimes one plots the absorption A = 1-T versus the wavenumber. By measuring the absorption coefficient of 5C-1 over a wide range of concentrations, it is found that the absorption of the SFO's is proportional to the concentration of iron. Therefore, we reduce ε to a mole of iron. The results are given in Table 7.

Table 7. Molar Extinction Coefficients for SFO #5C-1

$\tilde{\nu}$ (cm^{-1})	CONC {Mol.(Fe)/Liter}	ε
$50x10^3$	$.224x10^3$	5,700
"	.112	6,000
"	.056	6,300
"	.028	6,700
"	.014	7,400
41.70	.224	4,500
"	.112	4,500
"	.056	4,500
"	.028	4,500
"	.014	4,600
$35.70x10^3$	.224	3,400
"	.112	3,400
"	.056	3,500
"	.028	3,400
"	.014	3,500
31.20	.224	2,800
"	.112	2,800
"	.056	2,800
"	.028	2,800
"	.014	2,800
"	.0035	2,800

Deviations from a constant ε, for a given wave length, might indicate that the absorption was due to some other species in solution or due to scattering by the large SFO particles. However, only at 50,000 cm^{-1} is the variation in ε consistently larger than the experimental error. At the other wavenumbers ε differs only at the lowest concentrations used. At the lowest concentrations the effective thickness of the solute reduced to a solid layer is less than the average particle size. This, of course, could cause a deviation in ε. But at 50,000 cm^{-1} we believe that scattering of the beam by the colloidal size SFO particles becomes significant and affects the accuracy of the absorption data. This is borne out by an experiment in which both the "reference" and "sample" cells were filled with the SFO solution, the "reference" having a concentration of half that in the "sample" cell. This tends to equalize the effect of scattering since its effect is not necessarily proportional to the number of scatterers. The results of this experiment are given below.

$\bar{\nu}$	(ST'D Method)	(SFO in both cells)
$50.0 \times 10^3 cm^{-1}$	6,000	5,000
41.7	4,500	4,400
35.2	3,400	3,400
31.2	2,800	2,800

Again the results support the conclusion that the deviation observed at $50 \times 10^3 cm^{-1}$ is not due to a different species but rather by scattering of the SFO's in solution.

A graph of the extinction coefficient ε versus wavenumber $\bar{\nu}$ gives rise to several observations. First, the range of variation of ε is large, its maximum is about 20,000 for some SFO's. These largest values are for wavelengths in the UV. The magnitude of ε increases with wavenumber and reaches a "plateau" at approximately 30,000 cm^{-1}, from there ε rises less steeply with wavenumber. The magnitude of ε(5,000 - 15,000) in the UV is very large for optical transitions, but it is consistent with the value observed in other Fe^{3+} complexes and ions.[3]

Second, it is seen in the ε versus $\bar{\nu}$ curves that the strong UV absorption band and its "tail" show some fine structure in the form of small "wiggles" or dips. These are due to forbidden optical transitions. This will be discussed further in the following section.

Experiment and Discussion

The absorption by the iron group elements in crystals and aqueous solution is reviewed in detail by Ballhausen.[4]

The extinction coefficient for the ions in the iron group such as Co^{2+}, Fe^{2+}, Ni^{2+}, have a small ε value in the visible and IR, but have much larger values in the UV. As an example, Co^{2+} ($CoC\ell_2$ in aqueous solution) has two bands in the visible.[5] One absorption maximum at $\bar{\nu}_o$ = 21,600 cm^{-1} has a maximum ε value of only 4.55, the other line at 19,430 cm^{-1} has ε = 2.66. A list of such ions along with a review of previous work can be found in a paper by Orgel.[6]

The small value for the extinction coefficient in the visible and IR correspond to transitions between energy levels of the $(3d)^5$ configuration of Fe^{3+}. Now electric dipole transitions between any two states of a $(3d)^n$ configuration are formally forbidden. This is a consequence of the Laporte rule, which states that only transitions between even and odd states give rise to electric dipole transitions. All levels of the $(3d)^n$ configuration are even to a first approximation. Several other types of transitions are possible, for example, the electric quadrupole transition and the magnetic dipole transition. However, the contribution to the extinction coefficient ε by such transitions is still too small to account for the absorption bands in the visible and IR.[7]

The reason that one observes absorption from these formally forbidden transitions is that in second order the energy states are actually mixtures of even and odd states. The mixing of the states can occur through spin-orbit coupling and through coupling of nuclear vibrations. An analysis of the mixing shows that the small absorption peaks observed in the visible and IR can be accounted for.

For the SFO's we have attempted to locate the position of the maxima of these small absorption peaks. The difficulty is, of course, that the absorption peaks are merely small indentations in the broad absorption band in the UV. The location of these maxima is found by observing the inflections in the plot of ε versus wavenumber. To do this it is to be noted that at a wavenumber $\bar{\nu}$ where absorption occurs due to two bands centered around different wavenumbers we have

$$I = \alpha_1 \alpha_2 I_o$$

where α_1 is the transmittance at $\bar{\nu}$ due to a band at $(\bar{\nu}_o)_1$ and α_2 is the transmittance at $\bar{\nu}$ due to a band at $(\bar{\nu}_o)_2$. Then at $\bar{\nu}$ we have

$$\varepsilon = (1/\ell C) \cdot \log I_o/I$$

$$= (-1/\ell C)(\log \alpha_1 + \log \alpha_2) \ .$$

Let us consider α_2 to be the transmittance due to the UV band and α_1 that due to the weaker band centered at $(\bar{\nu}_o)_1$ then α_1, α_2 and $(\alpha_1 \cdot \alpha_2)$ are depicted schematically in Fig. 25. The position of $(\bar{\nu}_o)_1$ is seen to be at the inflection point.

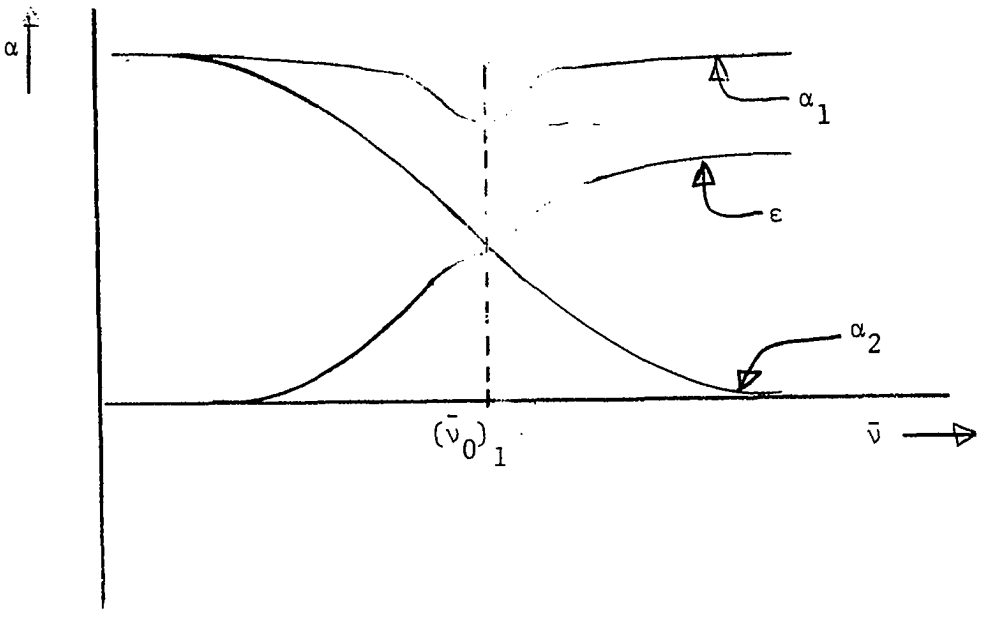

Figure 25. Method of separating small absorption from large broad absorption.

Hence, searching the curves of ε versus wavenumber for inflection points we can approximately locate the positions of the secondary absorption peaks. The results are given in Table 8 along with an estimate of possible error.

Transitions within the $(3d)^5$ configuration are formally forbidden and hence should give rise to small values of ε. Furthermore, such energy level differences correspond with visible light. Therefore, we attribute all of the absorptions listed in Table 8 to transitions within this configuration. The existence of levels of this type is supported by ESR spectra taken for several of the SFO's. These show that the g-values for the SFO's are 2.0±0.1. Theoretically, g = 2.0 for the ^6S ground state - [predicted ground state for $(3d)^5$].

For the higher lying levels it is possible that they are "mixed levels" i.e., dependent upon both the metal and ligand electronic states. Although, even in this case we should still have that the levels are primarily ferric levels.[8] This will be discussed later.

Table 8. Weak Absorption Peaks Observed for the SFO's.

$\bar{\nu}_o$ = 16,500±1,000 cm^{-1}	$\bar{\nu}_o$ = 21,500±1,000 cm^{-1}
5B-6	
10'-(7+8+9)	6A-1
14	6'-8
$\bar{\nu}_o$ = 22,500±1,000 cm^{-1}	**$\bar{\nu}_o$ = 26,500±1,000 cm^{-1}**
11-C	11A-3
11A-3	11-C
5C-1	10B-2
5B-6	10'-(7+8+9)
10B-2	5B-6
14	6'-8
10'-(7+8+9)	6A-1

Now consider the behavior of ε in the UV especially above 27,500 cm^{-1}. Absorption in this spectral region corresponds to transitions to the high lying levels referred to in the previous paragraph. In the UV region various factors can influence the absorption. First, the energies of the higher lying levels are most influenced by the surrounding atoms (ligands). Thus an electron in one of these states would be considered as "shared electron", e.g. one not bound exclusively

to the central ion. Transitions from the ground state of an ion to these levels are treated best by the molecular field theories.[9] In this theory some of the higher lying states are considered as predominately ligand levels and some as predominately metal levels. In general they are called mixed levels. The ground states are usually predominately metal ion levels. A transition between two mixed levels is called a charge transfer transition. The transition probability for a charge transfer transition can be quite large especially in comparison to those for transitions between two $(3d)^n$ levels. The charge transfer spectra of the iron group are in the wavenumber range of $10^4 cm^{-1}$. See McClure[10] and others.

A second factor that can contribute to the large absorption in the UV is that the higher states might arise from a $(3d)^4(4s)$, $(3d)^4(4p)$ or $(3d)^4(4d)$ configurations, so that electric dipole transitions would be formally allowed. Normally, however, transitions to these configurations are at higher energies (wavenumbers).[10]

In the ionic (Fe^{3+}) spectra of $FeCl_3$, Mulay and Selwood[11] have shown that only one strong band occurs in the UV. It has $\bar{\nu}$ = 41,700 cm^{-1} and an extinction coefficient of 6,000. In this study $HCLO_4$ is added to the solution to bring the pH below zero. This insures the formation of only one species of ion, namely Fe^{3+} or $\{Fe(H_2O)_6\}^{3+}$. Hydrolysis products and association species of ferric ions can be numerous in aqueous solutions but their formation is effectively prevented by the addition of $HCLO_4$, as shown by Mulay and Selwood.

A comparison of the absorption spectra of the stabilized ferric complexes (SFO's) with that of Fe^{3+} shows that the magnitudes of ε for the SFO's are the order of magnitude while the absorption band is correspondingly broader. In order to explain this greater width several other absorption spectra were taken. These are shown in Fig. 26. The first is the spectrum of $FeCl_3$ in 12.6 molar HCL. In this case the spectrum is typical of the associated complex $[FeCl_4]^{-1}$.[12] There is again an absorption peak at 41,700 cm^{-1}, but in addition two peaks of about the same strength at 31,900 cm^{-1} and 27,800 cm^{-1}. Also included in Fig. 26 is the spectrum of $FeCl_3$ in aqueous solution. This solution has been boiled from several minutes to insure formation of ferric hydroxide $Fe(OH)_3$.[13] Its spectrum closely resembles that of the SFO's in both magnitude of ε and width of the UV absorption band. The width is comparable to that observed in the spectrum of $[FeCl_4]^{-1}$ if we combine the three bands. Indeed the overall width is nearly the same for all the SFO's, $Fe(OH)_3$ and $[FeCl_4]^{-1}$ but the extinction coefficients do differ by about a factor of two in the UV-band. For all these solutions $\int_0^\infty \varepsilon d\bar{\nu}$, which is a measure of the strength of a particular transition, is roughly a constant for all the solutions discussed in this paragraph. Thus we conclude that the band in the UV arises from transitions to levels arising from configurations of the ferric ion of the type $(3d)^4(4s)$, $(3d)^4(4p)$, $(3d)^4(4d)$ or mixtures of these configurations with the ligand electrons. The ligands in the SFO's could be $(OH)^-$ or simply $(O)^{--}$ and H^+. Superimposed on this are the weak absorption peaks in the visible due to nearly forbidden transitions.

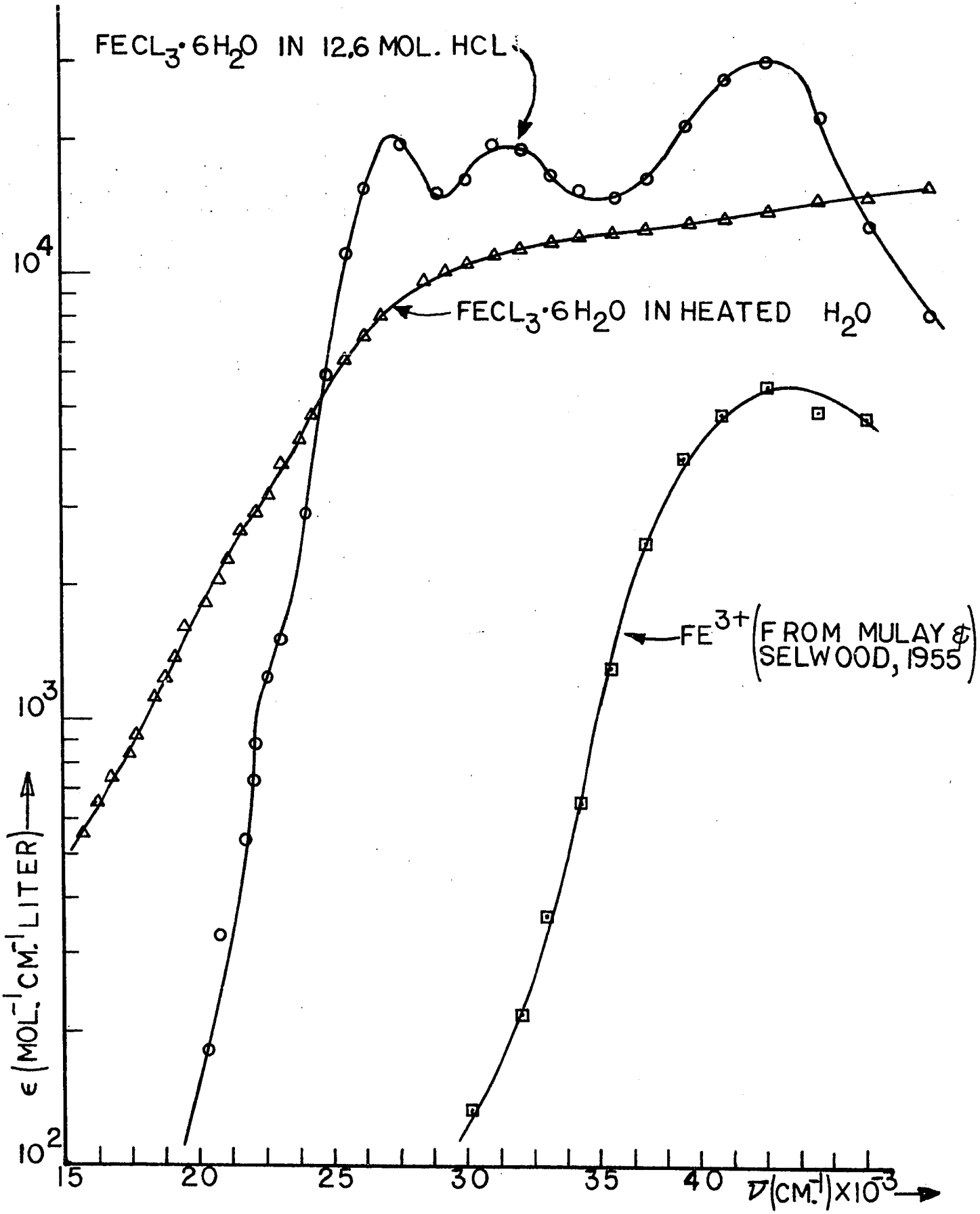

Figure 26. Extinction coefficients for some ferric salt solutions.

The total strength of the UV band is so large that its wings dominate the absorption in the visible. Dilute solutions of the SFO's appear red on illumination by white light because of the nearly complete absorption of the blue and green. Concentrated solutions of the SFO's appear black as no visible light is transmitted.

Data and Analysis

The maximum values of ε in the range 200 - 1700 millimicron are listed in Table 9. For the SFO's they were measured for 1-3 x 10^{-9} molar (Fe) concentrations.

Evidently, the high factions of 10, 6 and 5-(group C in Table 9)-have the same low value of ε = 5,800±150 at 50,000 cm^{-1}. Similarity in the structure of these three SFO's is also borne out by our X-ray diffraction analysis: these lattices resemble ferrites. The other fractions have ε values of about 10,600. Their structure resembles hydrous ferric oxides, however, with a variety of different magnetic structures.

Possibly that optical absorption classification is related to mixtures of different ferric complexes within a particular SFO. For example, species like $[Fe(OH)]^{2+}$ could predominate in some of the high fraction SFO's. That the small values of $\varepsilon_{Max.}$ in group C can be caused by formation $[Fe(OH)]^{2+}$ is supported by evidence from Mulay and Selwood.[14] According to their results as the percentage of $[Fe(OH)]^{2+}$ increases from zero to about 7 per cent of the Fe^{3+} concentration, the extinction coefficient at 41,750 cm^{-1} decreases. Indeed the Fe^{3+} band

Table 9. Maximum Values of ε in the Range 200-1700 millimicrons.

	$\varepsilon_{Max.}$	$\bar{\nu}(cm^{-1})$	Sample
	31,500	41.75x10	$[FeCl_4]^{-1}$
	20,000	31.87	"
A	21,500	27.62	"
	16,800	50.00	$Fe(OH)_3$
	10,000	50.00	14
	11,000	"	10'-(7+8+9)
	10,600	"	11-C
B	11,180	"	11A-3
	10,500	"	5B-6
	10,500	41.75	(Fe^{3+})
	5,900	50.00	10B-2
C	5,650	"	6A-1
	5,880	"	5C-1

a) 1 cm path length cell.

at 41,750 cm^{-1} is not even resolvable for the largest concentration of $[Fe(OH)]^{2+}$ and the extinction coefficient reaches a maximum at 50,000 cm^{-1} rather than at 41,750 cm^{-1}. This is similar to the position of ε_{Max} in the SFO's. We conclude that the SFO fractions of group C in Table 9 simply have a larger percentage of the species $[Fe(OH)]^{2+}$ than those of the group B complexes but concede that more work could be done to justify this conclusion. It is possible that the presence of such a species encourages the development of a ferrite structure which we observe in these fractions.

Oscillator Strengths for the SFO's

Finally, we shall examine the oscillator strength, the ratio of the actual absorption integral to that of classical oscillator. The oscillator strength "f" is given by the following relation.[15]

$$f = \frac{2.30 \times 10\ mc}{A\pi e^2} \int \varepsilon d\bar{\nu} \quad , \tag{31}$$

where

m = electronic mass,

c = velocity of light in vacuum,

A = Avogadro's number,

e = charge on the electron,

γ = function of the refractive index which is close to unity.

Substituting the numeric values of the constants it follows

$$f = 0.43 \times 10^{-8} \int \varepsilon d\nu \tag{32}$$

Most often a gaussian envelope is used as a first approximation of the ε versus $\bar{\nu}$ curve. However, the large variation of magnitude in ε makes it logical to plot log ε versus $\bar{\nu}$. From these graphs it is seen that the largest values of $\varepsilon(\geq 10^4)$ all lie in the UV.

Figures 27 through 31 show that the log ε vs $\bar{\nu}$ curves can be divided into two regions. One bounded by the instrument cut-off wavenumber of 50,000 cm^{-1} at one side and the sharp corner at approximately $\bar{\nu}$ = 25,000 cm^{-1}. The other region then is bounded by $\bar{\nu}$ = 0 and $\bar{\nu}$ = 25,000 cm^{-1}. Of course, the line used to approximate log ε has a different slope and intercept for these two regions. With this approximation then

$$\log \varepsilon = k\bar{\nu} + \log b \qquad (33)$$

where k the slope of the line and log b the intercept at $\bar{\nu}$ = 0 can be read from the experimental curves. Also, substituting Eq. (33) in the formula for the oscillator strength it follows that

$$f = 0.43\times10^{-8}\int e^{2.30(k\bar{\nu}+\log b)}d\bar{\nu} \ , \qquad (34)$$

and hence

$$f = \frac{0.43\times10^{-8}}{2.3}\left(\frac{b}{k}\right)\left[10^{k\bar{\nu}2} - 10^{k\bar{\nu}1}\right] \ . \qquad (35)$$

Here $\bar{\nu}_1$ and $\bar{\nu}_2$ are the boundary wavenumbers of this line.

Table 10 gives a list of the oscillator strengths for the SFO's as found by this method. Also given are the boundary wavenumbers.

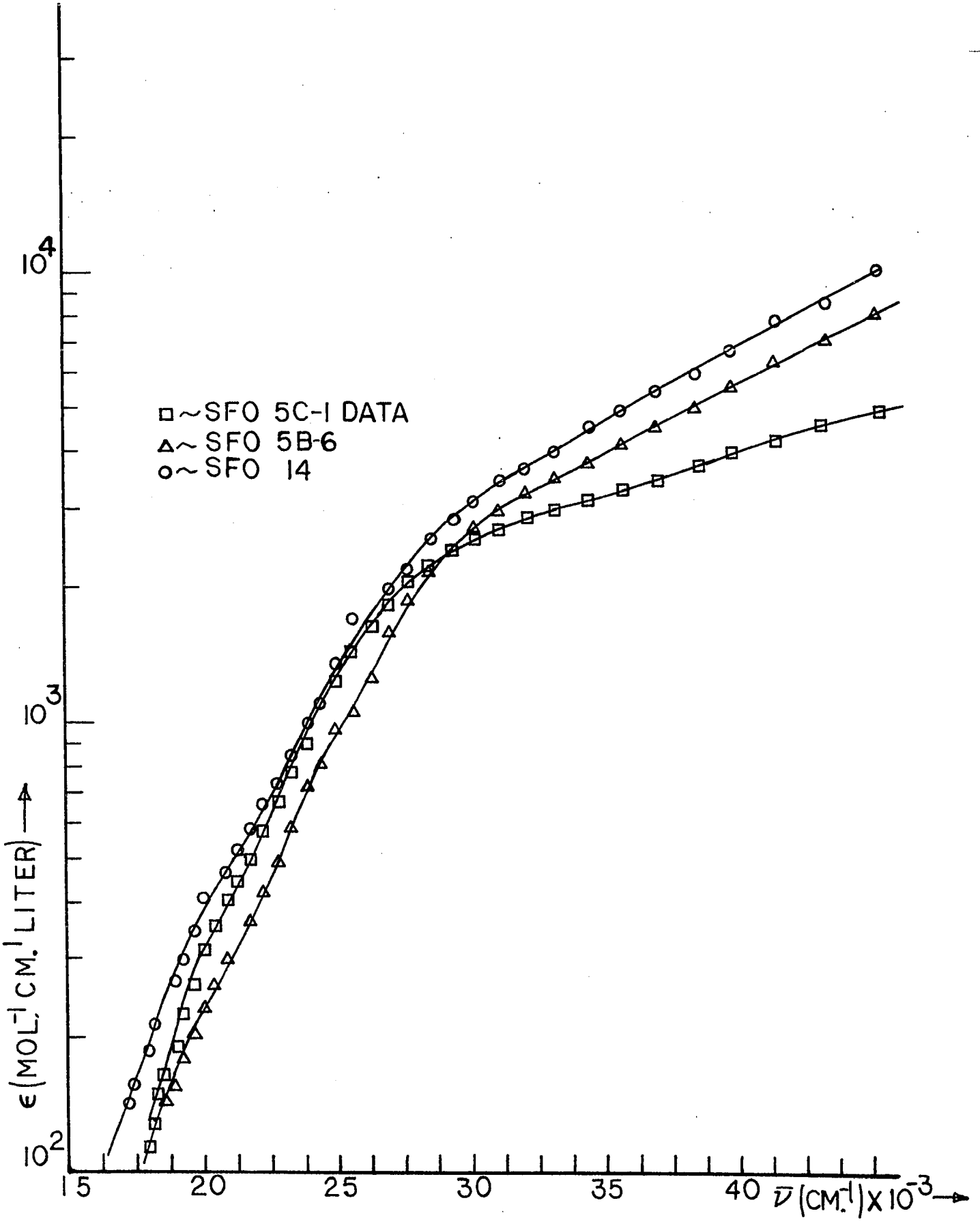

Figure 27. Extinction coefficients of SFO's #5C-1, #5B-6 and #14.

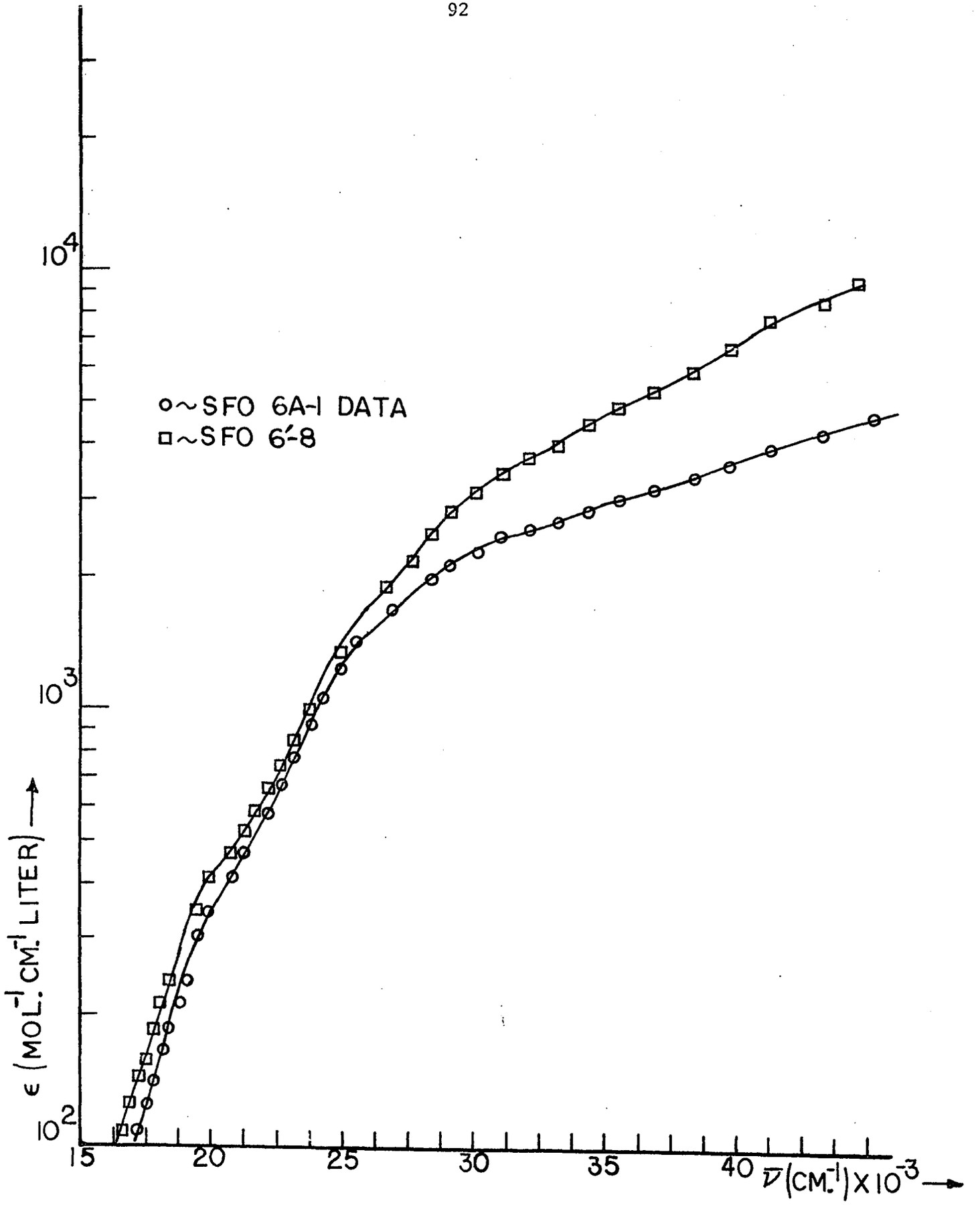

Figure 28. Extinction coefficients of SFO's #6A-1 and #6'-8.

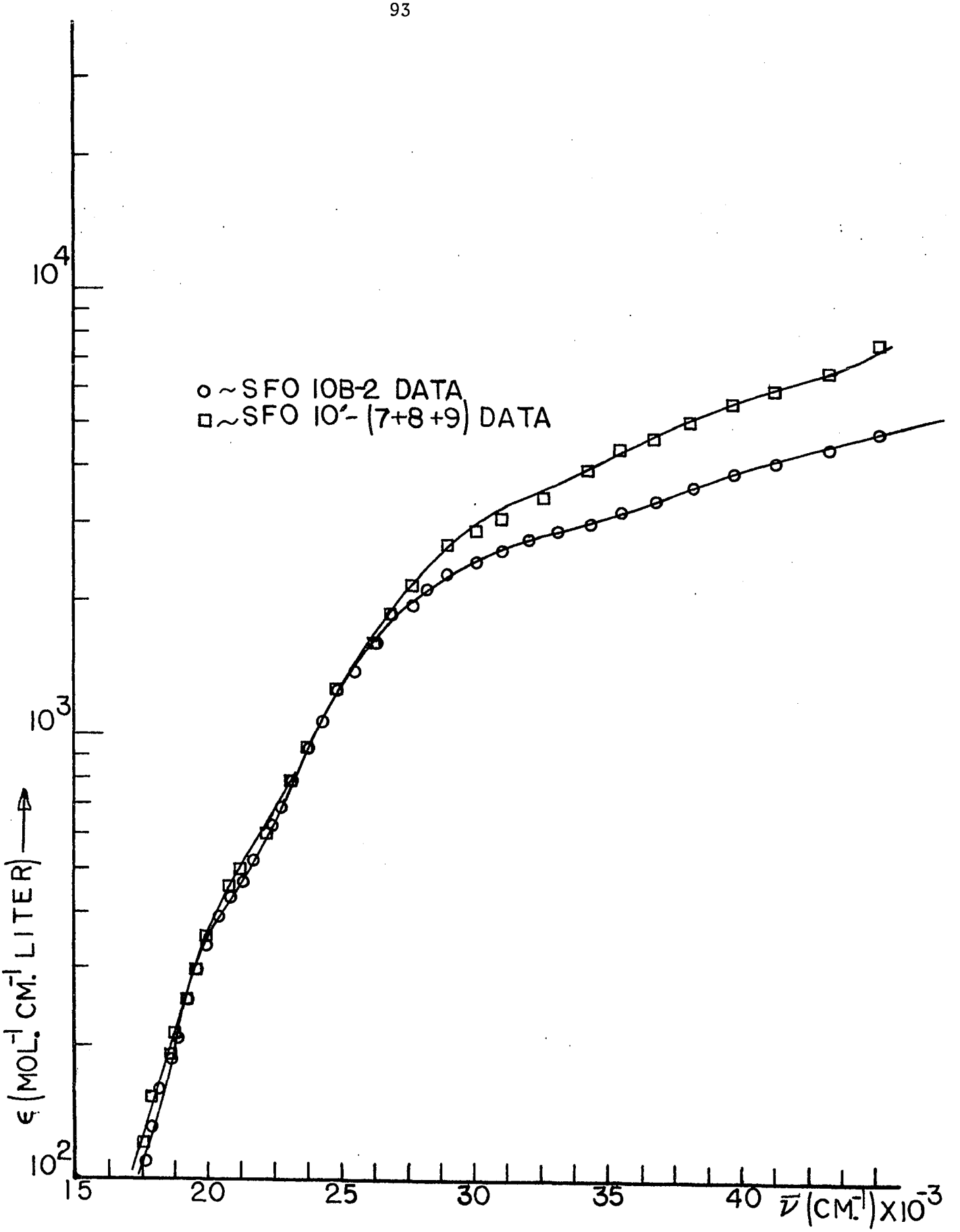

Figure 29. Extinction coefficients of SFO's #10B-2 and #10'-(7+8+9).

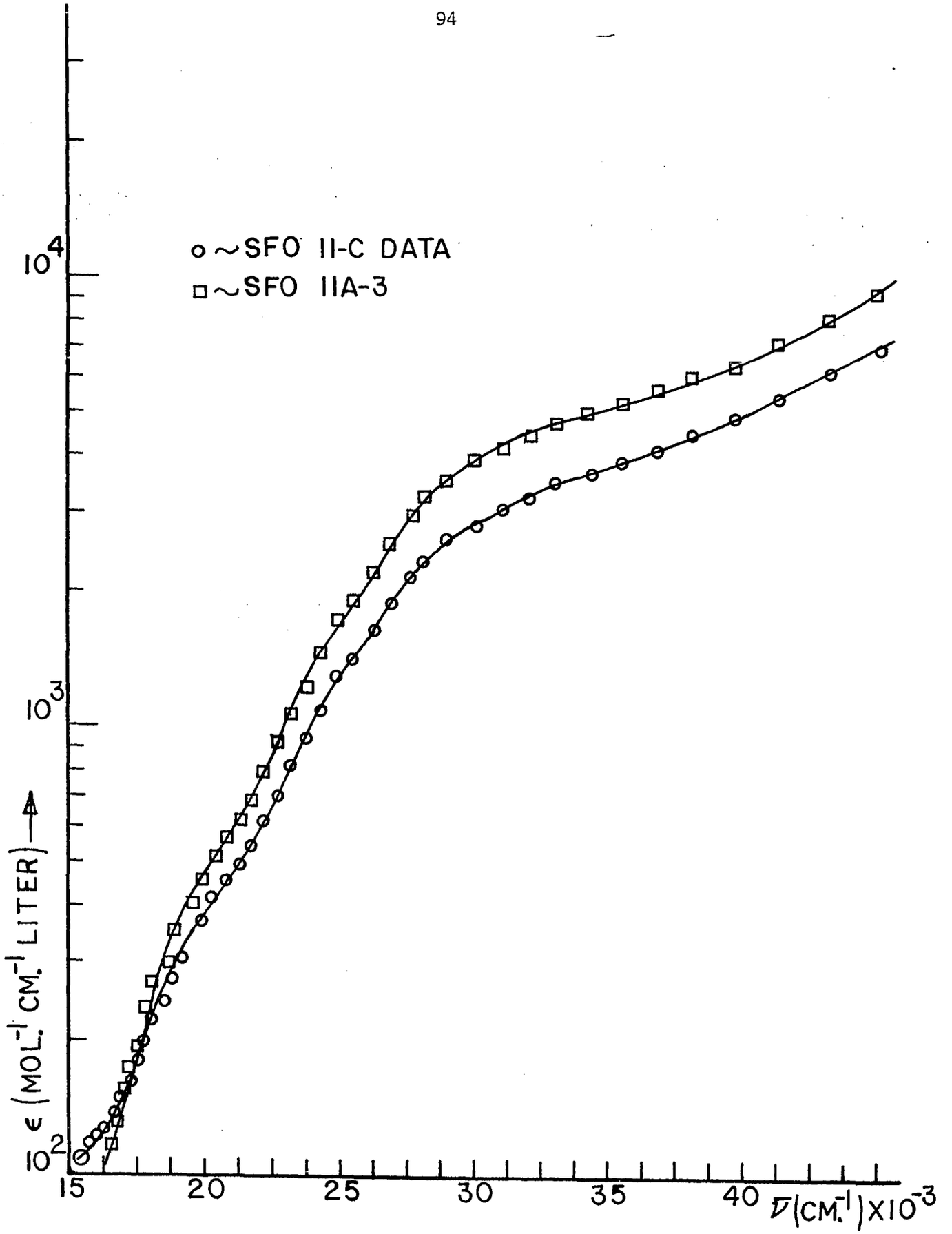

Figure 30. Extinction coefficients of SFO's #6a_1 and #6'-8.

Table 10. Oscillator Strengths

Sample	$\bar{\nu}_1$	$\bar{\nu}_2$	$\bar{\nu}_3$	$f(\bar{\nu}_1 \rightarrow \bar{\nu}_2)$	$f(\bar{\nu}_2 \rightarrow \bar{\nu}_3)$
$Fe(OH)_3$	$15x10^3$	$27.5x10^3$	$50x10^3$	.03	2.02
5C-1	15	27.5	50	.04	0.37
5B-6	16.3	29.3	48	.04	0.48
6A-1	14	27.0	50	.03	0.31
6'-8	15	27.5	45	.04	0.66
10B-2	15	27.8	47.8	.04	0.36
10'-(7+8+9)	15	28.8	47.8	.04	0.56
11A-3	10	28.	48.5	.01	0.64
11-C	10	28.8	50.	.05	0.47
14	15	28.5	45.3	.05	0.62

Note that the oscillator strengths of the SFO's also reflect the classification in Table 10 above. The oscillator strengths can be used in the calculation of the magneto-optic rotation.

The sum of the oscillator strengths for all the transitions originating in one particular level, including the transitions to the lower states with a minus sign, obeys the following relation[16]

$$f = \text{total number of electrons} \tag{36}$$

$$= 5 \text{ for ferric ions.} \tag{37}$$

Thus from Table 10 we see that for the SFO's the contribution to the oscillator strength in the region of observed wavenumbers is only about 10 per cent of the total oscillator strength. This simply means that the strong UV band extends further into the far UV region. We were not able to observe this region because of the optical limitation of the instruments used.

The $Fe(OH)_3$ oscillator strength is considerably larger - almost 40 per cent of the total. For $Fe(OH)_3$ we are observing a greater fraction of the UV at wavenumbers below 50,000 cm^{-1}.

REFERENCES

1. Beckman Instruments Company, Fullerton, California.
2. *Ibid.*
3. Gamlen, G. A. and D. O. Jordan, Jour. Amer. Chem. Soc. 156, 1435 (1953).
4. Ballhausen, C. J., Intro. to Ligand Field Theory (McGraw-Hill Book Company, Inc., New York, 1962)p. 226.
5. Jörgenson, C. K., Acta. Chem. Scand. 8, 1495 (1954).
6. Orgel, L. E., Jour. Amer. Chem. Soc. 23, 1004 (1955).
7. Griffith, J.S., Theory of Transition Metal Ions (Cambridge Univ. Press, Cambridge, 1961) Chap. II.
8. Ballhausen, C. J., *loc. cit.*
9. *Ibid.*
10. McClure, D. S., Solid State Physics 8, (Academic Press, New York, 1959).
11. Mulay, L. N. and P. N. Selwood, J. Amer. Chem. Soc. 77, 2693 (1955).
12. Gamlen, G. A. and D. O. Jordan, *loc. cit.*
13. Rabinovitch, E., and W. H. Stockmayer, J. Amer. Chem. Soc. 64, 335 (1942).
14. Mulay, L. N. and P. N. Selwood, *loc. cit.*
15. Mulliken, R. S. and C. A. Rieke, Repts. Prog. Phys. 8, 231 (1941).
16. *Ibid.*

CHAPTER V

RELATED EXPERIMENTS

Electron Microscope Results

We chose six different SFO's for this study. Four of these were known from other data to consist of large particles. The other two samples were supposed to contain smaller sized particles. With the experience and facilities of the OU Medical Center the task of taking the photographs became quite simple. Mr. Warren Stinson is due our thanks here. Mr. Stinson became interested in these iron samples from the point of view of tissue staining.

A brief description of the procedure followed may be given. First aqueous solutions of the SFO's were prepared. Next the copper, open metal "grids" for the electron microscope were covered by coating them with Formvar[1]. After the Formvar had dried the grids were dipped into the solutions of the SFO's and then they were again allowed to dry. Next the grids were placed into an RCA model electron microscope. The various "frames" in the grids were scanned until one was found that showed good contrast between background and particles. Three photographic plates were then exposed and from these we analyzed the particle sizes. Great care was taken before any plates were exposed to insure

that the photographs would contain particles similar to those found in the other frames, hence typical for the specimen. Figure 31 is a print of one of the plates obtained by the method above.

The electron microscope was equipped with a special high magnification unit which raised the magnification to 101,500. This was used for all the plates. Note that the prints in Fig. 31 depend upon further photographic enlargement and hence are magnified more than 101,500.

In the SFO's the ferric complexes are stabilized by the addition of various types of organic polymers. These polymers are usually dextrins - a particularly long chain molecule consisting of glucose rings. We used a typical pure dextrin - corn dextrin - as a blank check on the electron microscope performance. Again the same techniques were used to prepare the grids. However, even at the highest magnification we never observed "particles" of the type found in the SFO plates. Evidently, the electron density of the polymers was so small that the organic polymers were not visible in this preparation. Hence, in the SFO's we should see only the ferric complexes because the electron density at the iron sites is considerable, since a large number of electrons is associated with the small ion. For example, Fe^{3+} has 53 electrons and the radius is 0.60 Angstrom whereas constituents of the polymers - $\{C, (OH)^-, H^+, O^{2-}\}$ -all have larger diameters and/or far fewer electrons.[2]

Hence the particles which are visible in the SFO plates are attributed to the ferric complexes. It is precisely these complexes that we examined with the magnetic techniques. A platform was built for holding the plates during examination. The platform includes bottom

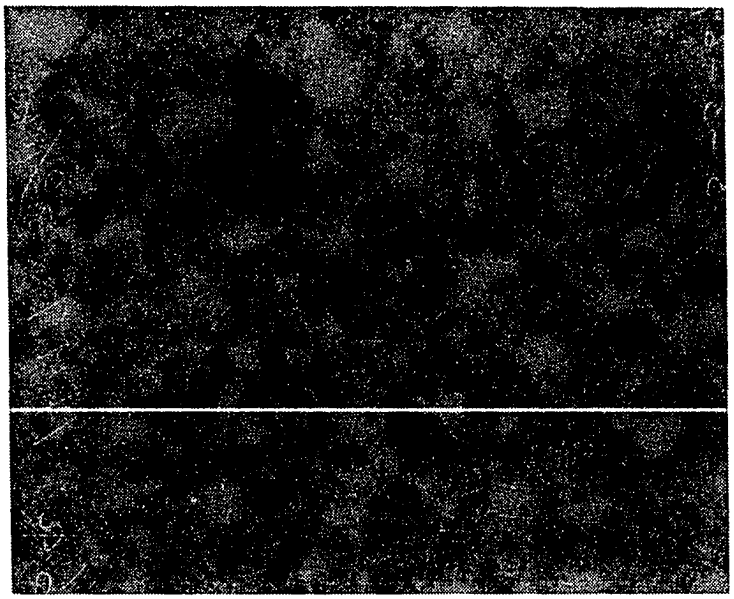

SFO #6A-1

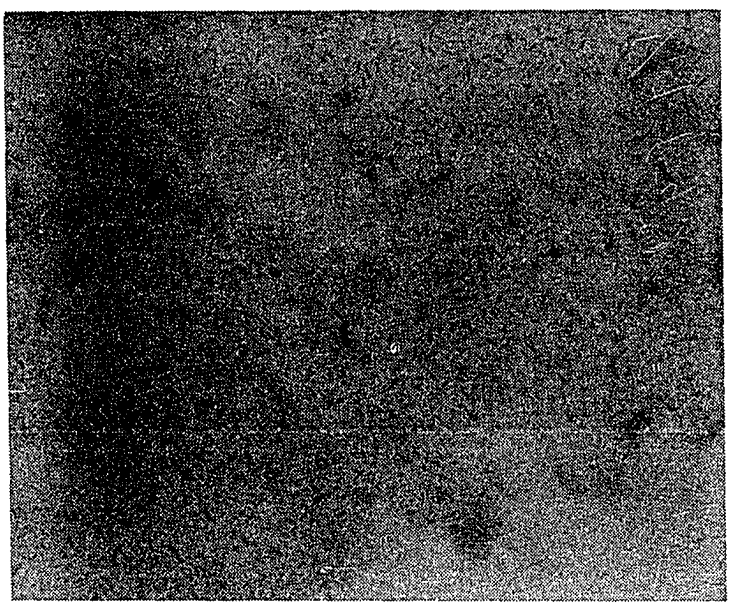

SFO #14

Figure 31, Photomicrographs of some SFO's.

illumination of the plates and a microscope equipped with a standard eyepiece. The microscope provided some magnification but most importantly it allowed the use of the filar attachment which permits size measurements without parallax. Normally about thirty different particles were measured on each plate. For all but SFO #14 the particles appeared approximately spherical. Hence only one number - the diameter - can characterize the particle size. For SFO #14 the length and width of the particles was measured. Of course, the true size of the particles had to be calculated considering the electron microscope magnification as well as the magnification of the eyepiece.

A summary of the results is given in Table 11 along with the data obtained from X-ray diffraction.[3]

Table 11. Comparison of Particle Size Data.

ELECTRON MICROSCOPE DATA					X-RAY DATA	
SFO	$\bar{D}_1$	σ_1	$\bar{D}_2$	σ_2	D_1	χ
6A-1	45Å	15Å			42	$30,500 \times 10^{-6}$ cgs./gram.
10A-1	31	8			34	7,900
5-1	23	5			22	195
11A-2	20	4			18	175
11-9	16	3			n.a.	122
11-15	14	2			n.a.	12
14	152	17	49	11	>69Å	43

In the table $\overline{D}_1$ is the average particle diameter - or length in the case of SFO #14 - and $\overline{D}_2$ is the average width of the particles of SFO #14. σ_1 and σ_2 are standard deviations of D_1 and D_2, respectively.

In our interpretation of the numbers found, several points should be stressed. When the SFO samples were fractionated with the Sephadex column it was found chemically that the heavy fractions, like 5-1, 6A-1, 10A-1, had the largest per cent iron content. Also the magnetic susceptibilities were found to be large for the heaviest fractions and small in the lightest fractions of the particular SFO. This suggested that in the heavy fractions the iron complexes exist in large domains. These exhibit cooperative effects like those observed in ferromagnetism. Similar behavior has been observed in polycrystalline iron and is often referred to as superparamagnetism.[4] Each domain moment behaves like a magnet subject to heat motions.

The electron microscope data indeed bear out our initial assumptions about the particle sizes, i.e. the largest particles have the largest susceptibilities. Only for #14, an extremely small susceptibility value occurs. This must be due to the fact that the ferric ions are antiferromagnetically aligned. It is simply a different ferric complex and not a discrepancy of our model otherwise. The three fractions of SFO #11 also show that the particle sizes are largest in the heaviest fractions.

Next it should be pointed out that the standard deviations "σ" are a reflection of the distribution of particle sizes. This is especially important in SFO #10A-1 and 6A-1. In these one can observe a relatively broad distribution of particle sizes on first sight. This is probably due to the method of preparation of these SFO's.

One can draw an interesting conclusion by comparison of the data obtained by the X-ray and electron microscope methods. In principle the X-ray method measures the crystal size whereas the electron microscope measures the particle size be it crystalline or random. So it should hold that

$$D_{X\text{-}RAY} \leq D_{E.M.}$$

Now we notice for the first four SFO's that within the experimental error the two methods give the same results for the particle sizes. Hence, the ferric complexes seem to be single microcrystals.

Other evidence for this conclusion comes from electrical resistance data on SFO #5C-2 which is very similar to #5-1. Its resistance can only be accounted for by using microcrystals similar to Fe_3O_4. Likewise, the antiferromagnetic alignment of SFO #14 suggests the presence of a regular structure within the ferric complex.

EPR Measurements

Information concerning the ground state of the iron in the ferric complexes can be obtained by measuring the absorption in the microwave region. With a Varian type 4502 EPR equipped with a 100 KC modulation unit we measured the "g-values" of the SFO's. Our thanks to Mr. Robert DeKinder, who made the actual runs for us on the EPR equipment. The values of g are determined by sweeping the magnetic field at a fixed microwave frequency and observing the position of the maximum absorption. At this position the following equation holds.

$$E_2 - E_1 = h\nu = g_{eff.}\mu_\beta H_R \qquad (38)$$

where

$E_2 - E_1$ = energy difference of two atomic states

ν = microwave frequency

μ_B = Bohr magneton

H_R = value of magnetic field at maximum absorption

The frequency ν and field H_R are read from the instrument. Together with the constants μ_B and h, "$g_{eff.}$" for the particular SFO then can be calculated.

The microwave absorption observed was all of the "broad band" type. This is probably related to the polycrystalline nature of the samples and to the interactions between the iron atoms. The experiments were performed at room temperature.

A brief explanation of the phenomenon involved can be based on the work of Meijer.[5] Considering for the moment free ferric ions the ground state is ^6S. This follows from Hund's Rule for five (5) 3d electrons. The degeneracy of the ^6S level for free ferric ions is removed by the electric field of the surrounding atoms. However, the ^6S level is unique in that the angular momentum is zero. Thus the spin-orbit perturbation is zero in the first order and of course since L = 0 there is no "quenching" of the angular momentum.

Meijer shows that in a magnetic field H the energy levels for $(Fe)^{3+}$ are given by

$$\begin{aligned} E_{\pm 5/2} &= \{\pm 5\mu_B + a/2 \pm (90c^2/8 + 5a^2/16)/2\mu_B H\}H \\ E_{\pm 3/2} &= \{\pm 3\mu_B + 3a/2 \mp (15c^2/14 - 5a^2/16)/2\mu_B H\}H \\ E_{\pm 1/2} &= \{\pm \mu_B + a \mp 3c^2/2\mu_B H\}H \end{aligned} \qquad (39)$$

where the "a" terms are due to nearly cubic electric fields of the surrounding atoms and the "c" terms are due to the trigonal electric field component.

The energy difference ΔE for the five allowed transitions are found from Eq. (39) to be

$$\begin{aligned} (\Delta E)_{5/2\to 3/2} &= 2\mu_B H \pm 2a + (15c^2)/2\mu_B H \\ (\Delta E)_{3/2\to 1/2} &= 2\mu_B H \mp 5a/2 + (5a^2/16 - 3c^2/4)2\mu_B H \\ (\Delta E)_{1/2\to 1/2} &= 2\mu_B H - 6c^2/2\mu_B H \end{aligned} \qquad (40)$$

Considering that the experiment shows a broad line we are interested only in the average value of (ΔE), we get from Eq. (40),

$$\overline{(\Delta E)} = \{2\mu_B + [(4\ 5/2)c^2 + 10a^2/16]/10\mu_B H\}H \tag{41}$$

Using the Eq. (38) defining $g_{eff.}$ and Eq. (41) above, we find

$$g_{eff.} = 2 + [(4\ 5/2)c^2 + 10a^2/16]/20(\mu_B H)^2. \tag{42}$$

The constants "a" and "c" are best determined by experiment. Meijer gives the values as

$$\begin{aligned} |a| &= 0.0128\ cm^{-1} \\ |c| &= 0.016\ cm^{-1} \end{aligned} \tag{43}$$

Thus for ferric ions placed in the field used by us, $\mu_B H = 0.2\ cm^{-1}$, it follows from Eqs. (42) and (43) that

$$g_{eff.} = 2.01. \tag{44}$$

In general, crystalline field effects tend to broaden the absorption lines, and tend to shift g to a slightly higher value.

Experimentally, we found the values for $g_{eff.}$ as given in the Table 12. Indeed, these tend to exceed the g = 2 value, and are nearly equal to the value predicted by theory in Eq. (44).

Table 12. $g_{eff.}$ Values Obtained by EPR Measurements.

$g_{effective}$	Compound
2.03	$Fe(NH_4)(SO_4)_2 \cdot 12H_2O$(ferric)
2.09	SFO #11-13
2.04	SFO #11-5
2.04	SFO #5C-2
1.99	SFO #14
2.21	$Fe(NH_4)_2(SO_4)_2 \cdot 6H_2O$(ferrous)

This data established that the electronic ground state of the iron is closely akin to that of Fe^{3+} (ferric ions). The $g_{eff.}$ obtained for a ferrous compound $Fe(NH_4)_2(SO_4)_2 \cdot 6H_2O$ was also measured for comparison, see Table 12. Its value 2.2 strongly exceeds 2.0. The ground state of Fe^{2+} is ^5D and hence, unlike Fe^{3+} the angular momentum is not zero. It directly contributes to the g value.

Effect of Pressure on the Resistance

In general one can write for the conductivity

$$\sigma = ne\mu \tag{45}$$

where the carrier density n is determined by the thermal excitation of the electrons into the conduction band, and the mobility μ depends upon

the various scattering processes in the bulk of the sample or between the micro crystals. This was already pointed out in the discussion of the temperature dependence of the conductivity.

Because the current-voltage characteristic is not linear, a barrier to electron conduction exists in the specimen as well. The electronic-sample connection makes only a minor contribution here. Therefore, the interfaces inside the specimen must present barriers, electron "tunneling" could occur. This should be strongly pressure dependent.

We picture our samples as ferric complexes of various sizes, separated by a few glucose polymer chains. The resistance of the pure polymer by itself is orders of magnitude larger than that of the iron oxides. Now on application of pressure to an SFO the organic chains will deform so that the distance between the ferric complexes becomes less. This should produce a lower sample resistance. In order to test this pressure dependence at various temperatures a pressure cell was built. We used conical shaped plugs sealed with epoxy to make the electrical connections. This held a pressure of 3 kilobar at 150 °C, while its leakage resistance was greater than 10^7 ohms. A standard hydraulic pump capable of 40,000 psi generated the pressure in the cell. An oil bath and measuring instruments similar to that described in Chapter III was again used.

In our experiment we indeed do observe a significant resistance decrease. However, a relaxation phenomenon in the opposite direction occurs hereafter. This process is sketched in Fig. 32. A

summary of the pertient data from this figure is given below in Table 13.

Table 13. Resistance Relaxation Data for SFO #5A-4.

	$\lim_{t\to\infty}(R/R_o)$		Time Constant (Sec.)	
	P = 1.35 KBAR	After release	1.35 KBAR	After release
T = 25 °C	1.20 ± 005	0.991	175	100
T = 131°C	1.278	1.01	118	112

After the pressure is applied the resistance initially decreased, but then it slowly "relaxes" till the resistance becomes equal to - or even greater than - the resistance at ≈1 atm. On release of the pressure the reverse situation occurs. This type behavior had been observed before in the SFO's for the magnetic susceptibility as a function of pressure.[6] In those studies the time constant was found to be 15-30 seconds. In the resistance measurement the time constant is 60-120 seconds. The results can be explained by assuming that the sample does at first compress uniformily. The distances between atoms decrease and hence the resistance. Thereafter, a viscous type rearrangement takes place, more rapidly at higher temperatures. This could mean that the microcrystalline structure is slowly being distorted, perhaps mostly on the outside. In principle this would be possible for the gellike hydrous ferric oxides. It should give rise to a decreased mobility. However,

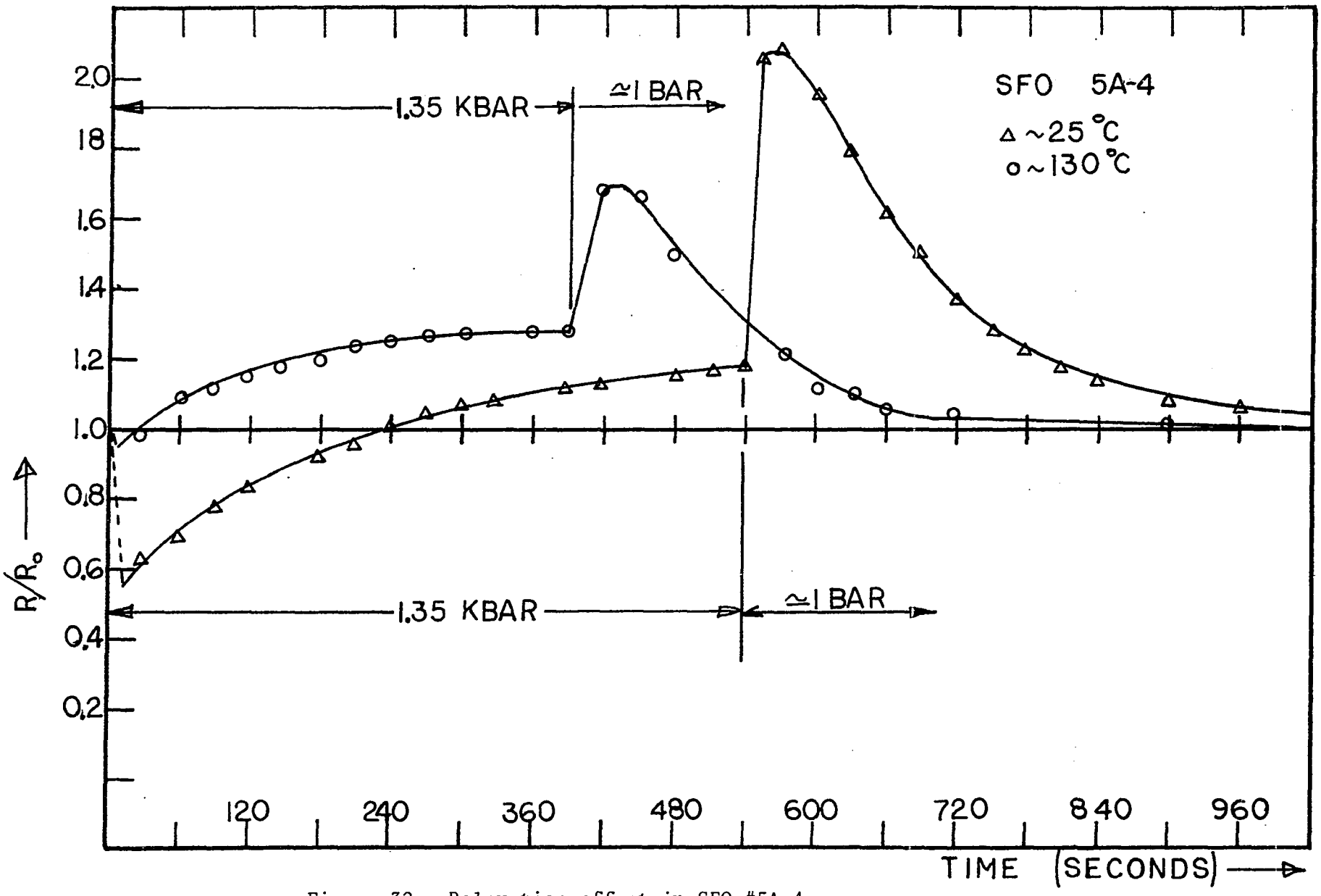

Figure 32. Relaxation effect in SFO #5A-4.

it is also possible that oil slowly penetrates into the specimen and thus releases the interparticle stresses. This will again separate them and give rise to the increase in resistance. Further work is needed here to determine the exact causes of this phenomenon.

In Fig. 33 the resistance of SFO #5A-4 as a function of temperature has been plotted. This has been given at ≈1 bar, 0.34 and 1.35 kilobars. The data plotted are for the extrapolated initial change in the resistance observed on application of the pressure. This we assume to be a measure of the change in polymer length, or distance between microcrystals and hence the change in "tunneling". Evidently, these changes are quite large. For instance the change is 55 per cent between 1 bar and 1.35 kilobar at 52.5 °C.

However, one also sees that the activation energy - determined by the slope of R vs 1/T changes only 7 per cent from atmospheric to 1.35 kilobar. This shows that the number of electrons for the conduction which is a function of the activation energy-(and hence the slope of R versus 1/T)-is little affected by the pressure. The mobility of these electrons is determined, however, by the distance between the ferric complexes. This distance is determined by the polymer and hence sensitive to pressure. This dependence of the mobility on pressure makes the conductivity a function of pressure as can be seen in Eq. (45). The "dip" at $10^3/T = 2.6$ is most likely due to a measurement error.

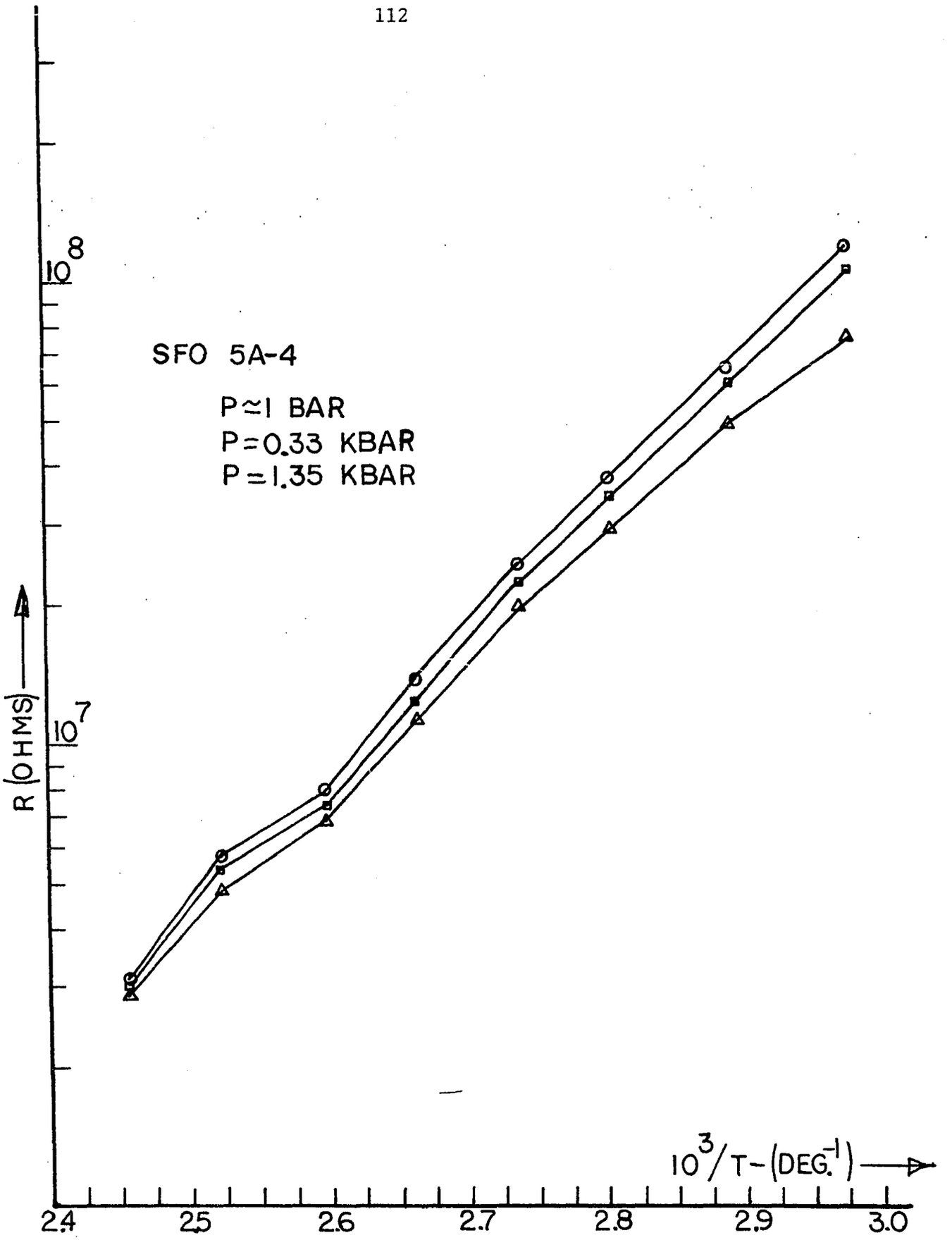

Figure 33. Temperature dependence of the resistance of SFO #5A-4 at several pressures.

Photoconductivity

An attempt was made to determine the energy levels - or possibly band edges - in the SFO's by studying photoconductivity. Thus at frequencies at or near that corresponding to the difference in energy between the ground and an excited level - or band - we should observe an increase in conduction. The electrons which are excited into the upper level have a greater mobility than those in the ground state. The optical absorption coefficients of the SFO's are large in the visible and IR and hence we did expect to observe some photo effect.

Our experimental setup is quite simple and is pictured schematically below.

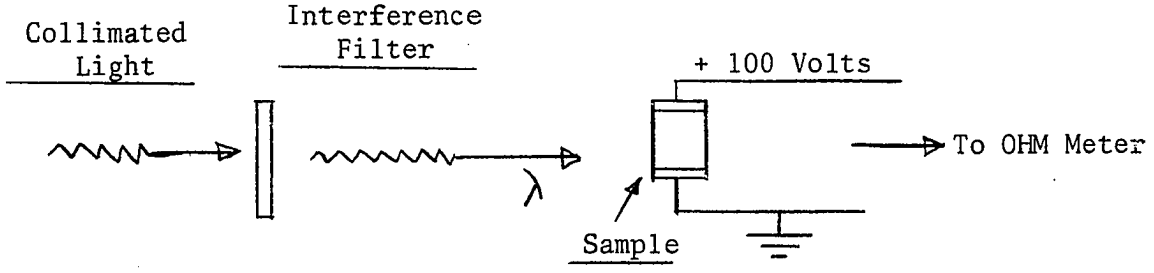

We attempted to observe photoconductivity at room temperature (25±3 °C) and also at liquid nitrogen temperature (77 °K) by immersing the sample in a partially silvered dewar. Data were taken at wavelengths of 0.4 microns to 1.7 microns.

No results were found that could positively be identified as photoconduction. At room temperature resistance changes of the order of 1 per cent between the "dark" and "illuminated" sample resistance

were observed. However, it is believed that this is due to increased conduction because of localized heating of the sample by the light, since no such affect was observed at 77 °K. The photo process then is not too productive in exacting electrons. The bulk of the conduction electrons then must originate in the thermal excitation. Quite probably the penetration of the light is not sufficient and the photo electrons are immediately trapped at the surface. It should also be kept in mind that the lifetime of the electrons in the conduction band is rather small. Of course, we are aware that the effect may be smaller than our limit of measurement. This sensitivity was about ±0.1 per cent resistance change.

REFERENCES

1. Shawinigan Products Corp., 350 Fifth Avenue, New York 1, New York.
2. Kittel, C., Intro. To Solid State Physics, 2nd Ed. (John Wiley and Sons, Inc., New York, 1961) pp. 82-83.
3. Wilson, D., M.S. Thesis (in preparation) University of Oklahoma, Norman, Oklahoma, 1968.
4. See, for example, Bates, L. F., Modern Magnetism (Cambridge Univ. Press, 1963) pp. 293-294.
5. Meijer, P., Physica 17, 899 (1951).
6. Wilson, D. M., *loc. cit.*

CHAPTER VI

THIN FILMS

Introduction

In order to obtain insight in the ferromagnetic contribution we examined the Faraday rotation of pure metal films of iron, cobalt, nickel and copper. All data were taken at room temperature, 23±2 °C, and for several wavelengths in the visible from 436 mμ to 685 mμ. The metal films were produced by vacuum evaporation on to cover slips. The thickness of the films have been measured. The transmission coefficients are 0.5 to 10 per cent for the wavelengths used.

Equipment

A standard type vacuum system was used for the evaporation of the films. A schematic diagram is given in Fig. 34.

The diffusion pump was connected to the baseplate by a short 2" diameter tube so that a high pumping speed could be maintained. The diffusion pump[(1)] had a pumping speed of 200 liters sec. at 10^{-5} Torr. This was sufficient to hold the pressure below 10^{-4} Torr during the evaporation. The vacuum valve made it possible to remove finished slides and reload without turning the diffusion pump off.

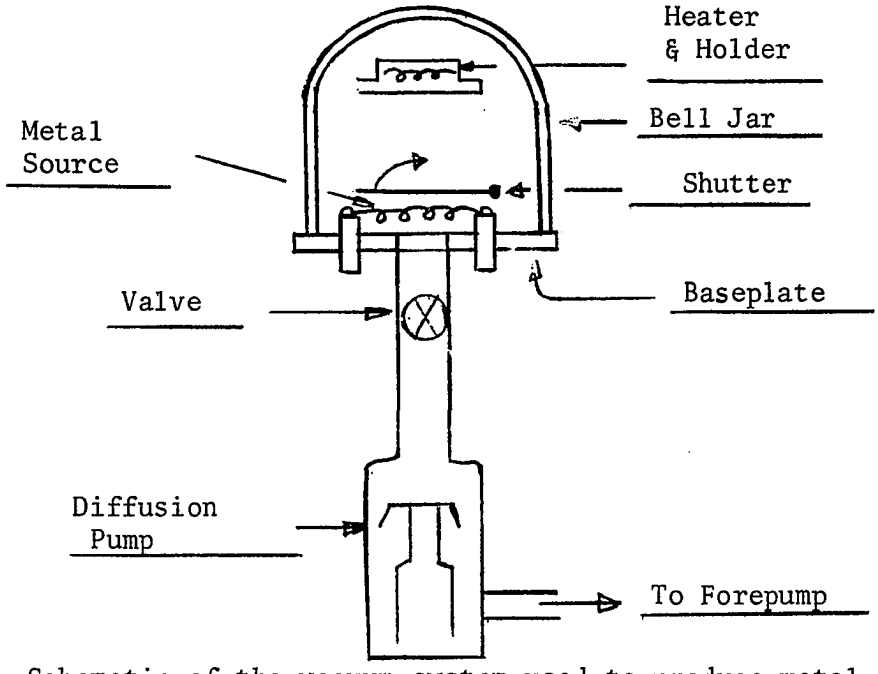

Figure 34. Schematic of the vacuum system used to produce metal films.

The diffusion pump is silver soldered to the baseplate. The baseplate has inserts for a thermocouple and a Phillips ionization gauge measuring the pressure. There are also a rotary feedthrough, actuating the shutter, and six current plugs. Four of these were for low current, approximately 10 amperes. They were isolated from the baseplate by a high resistivity epoxy[2] with a leakage resistance of better than 10^{14} ohms. The other two high current leads are used as the evaporation source leads.

The metal source consisted of four braided strands of .015" tungsten wire wound in a spiral of about 3/8" diameter. The metals to be evaporated were cut into strips about one fourth inch long and crimped onto the spiral. Crimping the wires onto the tungsten provided for a good heat transfer and consequently all metal melted at the same

time. This was necessary because nickel and cobalt will eventually alloy with the tungsten causing the filament to fail.[3] This crimping procedure as well as the cleaning and electropolishing[4] of the tungsten wire made it possible to do an entire evaporation in less than two minutes. And none of the filaments failed. The short evaporation time also resulted in purer films since fewer residual gas atoms could strike the substrate surface during deposition.

Most of the metals used as source were of high purity. A list of the suppliers and purity are:

Metal	Supplier	Purity
Nickel	A. D. Mackay Company	99%
Copper	Electronics Space Prod.	99.999%
Iron	Unknown	Unknown
Cobalt	Alfa Inorganics Company	99.7%

The substrates were microscope cover slides, 0.865" square and .010" thick. These were cleaned with a standard cleaning solution[5] and washed in distilled water. After drying they were placed in the bell jar and baked by the heater for approximately 30 minutes at about 200 °C. Then the slides were allowed to cool. Evaporation onto cold slides should decrease the strain set up in metal films that are evaporated onto hot substrates. The adhesion of the films did not seem to be diminished by evaporating onto cold substrates.

After the films had been prepared in the vacuum system, they were stored in a vacuum dessicator jar. No gross deterioration of the films has been observed except for the copper films. For the copper films we measured the Faraday rotation within an hour after the films were produced.

Thickness Measurement

The thickness of the films was measured by the method of Fizeau fringes as described by Tolansky.[6] This method does not depend upon physical properties of the films such as its index of refraction, density, etc. Because in thin films these properties do not have the bulk values it was felt best not to use a method that deponds upon these.

A schematic diagram of the optical system is shown in Fig. 35.

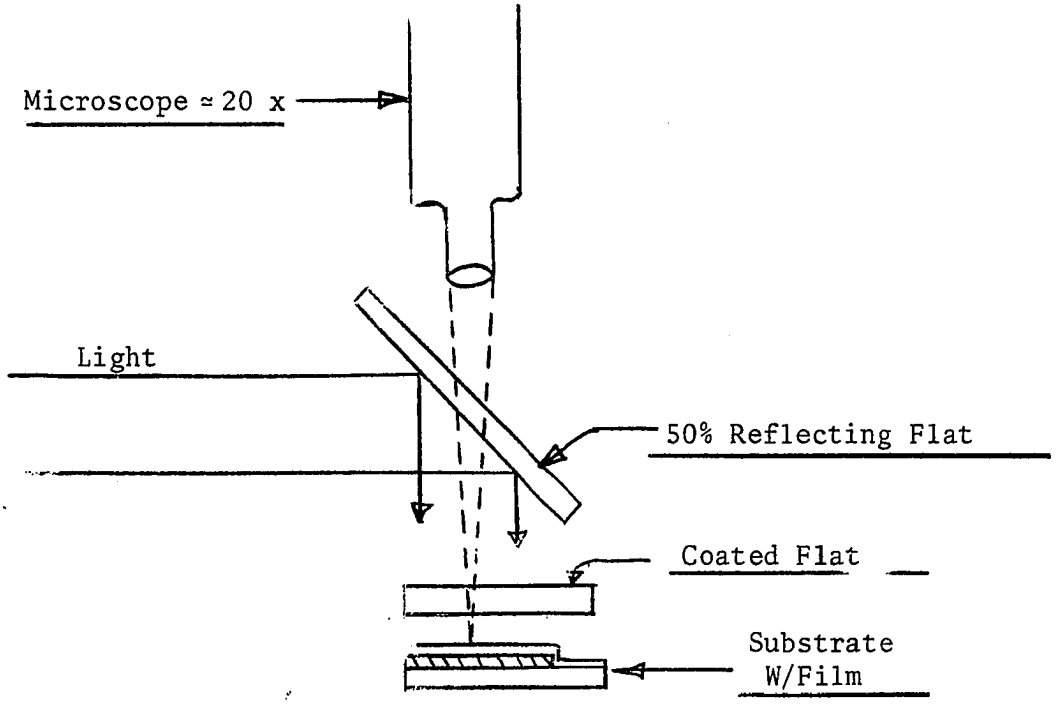

Figure 35. Schematic of apparatus used to measure thickness of the metal films.

The metal film does not cover the entire substrate so that a "step" exists at the edge of the metal film. The height of this step is to be measured. Therefore, the entire substrate is covered with a

layer of evaporated aluminum so that the film is ≃ 100 per cent reflecting. The optical flat is coated until it is about 95±3 per cent reflective. This high reflectivity is important in order to keep the fringe width as narrow as possible. See Tolansky. The optical flat is then brought close to the film, with its plane inclined to that of the film and a fringe pattern is set up with the fringes running perpendicular to the step in the film. In this case a fringe pattern will be observed as is indicated in the diagram below.

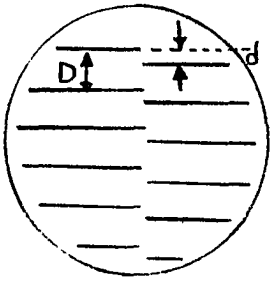

Evidently the film thickness "t" is given by

$$t = (d/D)\lambda_D$$

where λ_D is the wavelength of light used, (5890Å), while d and D are the measured distances indicated above.

With this technique it is possible to measure thickness of films the order of $\lambda/1000$ thick. But it is extremely important that all of the following conditions are met

1) The mirror on the flat must be 95±3 per cent reflecting.
2) The optical flat and film to be measured must be brought together to within about one wavelength.
3) The light source must be monochromatic.

The thickness of the films determined by this technique and used in the measurement of the Faraday effect are given in Table 14.

Table 14. Thickness of Films Used in the Study of Faraday Rotation.

Film	Thickness
Cobalt	900±150 Å
Iron	780±50
Nickel	1180±180

Faraday Effect Data and Analysis

The Faraday effect has been measured at 436 mμ, 478 mμ, 515 mμ, 546 mμ, 585 mμ, and 661 mμ. The results for T = 23±2 °C are displayed in Figs. 36 through 42. It was necessary to substract the rotation of the substrate. The rotation of the film, Θ_0, is given by

$$\Theta_0 = \Theta - \alpha,$$

where Θ is the rotation of film and substrate, while α is the rotation of the substrate. The Verdet constant, V, of the film then is

$$V = (\Theta_0 - \alpha)/H\ell$$

where Θ and α are expressed in degrees of arc, H is the external magnetic

field in gauss, and ℓ is the film thickness in cm. Figures 36 through 38 show the dependence of the rotation Θ_0 upon the external magnetic field H. In these curves the rotation was measured for both increasing and decreasing values of H. The rotations were also measured on reversing H. There is some hysteresis in the rotation for the three ferromagnetic films of cobalt, iron, and nickel. Comparing the two field direction in the case of nickel there is at most a difference of 20 per cent. In the other ferromagnetics and copper it is less.

Except for nickel, the ferromagnetics do not saturate at the fields used. But they do in all cases for fields of 90 kilogauss. At small values of H, Θ_0 is essentially proportional to the external field at all wavelenghts. The rotation of nickel is also proportional to H well below the saturation value.

To explain the dependence of the rotation on the magnetic field in ferromagnetics several theories have been proposed. Argyres'[7] theory explains the ferromagnetic rotation on the basis of a band model. He considers a particular domain. Thus the role of the magnetic field is simply to align the domains. His theory is best applied to bulk ferromagnetics. A somewhat qualitative theory proposed by Stoner and Wahlforth[8] considers this aspect of the magnetization in thin films. They take into account the demagnetization and crystalline field effects.

We shall consider this theory as far as it applies to the magnetization of our films. For thin films the magnetization vector tends to lie in the film plane. Hence, the magnetic field H which is always

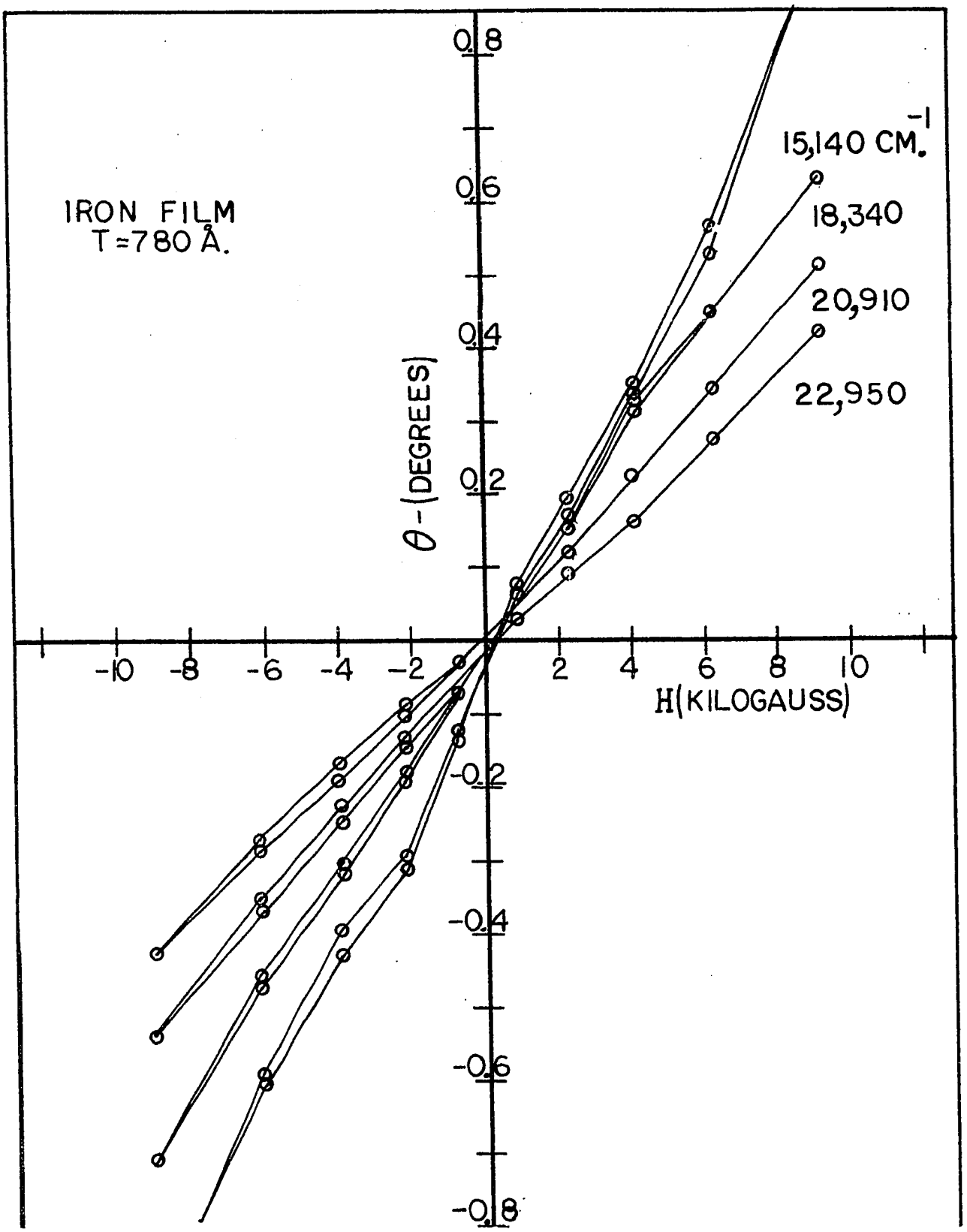

Figure 36. Faraday rotation of thin iron film as a function of magnetic field.

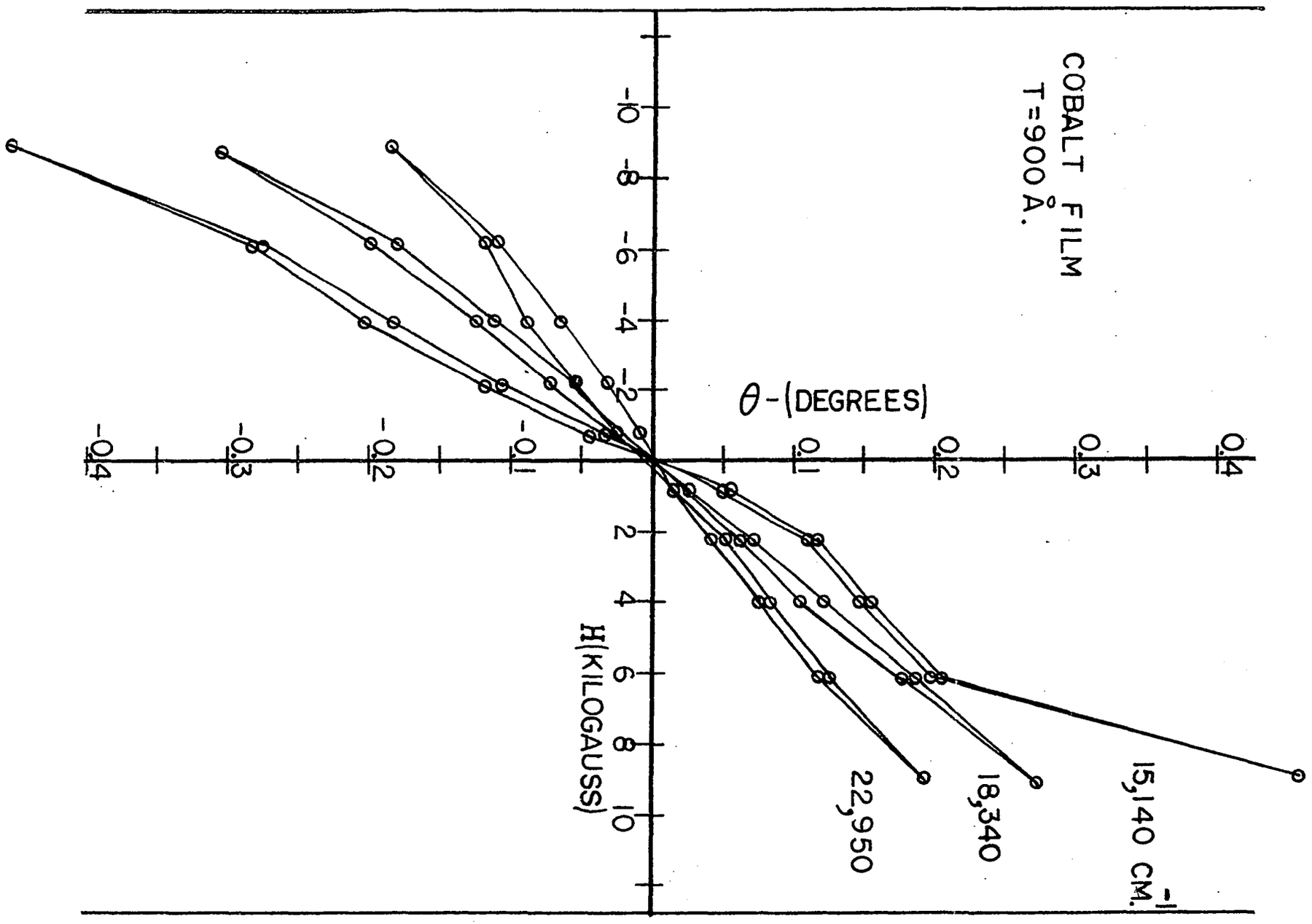

Figure 37. Faraday rotation of thin cobalt film as a function of magnetic field.

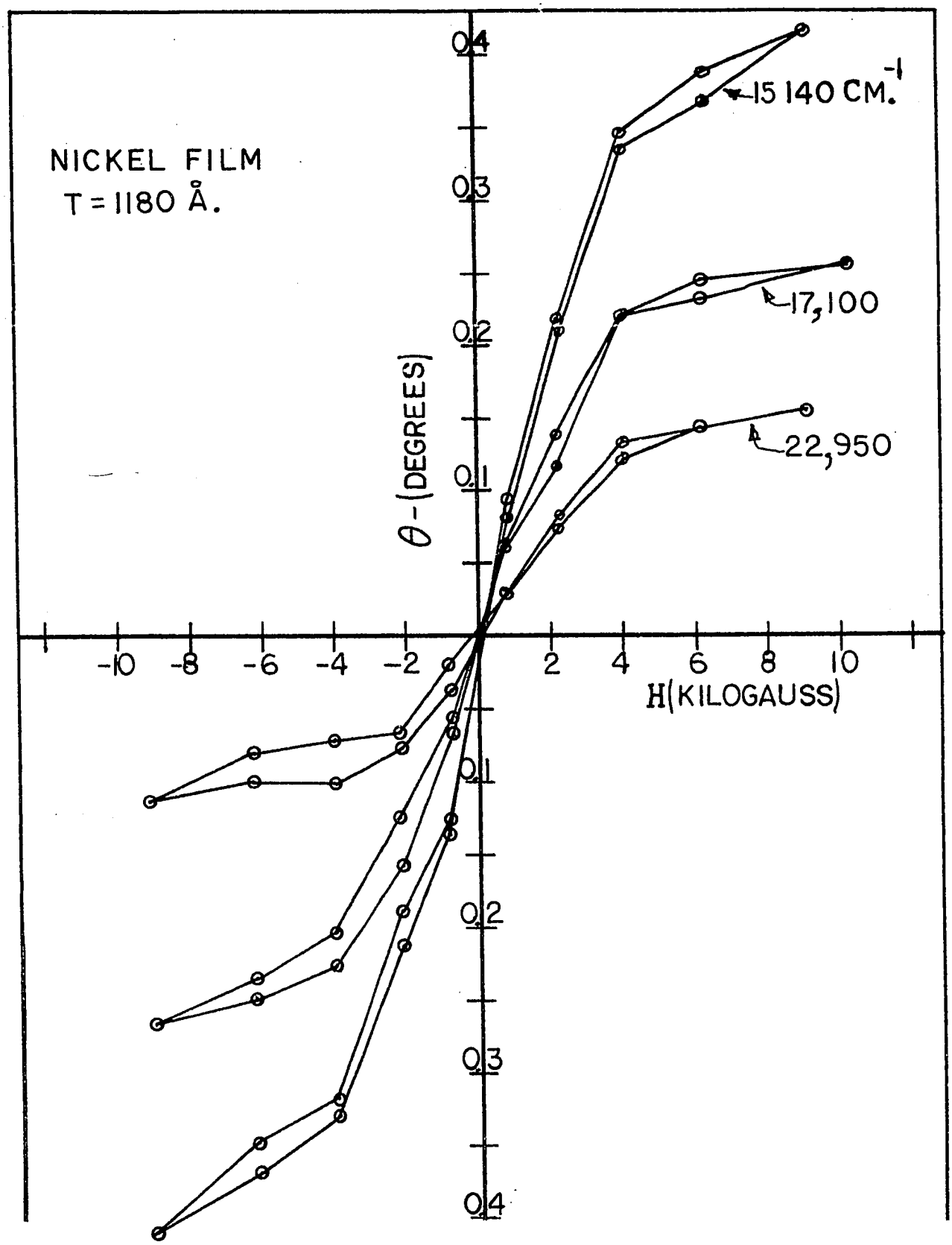

Figure 38. Faraday rotation of thin nickel film as a function of magnetic field.

perpendicular to the film plane will not be very effective in aligning domains as it would in a bulk ferromagnetic sample. A similar situation exists in single ferromagnetic crystals where one has certain "easy" directions and "hard" directions. Such cases are analyzed on the basis of an antisotropic crystalline, interaction energy which is expressed as K $\sin^2\Theta$. Adopting this model for the thin films we have that the total energy of the ferromagnetic domain in the field H is

$$E_H = K\sin^2\Theta - MH \sin\Theta.$$

M is the net magnetization of the domain while Θ is the angle between magnetization vector and the film plane.

To find the equilibrium magnetization we differentiate with respect to Θ and find for an extremum

$$\frac{\partial E_H}{\partial \Theta} = 0 = 2K \sin\Theta \cos\Theta - MH \cos\Theta \ . \qquad (46)$$

Hence $\sin\Theta = MH/2K$ or $\Theta = \pi/2$. Then it follows for the induced magnetization

$$M_H = M\sin\Theta = (M^2/2K)H \ . \qquad (47)$$

Thus a graph of M versus H, will result in a straight line through the origin up to the point where $\sin\Theta = 1$, then saturation occurs. This magnetization gives rise to the so-called "hard direction hysteresis loop" shown below.

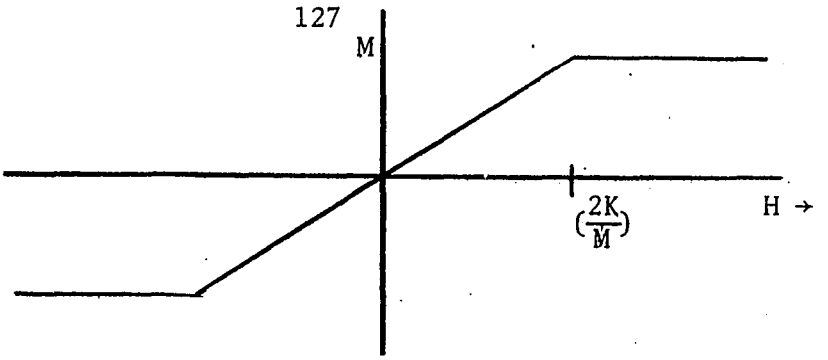

Evidently the curves for the Faraday rotation are similar to the hysteresis loop shown above. Because we omit the differences between H_{ext} and H_{int} the loop is just a single line. No hysteresis shows up. Thus Θ = Const.$\cdot M_H$ is usually referred to as Kundt's Law.[9]

In the references the equation is often written as

$$\Theta = KM/\ell \ ,$$

where ℓ is the sample thickness and K, Kundt's constant, and has been determined for various materials.

Table 15. Verdet Constants in the "Linear" Regions for Several Ferromagnetics.

λ	Co	Fe	Ni
661 mμ	5.5 deg/g.cm.	11.5 deg/g.cm.	8.6 deg/g.cm.
546	3.3	9.7	-
478	-	7.1	-
436	2.2	5.1	4.7

Table 16. Saturation Rotation for Nickel.

λ	Θ_0SAT. (Deg/cm.)
661 mμ	3.8×10^4
470	2.0×10^4
470	1.7×10^4
436	1.3×10^4

Tables 15 and 16 give the Verdet Constants in the linear regions and the saturation rotations for nickel at the wavelengths used.

The rotation by the copper films was found to be very small. The maximum rotation observed, .015 degrees is barely greater than the experimental uncertainty of .01 degrees. Hence, the field dependence will not be analyzed, but this measurement provided a useful check on the procedure.

Analysis of Wavenumber Dependence

In Figs. 39 through 42 the dependence of the rotation upon the wavenumber is given. For paramagnetic or diamagnetic rotations this frequency dependence is very pronounced. However, in the ferromagnetics there is little variation in the frequency dependence. Perhaps the nickel film has a peak centered at about 18,500 cm^{-1}. This could be due to resonance between two narrow (3d) bands corresponding

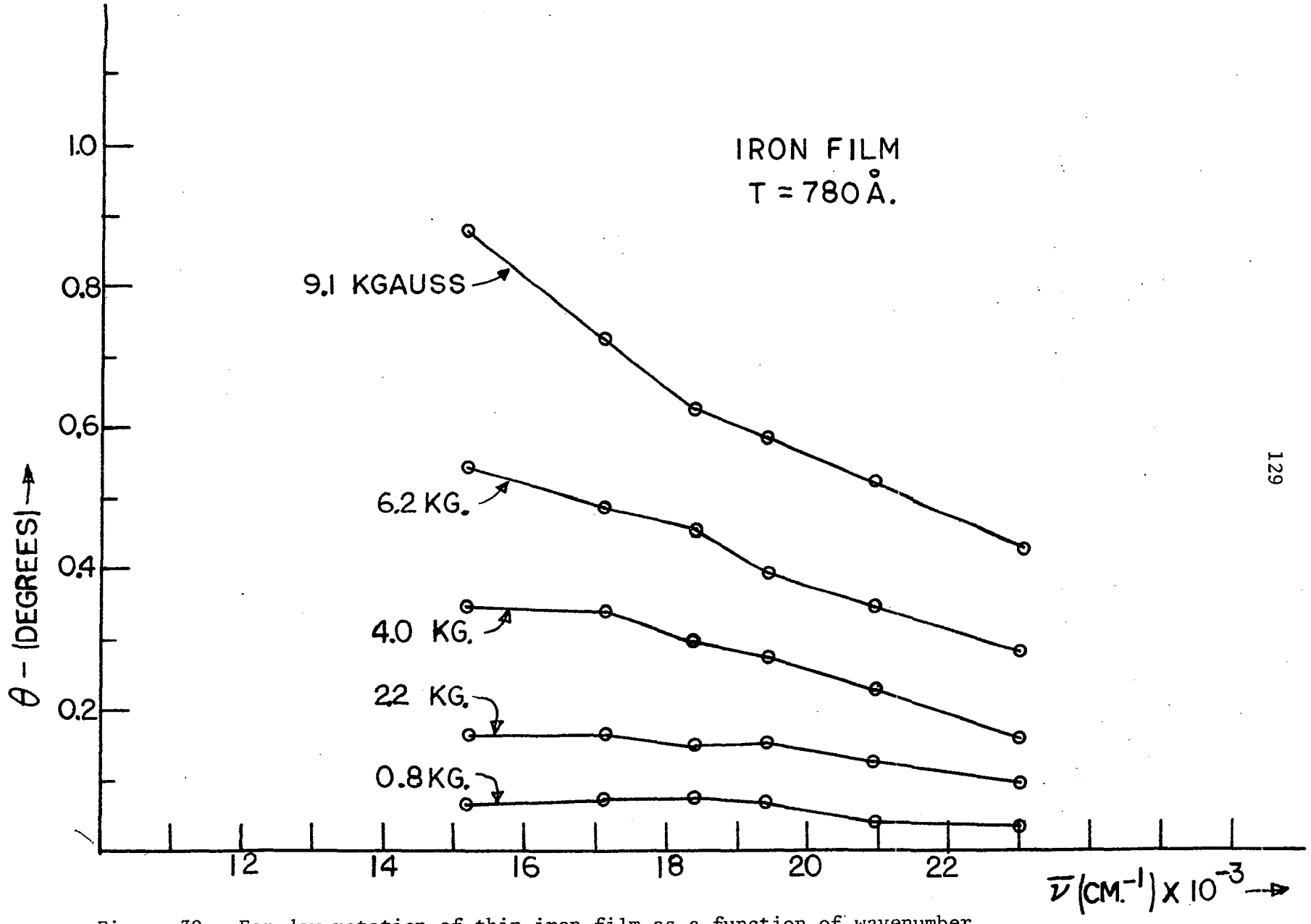

Figure 39. Faraday rotation of thin iron film as a function of wavenumber.

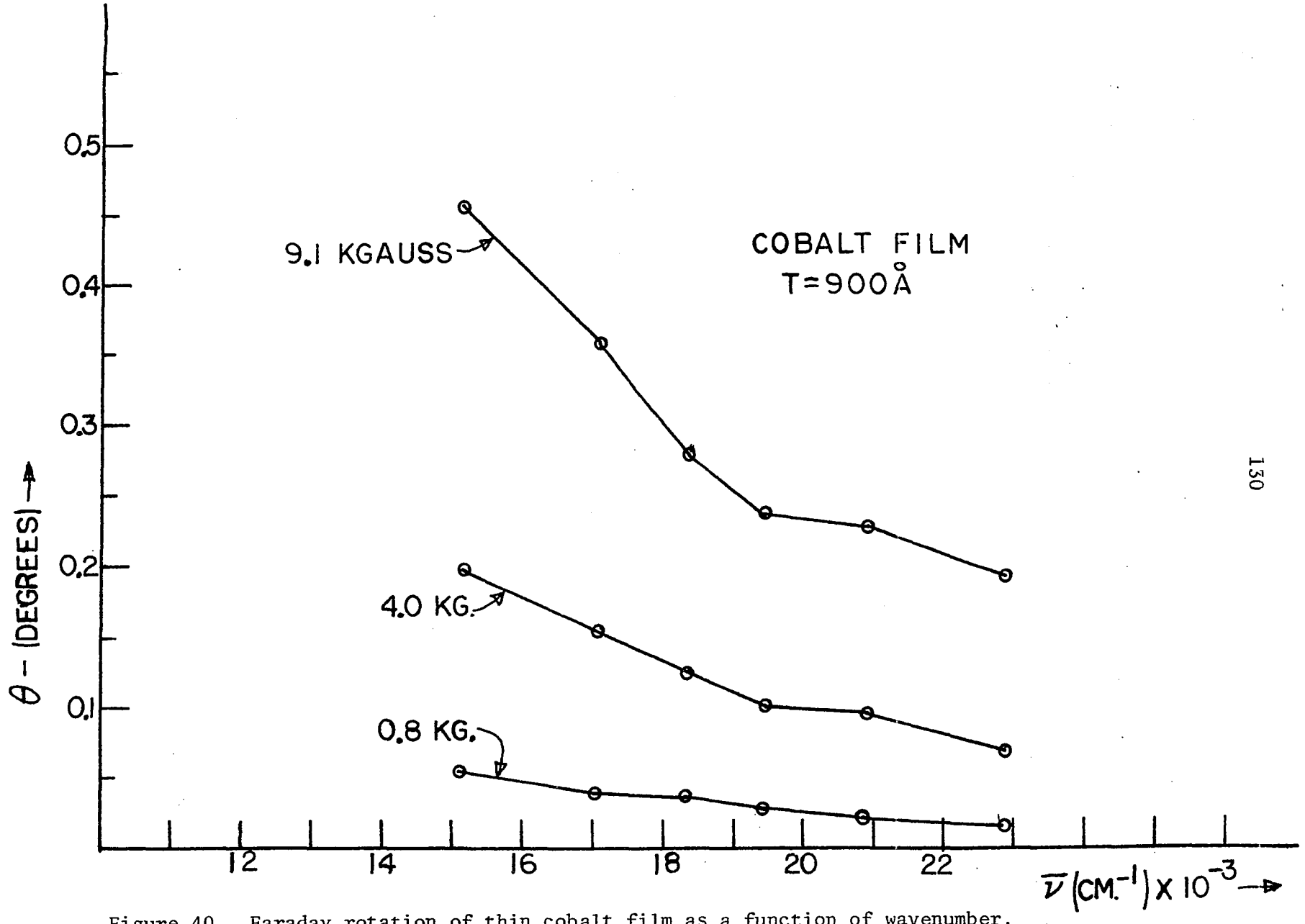

Figure 40. Faraday rotation of thin cobalt film as a function of wavenumber.

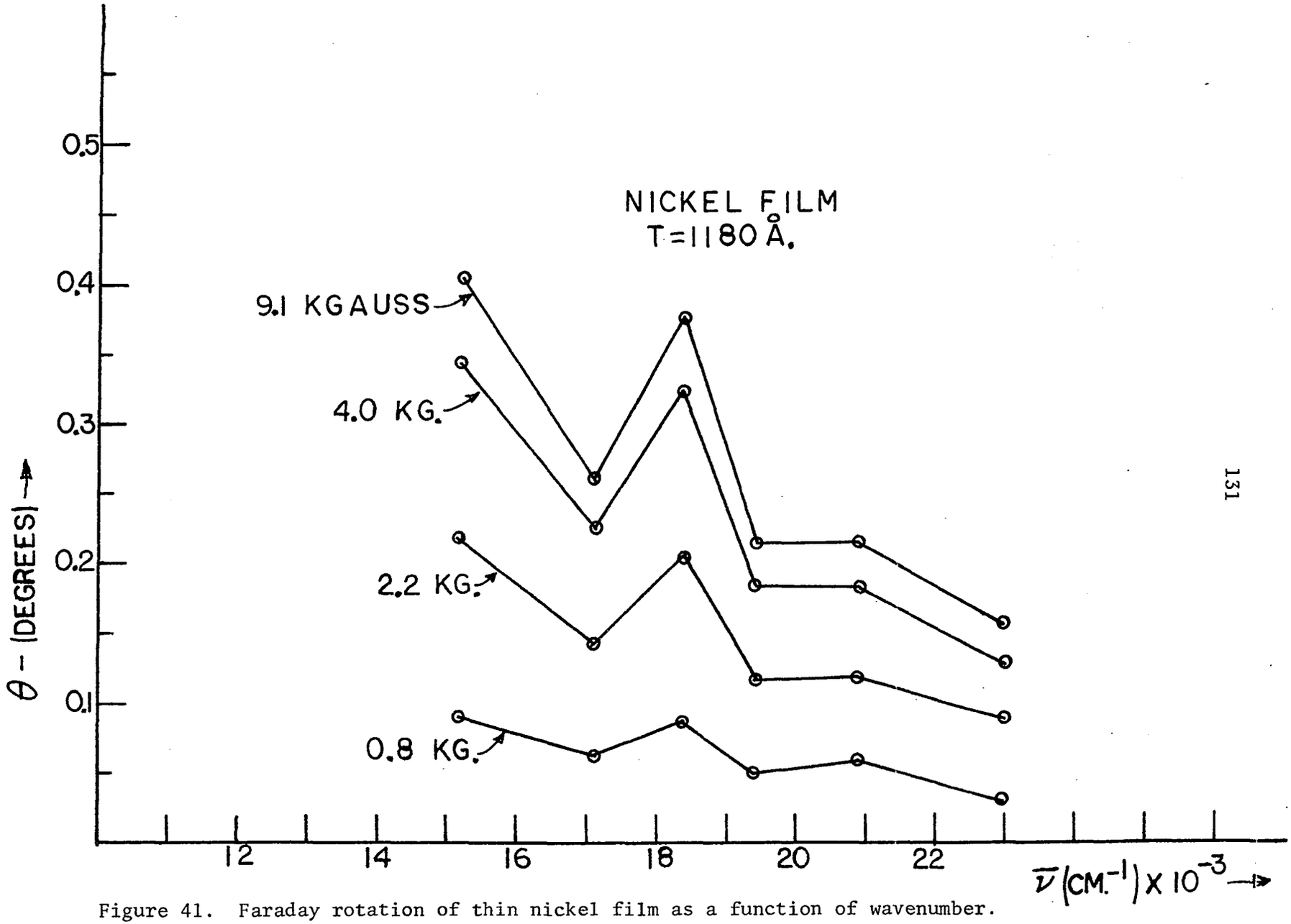

Figure 41. Faraday rotation of thin nickel film as a function of wavenumber.

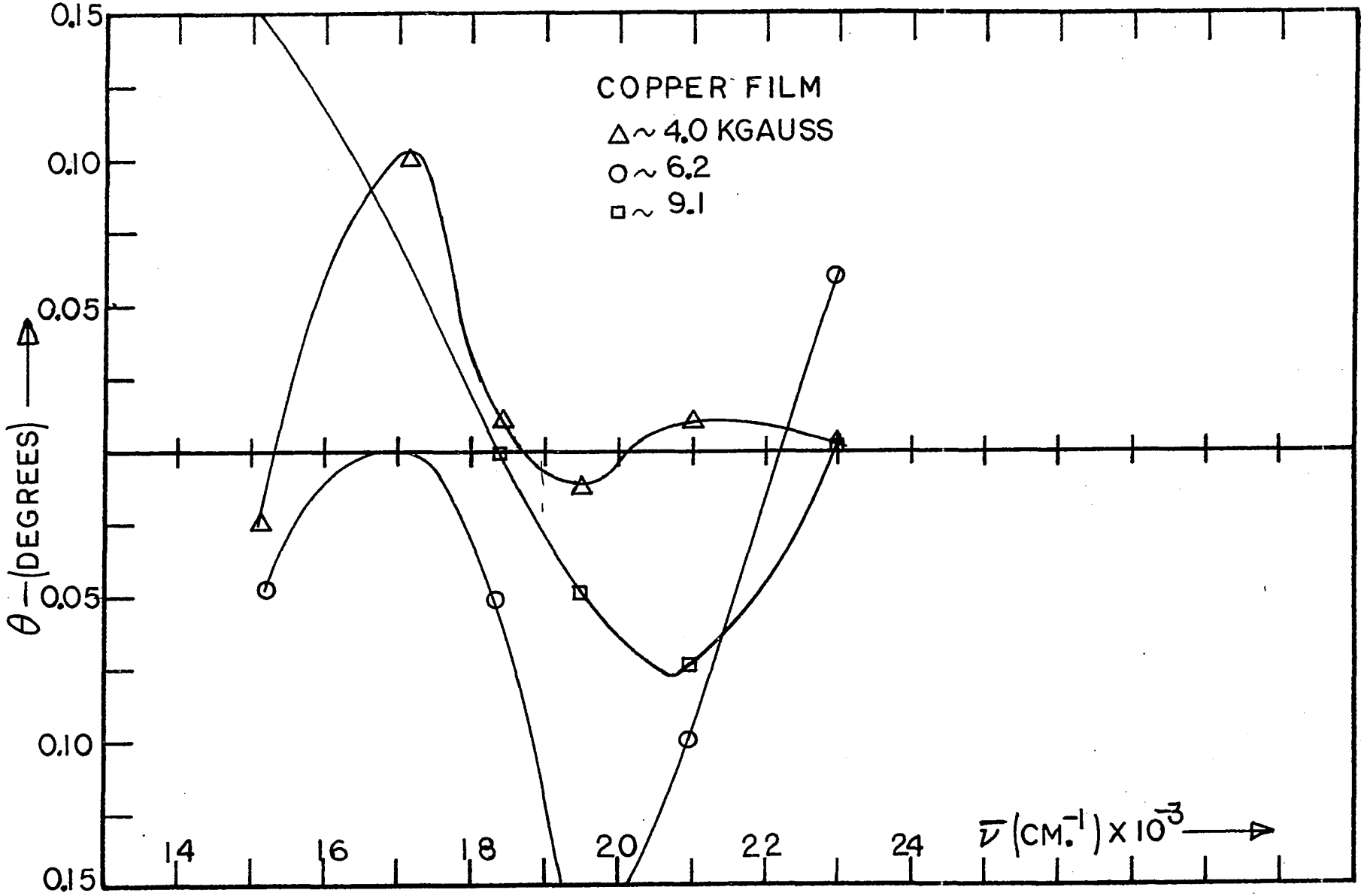

Figure 42. Faraday rotation of thin copper film as a function of wavenumber.

to an energy difference of 2.7 eV. According to the data for nickel the peak is roughly symmetrical about the wavenumber 18,500 cm^{-1}. We now plot the maximum height of the peak itself, hence

$$\Theta_R = \Theta_0 - \Theta_B \tag{48}$$

versus H. Here Θ_R is the rotation due to "resonance" only Θ_0 is the total observed rotation and Θ_B is the rotation due to the background rotation. The result is given in the Fig. 43.

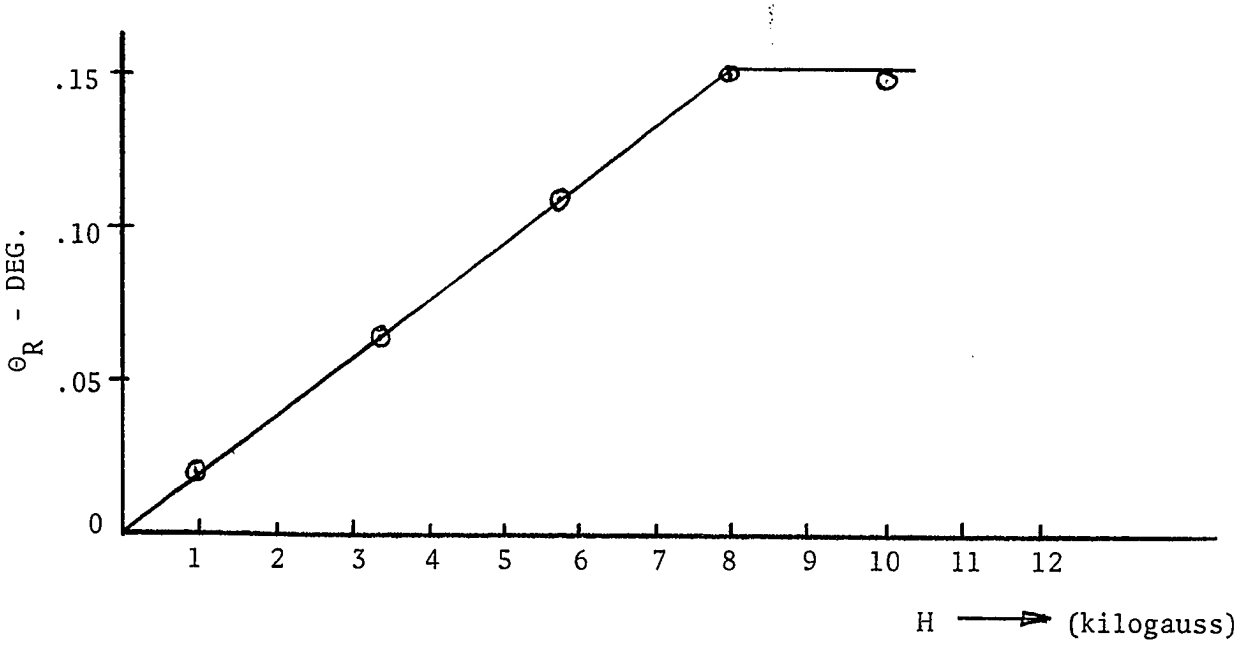

Figure 43. Field Dependence of the Rotation Θ_R at 18,500 cm^{-1}.

Again a typical ferromagnetic curve as observed in the "hard" direction shows up.

REFERENCES

1. Consolidated Vacuum Corp., Type VMF-21, Air cooled.
2. Emerson and Cuming, Inc., "Eccobond" Type 99, one part epoxy.
3. Dushman, S., Scientific Foundations of Vacuum Technique (John Wiley and Sons, Inc., New York, 1949), pp. 757-764.
4. Rosebury, F., Handbook of Electron Tube and Vacuum Techniques (Addison-Wesley Publishing Co., Inc., Reading, Mass. 1965) pp. 1-33.
5. *Ibid.*
6. Tolansky, S., Multiple Beam Interferometry (Clarendon Press, Oxford, 1948).
7. Argyres, P., Phys. Rev. 97, 344 (1955).
8. Stoner, E. C., and E. P. Wohlfarth, Phil. Trans. A, 240, 599 (1948).
9. Schütze, W., Handbuch Der Experimental Physik (Akademische Verlagsgesellschaft M.B.H., Leipzig. 1936) Vol. 16, pp. 184-199.

CHAPTER VII

SUMMARY

This thesis gives the results of an extensive review of the magneto-optic properties of a group of commercially prepared, stabilized ferric oxides. These SFO's were initially selected and studied because of their interesting pressure dependent Faraday effect. To better understand and theoretically analyze this phenomenon the present work was begun.

First the commercial SFO's were size fractionated because of the rather continuous range of particle sizes. The ferric oxide particle sizes were measured by X-ray and electron microscope techniques. The magneto-optic and magnetic properties are dependent on the size and, of course, was the reason for the initial fractionation.

The dispersion of the magneto-optic rotation-MORD-was measured for a high and low end fraction. This data was fitted by theoretically predicted functions. From these it is found that the high end fractions tend to have a larger paramagnetic rotation than do the low ends. This is attributed to the fact that the high fraction has a greater number of magnetic moments which can be aligned by the magnetic field in a manner similar to ferromagnetic alignment. However, the size of the ferric oxide particles which is in general less than 50 Angstroms limits the

number of magnetic moments to about 10^3 so that a superparamagnetic rather than a ferromagnetic effect takes place. This superparamagnetic effect is the cause of the large paramagnetic term in the theoretical expressions of the Faraday effect. It is found also that the magnitude of this term is related to particle size in general so that the high end fractions have a larger paramagnetic FR term than the low end fractions.

Also the MORD was studied for SFO's obtained from different sources. A total of five (5) different SFO's were studied. The behavior was similar except for SFO #14 for which the FR depends linearly on H. This is attributed to a antiferromagnetic alignment of the magnetic moments so that only the diamagnetic component-(which is proportional to H)-of the Faraday rotation remains.

The fitting of the experimental data constitutes somewhat of a test of the new theory in that both the wavenumber and H dependence of the FR could be fitted for the most part to within experimental error. Some deviations between theory and experiment still remain but the sample definition and experimental error did not justify further analysis.

In connection with the FR measurements the optical absorption spectra of the SFO's was measured. It was found that the absorption is due to a strong, broad absorption band in the UV so that the wings of this band dominate the absorption in the visible. The position of the other absorption bands were found to be at $16{,}500 \pm 1{,}000$ cm^{-1},

21,500±1,000 cm^{-1}, 22,500±1,000 cm^{-1}, 26,500 cm^{-1}±1,000 cm^{-1} and 32,000±2,000 cm^{-1} for the SFO's. The positions of these absorption bands was used in fitting the MORD's. The optical absorption spectra was compared to the spectra of several other ferric salt solutions and in particular it was found to be very similar to that of colloidal ferric hydroxide. Also it was found that the high fractions of the SFO's had extinction coefficients of 5,700±200$\{cm^{-1}\cdot[mole(Fe)]^{-1}\cdot liter\}$ whereas the low end fractions and SFO #14 had values of about twice this number.

A study of the electrical properties was undertaken after it was found that the resistance of the samples was strongly temperature dependent. The resistance varied exponentially as T^{-1}. Consideration of the theoretical explanation of this phenomenon led to the hope that these studies would enable us to determine the energy of the excited energy levels of the SFO's. The interpretation of the results was complicated, however, by the conduction due to the organic polymer of the SFO. SFO #5C-1 is the exception in that its resistance is very similar in magnitude to that of Fe_3O_4. The activation energy of this SFO is also quite similar which leads us to believe this particular SFO is simply stabilized Fe_3O_4 or $Fe_3O_4\cdot\chi H_2O$. A study on the pressure dependence of the sample resistance was undertaken to try to understand the mechanism of the electrical conduction. We found that the resistance changed sharply on application of about 1 kilobar but that activation energy changed little if any. We interpreted this to mean that the organic polymer which separates the ferric complexes is easily deformed

by pressure with the resulting effect that the resistance decreases sharply.

A tendency of the sample resistance to "relax" after initial application of pressure and again after its release was also observed. This effect is also observed in the magnetic susceptibility and is probably due to either a slow rearrangement of the surface atoms of the ferric oxide complex or to penetration of the pressurized oil into the porous sample and which tends to release the pressure.

Several short term studies of the SFO's were made. First, electron microscope photomicrographs were taken. We were able to observe and measure the size of the ferric oxide complexes within the SFO's. The organic polymer because of its much smaller electron density was not observed. The photo-micrographs showed that the high end fractions had the largest size ferric oxide particles, and vice versa. The particles were roughly spherical with the biggest observed diameters belonging to SFO #6A-1. This diameter was 45 Angstroms. The smallest particles observed were one of the low end fractions of SFO #11. They had a size of 20 Angstroms which is close to the limit of the resolving power of the electron microscope. Comparison of the electron microscope data and X-ray data led to the interesting conclusion that the ferric oxide complexes were actually microcrystalline. We had expected this from the magnetic properties but this proved an interesting confirmation.

A second brief study was made of the EPR spectra of the SFO's. From this study we were able to determine the spectroscopic splitting factor "g_{eff}" for the SFO's. For all the SFO's g_{eff} is slightly greater than 2.0. This is about what one expects for a ferric complex with a small amount of "zero field splitting".

Finally films of iron, cobalt, nickel and copper were vacuum deposited onto glass substrates. The Faraday rotation of each of these was then measured. For the ferromagnetic samples it was found that the Faraday rotation tends to saturate at fields near 10 kilogauss. In a bulk ferromagnetic this saturation takes place at much smaller fields. A brief theoretical analysis of this phenomenon is given. It is assumed that the ferromagnetic film is so thin that domains with a strong ferromagnetic component are in the film plane and hence are essentially perpendicular to the external field H. It is shown that this model could lead to Faraday rotation which is proportional to the magnetization of the ferromagnetic.

The thickness of the films was measured by use of a multiple beam technique. This allowed us to give values of the Verdet constant in the low field, linear, region of FR. Also the approximate saturation Verdet constant is given. These values are somewhat smaller than the saturation rotation values usually quoted for bulk samples and is probably due to the thin film characteristic of the sample. Very small rotations of the order of experimental error were observed for copper films.